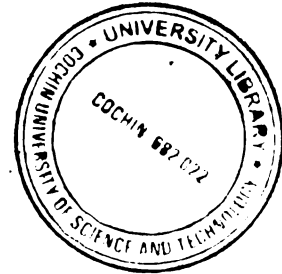# Investigations of Optical Interaction Processes in Certain Photonic Materials Using Z-scan and Thermal Lens Techniques

Santhi A

INTERNATIONAL SCHOOL OF PHOTONICS
COCHIN UNIVERSITY OF SCIENCE & TECHNOLOGY
COCHIN-682 022, INDIA

PhD THESIS SUBMITTED TO
COCHIN UNIVERSITY OF SCIENCE AND TECHNOLOGY
IN PARTIAL FULFILLMENT OF THE REQUIREMENTS FOR THE
DEGREE OF DOCTOR OF PHILOSOPHY

SEPTEMBER 2006

Investigations of Optical Interaction Processes in Certain Photonic Materials Using Z-scan and Thermal Lens Techniques

PhD Thesis

Author
Santhi A
International School of Photonics
Cochin University of Science and Technology
Cochin - 682 022
India
email- santhia.a@gmail.com, santhiannie@yahoo.com

Research Supervisor
Dr. V P N Nampoori
Proefessor, International School of Photonics
Cochin University of Science and Technology
Cochin - 682 022
email- nampoory@gmail.com

Research Co-guide
Dr. P Radhakrishnan
Proefessor, International School of Photonics
Cochin University of Science and Technology
Cochin - 682 022
email- radhak@cusat.ac.in

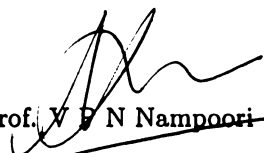International School of Photonics, Cochin University of Science and Technology, Cochin - 682 022

September 2006

CERTIFICATE

Certified that the work presented in the thesis entitled "Investigations of Optical Interaction Processes in Certain Photonic Materials Using Z-scan and Thermal Lens Techniques" is based on the original work done by Ms. Santhi A, under my guidance and supervision at the International School of Photonics, Cochin University of Science and Technology, Cochin - 22, India and has not been included in any other thesis submitted previously for award of any degree.

Cochin 682 022

15th September 2006

Prof. V P N Nampoori

(Supervising guide)

DECLARATION

Certified that the work presented in the thesis entitled "**Investigations of Optical Interaction Processes in Certain Photonic Materials Using Z-scan and Thermal Lens Techniques**" is based on the original work done by me, under the guidance and supervision of Dr. V P N Nampoori, Professor, International School of Photonics, Cochin University of Science and Technology, Cochin - 22, India and has not been included in any other thesis submitted previously for award of any degree.

Cochin 682 022

15th September 2006   Santhi A

Preface

Characterization of photonic materials were carried out using two very interesting techniques, Z-scan and Thermal lens. The z-scan is used for determination of nonlinear optical properties, whereas thermal lens effects was used for determination of fluorescence quantum yield. So the thesis is presented as two sections, one for Z-scan Techniques and the other for Thermal Lens Techniques. It comprises seven chapters.

Chapter1 - This gives an introduction to nonlinear optics, and some techniques for nonlinear optical material characterization. Among the various nonlinear optical interaction processes, the following processes are discussed in detail. Sum and Difference frequency generation, Optical Parametric Oscillation and Third Order Polarization of which Third harmonic generation (THG) and Intensity dependent Refractive Index (IDRI) are interesting consequences. Other processes described are Self Focusing, Optical bistability, Kerr-lens mode locking (KLM), Self-phase modulation, parametric amplification, and parametric generation, Spontaneous parametric down conversion and Optical rectification. Other important processes that are mentioned are Cross-phase modulation (XPM), Nonlinear Light Scattering- Stimulated Brillouin Scattering and Stimulated Raman Scattering, Optical phase conjugation and Two-photon absorption. It also deals with Nonlinear Optical Materials and some of the Measurement Techniques. Here various methods for nonlinear material characterization are described with special emphasis to z-scan technique. The theoretical details and the methods to analyze and interpret the z-scan transmittance data are discussed in detail. Other methods like degenerate four-wave mixing, nearly degenerate three wave mixing etc are mentioned.

Chapter2 - In this chapter the experimental results for nonlinear optical absorption in metal phthalocyanines are included. Both open aperture and closed aperture z scan transmittance signals were recorded to study the refractive and absorptive nonlinearities. The samples chosen were metal phthalocyanines viz CoPc, NiPc, ZnPc and CuPc. Dimethyl Formamide (DMF) and Dimethyl Sulphoxide (DMSO) were used as solvents. The laser source was the Q switched Nd:YAG with 10 Hz repetition rate and a pulse width of 8 ns. As the nonlinear sample is scanned along the propagation path of a focused Gaussian

laser beam around its focus, the intensity characteristics of the beam induces a position dependant change of refraction inside the sample. The transmittance of the nonlinear medium through a finite aperture placed in the far field as a function of the sample position is measured. From an open aperture z scan signal, the nonlinear absorption coefficient β can be determined and the nonlinear refraction coefficient γ can be deduced from the closed aperture data. Optical limiting studies were also performed in ZnPc using the fundamental and second harmonic from the same laser source.

Chapter3 - Wavelength dependence of saturable and reverse saturable absorption (SA and RSA) of zinc phthalocyanine (ZnPc) was studied using 10 Hz, 8ns pulses from a MOPO in the wavelength range from 520-686 nm, which includes the rising edge of the Q-band in the electronic absorption spectrum. The nonlinear response is wavelength dependent and switching from RSA to SA has been observed as the excitation wavelength changes from the low absorption window region to higher absorption regime near the Q-band. The SA again changes back to RSA when we further move over to the infrared region. Values of the imaginary part of third order susceptibility are calculated for various wavelengths in this range. This study is important in identifying the spectral range over which the nonlinear material acts as RSA based optical limiter. A five level energy model is considered and the resulting rate equations are solved in transient regime and steady state regime to account for the spectral dependence of nonlinear absorption. Following the density matrix formalism, an expression for $\text{Im}(\chi^{(3)})$ in terms of excitation wavelength, the detuning factor, the line shape function etc. was obtained. This can be simulated to see how far it matches with the experimentally obtained results.

Chapter4 - An introduction to phtothermal and photo-pyro techniques is presented in this chapter. The various techniques discussed are photo thermal deflection, thermal lensing, photo acoustic method etc. Special emphasis is given to thermal lensing effects and applications. It also presents the relative advantages and disadvantages of each method.

Chapter5 - Fluorescence quantum yield (FQY) is the fraction of the molecules that emit a photon after direct excitation by a light source. It provides information on radiationless processes in molecules, and, in the assignment of electronic transitions. The need of a fluorescence standard can be eliminated if we go for photo-thermal method like thermal lens technique. It is a highly sensitive method, which can be used to measure the optical absorption and thermal characteristics of a sample. We use this technique to determine the effect of silver nano particles on the FQY of Rhodamine 6G and also to calculate the

FQY value of a newly synthesized chemical schiff base. We have proved that the presence of Ag sol reduces the quantum yield of Rh6G. A discussion is presented on the possible reasons for this decrease in FQY in terms of formation of charge transfer complexes. Also, we have observed that the presence of silver sol can enhance the thermal lens signal. The fluorescence spectrum of the schiff base, obtained from salicylaldehyde and 2-aminophenol is studied using an argon-ion laser as the excitation source and its FQY is determined using a thermal lens method. The quantum-yield values are calculated for various concentrations of the solution in chloroform and also for various excitation wavelengths. The high value of the FQY of this schiff base, will make this sample useful as a fluorescent marker for biological applications. Photo stability and gain studies will assess its suitability as a laser dye.

Chapter6 - We apply the theory of photo thermal lens formation and also that of pure optical nonlinearity, to account for the phase modulation in a beam as it traverses a nonlinear medium. It is used to simultaneously determine the nonlinear optical refraction and the thermo-optic coefficient. We demonstrate this technique using some metal phthalocyanines dissolved in dimethyl sulphoxide, irradiated by a Q switched Nd:YAG laser with 10 Hz repetition rate and a pulse width of 8 ns. A transient TL signal will be formed in liquid samples, in the nanosecond regime, which we exploit here to simultaneously determine thermo-optic coefficient, dn/dT and the nonlinear optical parameters. we considered the changes in refractive index due to purely optical nonlinearity and also that due to TL formation. This is demonstrated using CoPc and NiPc in DMSO.

Chapter7 - This chapter summarizes all the experimental results and gives a brief discussion about possible modifications and extensions to the work already done. Some of them are; spectral dependence of nonlinear refraction cross section, time resolved z-scan to clearly understand the nonlinear optical behavior, photo bleaching and gain studies of the schiff base to assess its suitability as a laser dye, and photo pyro technique to calculate the excited state absorption cross section and compare it with the values obtained using z-scan method.

Most of these results are published in peer reviewed journals and also presented in various conferences. **The publications are listed at the end of chapter 7**

Acknowledgements

I owe so much to so many as I reflect on this thesis. I thank my research advisor, **Prof. V P N Nampoori** and co-guide, **Prof. P Radhakrishnan**, for sharing their experience and knowledge with me. I am indebted to them for accepting me as their student, which resulted in a very important turning point in my academic life. I am also thankful to **Prof. V M Nandakumaran** for helping me at the time of my admission, and **Prof. C P Girijavallabhan** for showing sincere interest in various experiments I carried out in the laser lab.

My indebtedness also goes to those I worked with, on several research projects, including (but not limited to) **Vinu V Namboodiri, Jyotsna Ravi, A. Deepthi, K P Unnikrishnan** and **Achamma Kurian**. I am especially thankful to Vinu, with whom I did most of the high power laser experiments. He provided instant solutions to several of the LaTeX problems I had. It was a pleasure to be in the elite company of Jyotsna, Vinu, **Jijo, Pravitha** and **Rekha**, all of whom are special in their own ways, possessing superior problem solving ability and commonsense. I particularly acknowledge Jijo for all the help he provided whenever I had a crisis with computers!!

I had several other great friends (in addition to those already listed), and though I cannot name them all, I especially want to thank **Chitra** for her help and company when I needed it the most. I am thankful to her and also to sister **Ritty** and **Sajeev** for careful proof reading of my manuscript. My gratitude also goes to **Bino George**, for the clear illustrations in the first chapter of this thesis and for the beautiful cover design. He spent a lot of time for making whatever modifications I required. I am thankful to **Rajesh S**, for providing me with some useful programming tips in Matlab and Mathematica.

I also **thank the** other student members of the photonics family as well

as the other faculty, staff and students of the International School of Photonics. I am thankful to **Prof. V Ramakrishnan, Prof. M R P Kurup** and **Prof. J.Keshavayya** for their generosity with the most interesting and "freshly made" samples used in my experiments. I also acknowledge **Umadevi** and **U.L.Kala** for helping me in preparing some of those samples.

I would like to acknowledge the financial support of the Council of Scientific and Industrial Research, CSIR. I also acknowledge **NUFFIC, SPIE, CEFIPRA** and CSIR for providing me with partial travel grant that enabled me to attend some very good research conferences during my research life at ISP.

My parents, sister and brother, have been unbelievably supportive throughout my life, without which it would have been impossible to lead such a long student life as I had. I thank them for being with me always and for allowing me to choose my career.

<div align="right">

Santhi

</div>

Contents

List of Figures

List of Tables

Part I

Z-scan Technique

Chapter 1

Characterization of Nonlinear Optical Materials

"Truth is ever to be found in the simplicity, and not in the multiplicity and confusion of things."- Isaac Newton

ABSTRACT

A concise introduction to nonlinear optics and various nonlinear optical interactions are given in this chapter. A short survey of emerging nonlinear optical materials and some of the characterization techniques are also discussed here. This chapter briefly describes various nonlinear optical phenomena which can be used to probe the secrets of light-matter interaction. Description of z-scan is given as a separate section at the end. Only a brief and commonly used theoretical formalism of z-scan technique is provided in this section. Appropriate modifications and more details of data interpretations are given in succeeding chapters.

1.1 Nonlinear Optical Properties and Materials

Nonlinear optics is a broad field of research and technology that includes subject matter in the fields of physics, chemistry, biology and engineering. The diversity of nonlinear optics stems, in part, from the need for all-optical and electro-optical devices for applications in telecommunications, optical storage, and all-optical computing. In addition, many nonlinear optical effects have proved to be versatile probes of fundamental issues such as the electronic structure of compound semiconductors, phase transitions in liquid crystal films etc. Nonlinear optical materials use nonlinear dependence of the refractive index on

the applied electric field to produce other frequencies. Basic concepts of nonlinear optics and some of the important nonlinear optical materials are discussed below.

1.1.1   Introduction to Nonlinear Optics

The invention of the laser ushered in a new field of studies in optical phenomena in the early 1960s – 'nonlinear optics'. Because laser light can be sufficiently intense, it can actually change the index of refraction of a material through which it passes. Thus, the behavior of a transparent medium can depend on how intense the light is - a 'nonlinearity' that has led to such interesting phenomena as self-focussing of light and optical harmonic generation, resulting into the creation of new colors of light from a single color. Nonlinear optics is the study of phenomena that occur as a consequence of the modification of the optical properties of a material system in the presence of light. Nonlinear optical phenomena are nonlinear in the sense that they occur when the response of a material system to an applied optical field is a nonlinear function of the strength of the optical field. For example, second harmonic generation occurs as a result of the part of the atomic response that depends quadratically on the strength of the applied optical field[1]. In order to describe more precisely what is meant by an optical nonlinearity, lets us consider how the dipole moment per unit volume, or polarization $\tilde{P}(t)$, of a material system depends on the strength $\tilde{E}(t)$ of the applied optical field. In the case of conventional (i.e., linear) optics, the induced polarization depends linearly on the electric field strength in a manner that can often be described by the relationship

$$\tilde{P}(t) = \chi^{(1)} \tilde{E}(t) \tag{1.1}$$

where the constant of proportionality $\chi^{(1)}$ is known as the linear optical susceptibility. In nonlinear optics, the nonlinear optical response can often be described by generalizing Equation 1.1 by expressing the polarization $\tilde{P}(t)$ as a power series in the field strength $\tilde{E}(t)$ as

$$\tilde{P}(t) = \chi^{(1)} \tilde{E}(t) + \chi^{(2)} \tilde{E}^2(t) + \chi^{(3)} \tilde{E}^3(t) + \dots\dots$$
$$= \tilde{P}^{(1)}(t) + \tilde{P}^{(2)}(t) + \tilde{P}^{(3)}(t) + \dots \tag{1.2}$$

The quantities $\chi^{(2)}$, $\chi^{(3)}$ etc are known as the second and third - order nonlinear optical susceptibilities , respectively. Here $\chi^{(1)}$ is a second rank tensor, $\chi^{(2)}$, third rank tensor etc. It is also assumed that the polarization at time t depends

only on the instantaneous value of electric field strength, or that the medium is lossless and dispersionless. But in general, the nonlinear susceptibilities depend on the frequencies of the applied electric field, and the equations for polarization need to be modified. We call $\tilde{P}^{(2)}(t) = \chi^{(2)}\tilde{E}^2(t)$ as the second order nonlinear polarization and $\tilde{P}^{(3)}(t) = \chi^{(3)}\tilde{E}^3(t)$ as the third order nonlinear polarization. The physical processes that occur as a result of $\tilde{P}^{(2)}$ are distinct from those that occur as a result of $\tilde{P}^{(3)}$. Second order nonlinear optical interactions can occur only in noncentrosymmetric crystals, that is, in crystals that do not have inversion symmetry. Since liquids, gases, amorphous solids (such as glass), and even many crystals do display inversion symmetry, $\chi^{(2)}$ vanishes for such media, and consequently they cannot exhibit second order nonlinear optical phenomena. On the other hand, third order nonlinear optical interactions (i.e., those described by $\chi^{(3)}$) can occur both for centrosymmetric and noncentrosymmetric media[1]. An Important point to be noted is that in order to make the series in Equation 1.2 convergent, the ratio of $(n+1)^{th}$ to $(n)^{th}$ coefficient should be very much less than unity.

The most common procedure for describing nonlinear optical phenomena is by expressing the polarization $\tilde{P}$ in terms of the applied field strength $\tilde{E}$. The reason why polarization plays a key role in the description of nonlinear optical phenomena is that a time-varying polarization can act as the source of new components of the electromagnetic field. For example, the wave equation in nonlinear optical media often has the form

$$\nabla^2\tilde{E} - \frac{n^2}{c^2}\frac{\partial^2\tilde{E}}{\partial t^2} = \frac{4\pi}{c^2}\frac{\partial^2\tilde{P}}{\partial t^2} \tag{1.3}$$

where n is the refractive index and c is the speed of light in vacuum. We can interpret this expression as an inhomogeneous wave equation in which the polarization $\tilde{P}$ drives the electric field $\tilde{E}$. This equation expresses the fact that, whenever $\frac{\partial^2\tilde{P}}{\partial t^2}$ is nonzero, charges are being accelerated and generate electromagnetic radiation.

---

[1] It is interesting and useful to have an idea about the order of magnitude of NLO effects. Assume the nonlinearity is electronic in origin. Under conditions of non resonant excitation, $\chi^{(2)}$ will be of the order of $\frac{\chi^{(1)}}{E_{at}}$. For condensed matter, $\chi^{(1)}$ is of the order of unity, and therefore, $\chi^{(2)}$ will be of the order of $\frac{1}{E_{at}}$. Since E_{at}, the atomic electric field strength is given by $E_{at} = \frac{e}{a_0^2} = 2 \times 10^7 esu$ (-e is the charge of electron and a_0 the Bohr radius), $\chi^{(2)} \sim 5 \times 10^{-8} esu$ and $\chi^{(3)} \sim 3 \times 10^{-15} esu$
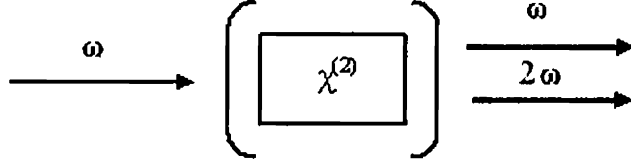
Figure 1.1: Geometry of second harmonic generation

1.1.2   Descriptions of Nonlinear Optical Interactions

Nonlinear optical interactions of laser fields with matter provide powerful spec-
troscopic tools for the understanding of microscopic interactions and dynamic
processes. A topic of keen interest in this field is the generation of higher har-
monics of the laser frequency, using the nonlinear response of atoms or plasma in
intense optical fields. The high fluence available from lasers enable such various
nonlinear phenomena to take place, some of which are described below.

Consequences of Second Order Polarization

1. **Optical Second Harmonic Generation (OSHG):** OSHG is a nonlin-
   ear process which leads to frequency doubling when an intense laser beam
   travels through a nonlinear optical medium[2].

   The second harmonic generation is illustrated schematically in Figure 1.1
   Here a laser beam whose electric field strength is expressed as

   $$\bar{E}(t) = Ee^{-i\omega t} + c.c \qquad (1.4)$$

   is incident on a crystal for which $\chi^{(2)}$ is non zero. The nonlinear polariza-
   tion that is created in such a crystal is given as

   $$\bar{P}^{(2)}(t) = 2\chi^{(2)}EE^* + (\chi^{(2)}E^2e^{-2i\omega t} + c.c). \qquad (1.5)$$

   We see that the polarization consists of a contribution at non-zero fre-
   quency (the first term) and a contribution at frequency 2ω (the second
   term). This latter contribution can lead to the generation of radiation

---

[2]The characteristic length for significant second harmonic generation under phase matched
condition is $L \sim \lambda E_a/E$ where E is the incident optical field and λ is its wavelength. For
$\lambda = 1\mu m$ we see that L= 1 cm for power density of $1MW/cm^2$ ($3 \times 10^6 Vm^{-1}$ incident field.)

at second-harmonic frequency. As an example, the Nd:YAG laser that operates at 1064 nm, produces radiation at wavelength 532 nm by SHG. Historically, nonlinear optics originated with the experimental observation of SHG by P. A. Franken, who in 1961 noticed that a weak optical signal at 347.1 nm could be generated in a quartz crystal when the material was illuminated with a high-power ruby laser at 694.2 nm [2]. Franken concluded that this new light source was due to the coherent mixing of two optical electric fields in the quartz so as to produce a "second harmonic" response in the bulk region of the material.

2. **Sum and Difference Frequency Generation (SFG and DFG)**: SFG and DFG refer to the generation of light with a frequency that is the sum or difference of two input frequencies in a nonlinear medium. (SHG is a special case of this). This technique is being used extensively to produce tunable laser pulses in the mid infrared region. This region of the spectrum is very important for the sensing of a great variety of (transient) molecular species. Femtosecond IR pulses can be used to interact selectively with the bonds in a molecule. The mid-IR region is ideally suited to determine the presence of specific molecules in a sample. Therefore, a great deal of effort has been invested over the last decade to produce femtosecond pulses tunable in the near- and mid-IR region. The vast majority of techniques now in use are based on parametric difference-frequency generation processes. When an optical field with two distinct frequency components are incident on a nonlinear medium, which is represented as,

$$\tilde{E}(t) = E_1 e^{-i\omega_1 t} + E_2 e^{-i\omega_2 t} + c.c \tag{1.6}$$

the second-order contribution to the nonlinear polarization can be written as[1]

$$
\begin{aligned}
\tilde{P}^{(2)}(t) &= \chi^{(2)} \tilde{E}^2(t) \\
&= \chi^{(2)}[E_1^2 e^{-2i\omega_1 t} + E_2^2 e^{-2i\omega_2 t} + 2E_1 E_2 e^{-i(\omega_1+\omega_2)t} + \\
&\quad 2E_1 E_2^* e^{-i(\omega_1-\omega_2)t} + c.c] + 2\chi^{(2)}[E_1 E_1^* + E_2 E_2^*]. \tag{1.7}
\end{aligned}
$$

The complex amplitude of the various frequency components are hence

given by

$$P(2\omega_1) = \chi^{(2)} E_1^2 ..... (SHG) \tag{1.8a}$$

$$P(2\omega_2) = \chi^{(2)} E_2^2 ..... (SHG) \tag{1.8b}$$

$$P(\omega_1 + \omega_2) = 2\chi^{(2)} E_1 E_2 ..... (SFG) \tag{1.8c}$$

$$P(\omega_1 - \omega_2) = 2\chi^{(2)} E_1 E_2^* ..... (DFG) \tag{1.8d}$$

$$P(0) = 2\chi^{(2)} (E_1 E_1^* + E_2 E_2^*) ..... (OR) \tag{1.8e}$$

where OR is 'optical rectification' and other acronyms are as mentioned before.

3. **Optical Parametric Oscillation (OPO)**: Optical Parametric Oscillation is the generation of a signal and idler waves using a parametric amplifier in a resonator. In the process of DFG, the presence of radiation at frequency ω_2 or ω_3 can stimulate the emission of additional photons at these frequencies. If the nonlinear crystal used in this process is placed inside an optical resonator, (as shown in Figure 1.2) the ω_2 and/or ω_3 fields can build up to large values. Such a device is known as optical parametric oscillator. This device is tunable because any frequency ω_2 (less than ω_1) can satisfy the condition $\omega_2 + \omega_3 = \omega_1$ for some frequency ω_3. In practice, one controls the output frequency by adjusting the phase-matching condition.[3] The applied field frequency ω_1 is often called the pump frequency, the desired output frequency is called the signal frequency, and the other unwanted frequency is the idler frequency.

4. **Optical Parametric Amplification (OPA)**: OPA the amplification of a signal input in the presence of a higher-frequency pump wave, at the same time generating an idler wave. This can be considered as DFG. A modern optical parametric amplifier is an extension of microwave parametric amplifier in optics employing the same principle. It essentially consists of two modes, as mentioned before, the signal and the idler (ω_s and ω_i respectively) coupled through a nonlinearity in a crystal (for example) having a $\chi^{(2)}$ coefficient by a strong pump mode at higher frequency

---

[3] How large should be an incident optical field to allow atoms and molecules to reveal their nonlinear properties? In most cases the incident field should not be negligible in comparison with the internal field E_a which binds together the electrons. $E_a \sim 3 \times 10^{10} Vm^{-1}$ and to obtain such fields an incident intensity of $10^{14} Wcm^2$ is required. But in practice this much intensity will not be necessary for materials to show their NLO behavior. It is because under specific conditions, the induced dipoles oscillate coherently with definite phase relationship. This will result in the radiated fields to add constructively. This constructive interference is termed as 'phase matching'.
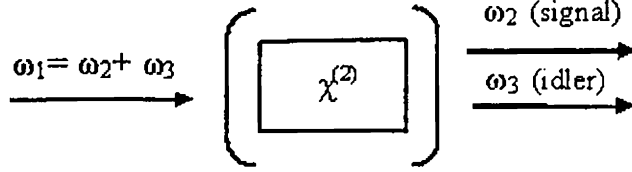
Figure 1.2: The optical parametric oscillator. The cavity end mirrors have high reflectivity at frequencies ω_2 and/or ω_3

ω_p, such that

$$\omega_p = \omega_s + \omega_i. \tag{1.9}$$

The pump is usually assumed to be in a larger amplitude coherent state and hence to produce a classically modulated interaction between the signal and the idler modes. If the signal and the idler frequencies are equal, the amplifier is said to operate in a degenerate mode. The optical parametric amplification can be treated as a three-wave mixed amplifying process. When the pump and the signal are injected into the nonlinear medium, they induce polarization with frequency $\omega_i = \omega_p - \omega_s$ through the second order optical susceptibility. At the same time, the idler signal coupled with the the pump, induces the polarization with frequency $\omega_s = \omega_p - \omega_i$. This generates intensity enhanced signal beam [5]. Because the pump is much stronger than the signal and the idler, if the phase matching condition is well satisfied, this nonlinear frequency mixing will act continuously along the space. This results in the optical parametric amplification.

The condition for energy conservation is given by Equation 1.9 and the condition for momentum conservation is

$$k_p = k_s + k_i. \tag{1.10}$$

If the three wave vectors are all in the same direction, this becomes,

$$n_p \omega_p = n_s \omega_s + n_i \omega_i. \tag{1.11}$$

The spatial variation of the optical fields in the nonlinear medium is given by the equations,

$$\frac{\partial E_1(z)}{\partial z} = \frac{i\omega_1}{2cn_1}\chi^{(2)}E_3(z)E_2^*(z)e^{-i\Delta kz} \qquad (1.12a)$$

$$\frac{\partial E_2(z)}{\partial z} = \frac{i\omega_2}{2cn_2}\chi^{(2)}E_3(z)E_1^*(z)e^{-i\Delta kz} \qquad (1.12b)$$

$$\frac{\partial E_3(z)}{\partial z} = \frac{i\omega_3}{2cn_3}\chi^{(2)}E_1(z)E_2(z)e^{+i\Delta kz} \qquad (1.12c)$$

where $\omega_i/c = k_i/n_i$ and $\omega_3 = \omega_1 + \omega_2$. In OPA, $\omega_3 = \omega(pump)$ and $\omega_1 = \omega(signal)$ and $\omega_2 = \omega(idler)$.
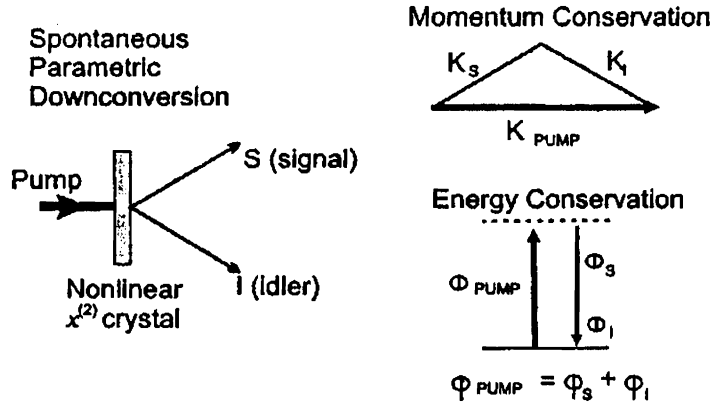
Figure 1.3: Wave vector diagram for SPDC

5. **Spontaneous Parametric Down Conversion (SPDC):** SPDC is an important process in quantum optics. A nonlinear crystal splits incoming photons into pairs of photons of lower energy whose combined energy and momentum is equal to the energy and momentum of the original photon. "Parametric" refers to the fact that the state of the crystal is left unchanged in the process, which is why energy and momentum are conserved (this is related to phase matching in nonlinear optics). The process is spontaneous in the same sense as spontaneous emission, it is initiated by random vacuum fluctuations. Consequently, the photon pairs are created at random times. However, if one of the pair (the "signal") is detected at any time then we know its partner (the "idler") is present. This then allows for the creation of optical fields containing a single photon. As of now, this is the predominant mechanism for experimentalists to create single photons (also known as Fock states).
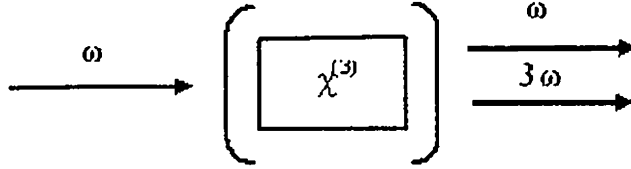
Figure 1.4: Geometry of third harmonic generation

Consequences of Third Order Polarization

Some of the important consequences of third order polarization are given below.

1. **Third Harmonic Generation (THG):** THG is the generation of light with a tripled frequency or one-third the wavelength of the incident radiation. Consider the third order contribution to nonlinear polarization,

$$\tilde{P}^{(3)}(t) = \chi^{(3)} \tilde{E}^3(t) \qquad (1.13)$$

   For electric field of the form

$$\tilde{E}(t) = \mathcal{E}cos(\omega t) \qquad (1.14)$$

   $\tilde{P}^{(3)}(t)$ will contain a term with frequency 3ω which is due to third harmonic generation. This is illustrated in Figure 1.4. When we consider the third order polarization, there is one component in it at the frequency of the incident field; this term leads to a nonlinear contribution to the refractive index experienced by a wave at frequency ω. The refractive index in the presence of this type of nonlinearity depends on the intensity of the laser light and leads to what is known as 'intensity dependent refractive index', (IDRI).

2. **Intensity Dependent Refractive Index (IDRI):** IDRI is defined as the change of the index of refraction in a material, due to the presence of intense optical waves. Third order polarization causes a modification in refractive index in such cases and is defined as

$$n = n_0 + n_2 I \qquad (1.15)$$

where n_0 is the linear refractive index and

$$n_2 = \frac{12\pi^2}{n_0^2 c} \chi^{(3)} \tag{1.16}$$

is an optical constant that characterizes strength of the nonlinearity. $I = (\frac{n_0 c}{8\pi} \mathcal{E}^2)$ being the time averaged intensity of the incident wave. Because the intensity has unit W/cm^2, the unit used for n_2 is cm^2/W. There are a variety of mechanisms that can cause the change in the index of refraction, and it has numerous applications. Self-focussing (defocussing) and optical bistability are two important consequences of the IDRI.

3. **Self Focussing**: One consequence of intensity dependent refractive index is self focussing. This can happen when a light beam of non uniform transverse intensity distribution, propagates through a material for which n_2 is positive. Under these conditions, the material effectively acts as a positive lens and causes the rays to curve towards each other, resulting in self-focussing. This is of great practical importance because, the intensity at the focal spot of the self-focussed beam is usually sufficiently large to lead to optical damage of the material. If the intensity of a light beam varies across its diameter, as is the case of Gaussian beams, then the refractive index of the material through which the beam propagates varies accordingly. Let us consider the case of a Gaussian beam. In the center of the beam the intensity is higher than at the edges. If $n_2 > 0$, the optical path length is larger at the center than at the edges, as in a converging lens. The beam is then focused as it propagates through the medium. If $n_2 < 0$, then the beam path is larger at the edge, and the beam will defocus [4]. In the case of self-focussing, if the nonlinear medium is of small path length, the focussing will occur outside the medium, and hence it cannot damage the material. But if the nonlinear medium is long enough, the focussing occurs inside the material and damage may occur for input intensities that are sufficiently high. Another interesting phenomenon that can take place inside a long nonlinear medium is the self-trapping of light. This takes place when the tendency of the beam to self-focus is compensated by its tendency to spread due to diffraction. Then, the beam has a constant diameter over a relatively large distance inside the material.

4. **Optical bistability**: Optical bistability means that for an input laser intensity, there are two possibilities of the output signal, exactly as with magnetic hysteresis[6]. In this case, the transmittance of an optical device,

may change from a low value to a high value for a sufficiently high intensity and remains at this value until the intensity is reduced by appropriate amount. Such a device can be realized with a Fabry-Perot interferometer containing a nonlinear medium (nonlinear Fabri-Perot interferometer). As in common bistable systems, here also, two output intensities are possible at a given input intensity. The device can be used as an optical memory element or as a switch in optical communication and in optical computing. If the input intensity is a given value I_b (with $I_l < I_b < I_h$), where I_l and I_h are the lower and upper limits, there are two possible output intensities. This situation corresponds to storing binary information. If a pulse of light is sent through the device, the system can make a transition to the higher state. If the input light is blocked momentarily, the system makes a transition to the lower state.

5. **Optical Kerr Effect:** Consider an isotropic liquid comprising asymmetric molecules placed in an electric filed. Its molecules tend to align themselves parallel to the direction of the field. Because the molecules are not symmetrical, this alignment causes the liquid to become anisotropic and birefringent. That is, a light wave which enters the liquid, splits into two waves traveling at different velocities. Due to this the material offers different refractive indices for different polarized light. This electric field induced birefringence in isotropic liquid is called the Kerr effect. If a constant field is applied, the liquid behaves as a birefringent crystal with indices n_o and n_e. The optic axis is parallel to the direction of the field. The birefringence is proportional to the square of the applied voltage. In other words, the change in refractive index is proportional to the square of the electric intensity of the external field.

6. **Kerr-Lens Mode locking (KLM):** It has been known for a long time that intense laser beams are subject to self-focussing when they propagate through optical media that have a nonlinear index of refraction. This Kerr self-focussing effect leads to slight changes in the spatial intensity profile of the resonator mode in laser oscillators. As a consequence, by introducing an intra cavity aperture, a power-dependent loss can be created. When carefully optimized, this passive amplitude-modulation mechanism favors a high intra-cavity power, i.e., mode-locked operation over free-running laser oscillation. Owing to the quasi-instantaneous response of nonresonant Kerr nonlinearities, the amplitude modulation induced by self-focussing is able to simulate ultra-fast saturable-absorber

action and support pulse formation down to the femtosecond regime in solid-state lasers that have long gain-relaxation times. The technique has been termed self mode-locking or Kerr lens mode locking(KLM)[7].

7. **Self-phase Modulation (SPM)**: SPM is another important nonlinear optical effect resulting out of light-matter interaction. An ultrashort pulse of light, when traveling in a medium, will induce a varying refractive index of the medium due to the optical Kerr Effect. This variation in refractive index will produce a phase shift in the pulse, leading to a change of the frequency spectrum of the pulse. Self-phase modulation is an important effect in optical systems that use short, intense pulses of light, such as lasers and optical fibre communication.

For an ultrashort pulse with a Gaussian shape and constant phase, the intensity at time t is given by,

$$I(t) = I_0 exp(-\frac{t^2}{\tau^2}) \qquad (1.17)$$

where I_0 is the peak intensity, and τ is half the pulse duration. If the pulse is traveling in a medium, the optical Kerr effect produces a refractive index change with intensity as given earlier (Equation 1.15). As the pulse propagates, the intensity at any one point in the medium rises and then falls as the pulse goes past. This will produce a time-varying refractive index:

$$\frac{dn(I)}{dt} = n_2 \frac{dI}{dt} = n_2 I_0 \frac{-2t}{\tau^2} exp(-\frac{t^2}{\tau^2}) \qquad (1.18)$$

This variation in refractive index produces a shift in the instantaneous phase of the pulse:

$$\phi(t) = \omega_0(t) - \frac{2\pi}{\lambda_0} n(I) L \qquad (1.19)$$

where ω_0 and λ_0 are the carrier frequency and (vacuum) wavelength of the pulse, and L is the distance through which the pulse has propagated. The phase shift results in a frequency shift of the pulse. The instantaneous frequency $\omega(t)$ is given by:

$$\omega(t) = \frac{d\phi(t)}{dt} = \omega_0 - \frac{2\pi L}{\lambda_0} \frac{dn(I)}{dt} \qquad (1.20)$$

and from the equation for dn/dt above, we get

$$\omega(t) = \omega_0 + \frac{4\pi L n_2 I_0}{\lambda_0 \tau^2} \ t \ exp(-\frac{t^2}{\tau^2}) \qquad (1.21)$$

Plot of $\omega(t)$ against t, shows the frequency shift of each part of the pulse. The leading edge shifts to lower frequencies ('redder' wavelengths), trailing edge to higher frequencies ('bluer') and the very peak of the pulse is not shifted. For the center portion of the pulse (between $t = \tau/2$), there is an approximately linear frequency shift (chirp) given by:

$$\omega(t) = \omega_0 + \alpha \ t \qquad (1.22)$$

where α is:

$$\alpha = \frac{d\omega}{dt}\bigg|_0 = \frac{4\pi L n_2 I_0}{\lambda_0 \tau^2} \qquad (1.23)$$

It is clear that the extra frequencies generated through SPM broaden the frequency spectrum of the pulse symmetrically. In the time domain, the pulse is not changed, however in any real medium the effects of dispersion will simultaneously act on the pulse. In regions of normal dispersion, the 'redder' portions of the pulse have a higher velocity than the 'bluer' portions, and thus the front of the pulse moves faster than the back, broadening the pulse in time. In regions of anomalous dispersion, the opposite is true, and the pulse is compressed temporally and becomes shorter. This effect can be exploited to produce ultrashort pulse compression.

8. **Cross-phase Modulation (XPM):** XPM is a nonlinear effect where the intensity of one beam influences the phase change of another beam. Cross-phase modulation is the change of the optical phase of a light beam caused by the interaction with another beam in a nonlinear medium, specifically a Kerr medium. This can be described by a change of the refractive index,

$$\Delta n(\lambda_2) = 2 n_2 I(\lambda_1) \qquad (1.24)$$

with the nonlinear coefficient n_2. Compared to the corresponding equation for SPM, there is an additional factor of 2. This factor 2 is valid for beams with the same polarization (for cross-polarized beams, it must be replaced by 2/3). XPM can be relevant under different circumstances. For example, it leads to an interaction of laser pulses in a medium, which

allows to measure the intensity of one pulse by monitoring a phase change of the other one (without absorbing any photons of the first beam). This is the basis of a scheme for quantum *nondemolition* (QND) measurements. The effect can also be used to synchronize two laser cavities using the same gain medium, in which the pulses overlap and experience XPM. In optical fiber communications, XPM in fibers can lead to problems with channel crosstalk. Sometimes it is said that cross-phase modulation can be used for channel translation (wavelength conversion), but in this context one typically refers to a kind of XPM which is not based on the Kerr effect, but rather on changes of the refractive index via the carrier density in a semiconductor optical amplifier.

9. **Nonlinear Light Scattering:**

   (a) Stimulated Brillouin Scattering- Brillouin Scattering occurs when light in a medium (such as water or a crystal) interacts with density variations and changes its path. The density variations may be due to acoustic modes, such as phonons, or temperature gradients. As described in classical physics, when the medium is compressed, the index of refraction changes and the light path bends.

   From a quantum point of view, Brillouin Scattering is considered to consist of interaction of light photons with acoustic or vibrational quanta (phonons). The scattered light has a wavelength that is changed slightly by a variable quantity known as the Brillouin shift; it is sometimes referred to as a 'red shift' since it may increase the wavelength of light in a spectrum. For intense beams (e.g. laser light) traveling in a medium, the variations in the electric field of the beam itself may produce acoustic vibrations in the medium via electrostriction. The beam may undergo Brillouin inelastic scattering from these vibrations (acoustic waves), usually in opposite direction to the incoming beam, a phenomenon known as Stimulated Brillouin Scattering (SBS). For liquids and gases, typical frequency shifts are of the order of 110 GHz (wavelength shifts of 110 pm for visible light).

   Stimulated Brillouin Scattering is one effect by which *optical phase conjugation* can take place[5]. In this process a very small part of photon energy transfers to the phonon, consequently a tiny frequency shift of the light wave is induced. When an intense laser beam or pulse propagates in the medium, the coherent acoustic wave will be
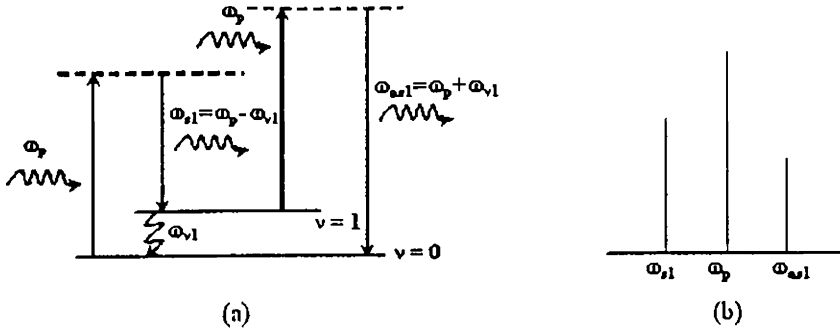
Figure 1.5: Raman scattering showing Stokes and Anti-Stokes lines

enhanced by the electrostriction and the scattered light wave is amplified coherently. As a result, the scattering process becomes SBS. This was predicted and calculated by Leon Brillouin in 1922, and was later observed experimentally in liquids. The wave number of frequency shift is only about 0.1 cm^{-1}.

(b) Stimulated Raman Scattering (SRS)- When a strong pump with frequency ω_p injects into some medium, such as hydrogen gas, liquid CS_2, or solid silica, a scattering radiation ω_{Raman} with considerable frequency red-shift is generated. The Raman scattering is the inelastic scattering of light waves by the vibration energy levels in the medium. In this process a part of photon energy, which equals the vibration level energy $\hbar\omega_{vibration}$, is transferred to the optic phonon. In this case a light wave with a shift of about 100 to 1000 cm^{-1} is produced and is called stimulated Raman scattering. Figure 1.5 shows the spontaneous Raman scattering spectrum. In Figure 1.5a, $\nu = 1$ is the real vibrational level and the left vertical line in 1.5 b is the red-shifted Stokes line $\omega_s = \omega_{s1}$ corresponding to $\nu = 1$ level scattering. The anti-Stokes process in Figure 1.5(a) is really a four-wave mixing, and the right vertical line in 1.5(b) is the blue-shifted anti-Stokes line ω_{as} for which no real level exists. Qualitatively, the first Stokes (stimulated) and anti-Stokes (FWM) are

$$\omega_{Stokes} = \omega_{pump} - \omega_{vibration} \tag{1.25}$$

$$\omega_{anti-Stokes} = 2\omega_{pump} - \omega_{Stokes} = \omega_{pump} + \omega_{vibration} \tag{1.26}$$
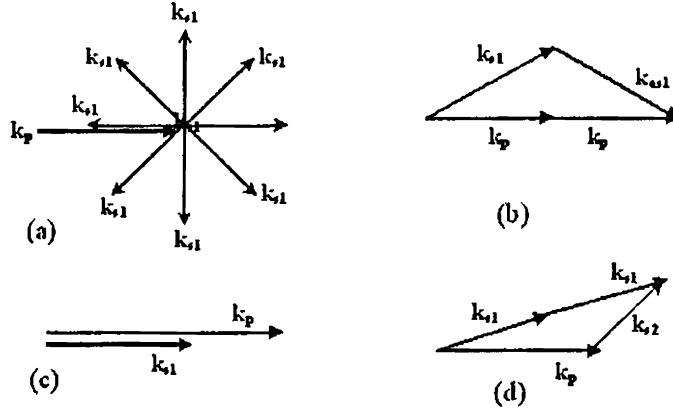
Figure 1.6: Wave vector diagram showing FWM process in SRS

If the injected laser beam or pulse are very intense, the scattered light wave will be amplified with significant gain (G_{Raman}) and enhanced coherently. As a result, the scattered process becomes stimulated raman scattering (SRS). At the same time, FWM reveals comparatively efficient and a series of spectrum lines corresponding to ω_{s2}, ω_{as2}, ω_{s3}, ... are obtained. These are all generated by FWM, and the wave-vector diagrams are shown in Figure 1.6.

10. **Optical Phase Conjugation:** It is possible, using nonlinear optical processes, to exactly reverse the propagation direction and phase variation of a beam of light. The reversed beam is called a conjugate beam, and thus the technique is known as optical phase conjugation (also called time reversal, wavefront reversal and retroreflection).

The most common way of producing optical phase conjugation is to use a four-wave mixing technique, though it is also possible to use processes such as SBS. A device producing the phase conjugation effect is known as a phase conjugate mirror (PCM).

For the four-wave mixing technique, we can describe four beams (j = 1,2,3,4) with electric fields as given in Equation 1.27.

$$\tilde{E}_j(\mathbf{x}, t) = \frac{1}{2} E_j(\mathbf{x}) e^{i\omega_j t - \mathbf{k} \cdot \mathbf{x}} + c.c \qquad (1.27)$$

where E_j are the electric field amplitudes. $\tilde{E}_1$ and $\tilde{E}_2$ are known as the

two pump waves, with $\tilde{E}_3$ the signal wave, and $\tilde{E}_4$ the generated conjugate wave. If the pump waves and the signal wave are superimposed in a medium with a non-zero $\chi^{(3)}$, this produces a nonlinear polarization field,

$$P_{NL} = \chi^{(3)}(\tilde{E}_3 + \tilde{E}_2 + \tilde{E}_3)^3 \qquad (1.28)$$

resulting in generation of waves with frequencies given by $\omega = \omega_1\omega_2\omega_3$ in addition to third harmonic generation waves with $\omega = 3\omega_1, 3\omega_2, 3\omega_3$.

As above, the phase-matching condition determines which of these waves is the dominant. By choosing conditions such that $\omega = \omega_1 + \omega_2 - \omega_3$ and $k = k_1 + k_2 - k_3$, this gives a polarization field,

$$P_\omega = \frac{1}{2}\chi^{(3)}\epsilon_0 E_1 E_2 E_3^* e^{i(\omega t - \mathbf{k}.\mathbf{x})} + c.c. \qquad (1.29)$$

This is the generating field for the phase conjugate beam, $\tilde{E}_4$. Its direction is given by $k_4 = k_1 + k_2 - k_3$, and so if the two pump beams are counter-propagating ($k_1 = -k_2$), then the conjugate and signal beams propagate in opposite directions ($k_4 = -k_3$). This results in the retro reflection. Further, it can be shown for a medium with refractive index n and a beam interaction length l, the electric field amplitude of the conjugate beam is approximated by

$$\tilde{E}_4 = \frac{i\omega l}{2nc}\chi^{(3)} E_1 E_2 E_3^* \qquad (1.30)$$

(where c is the speed of light). If the pump beams E_1 and E_2 are plane (counter-propagating) waves, then $\tilde{E}_4(\mathbf{x}) \propto \tilde{E}_3^*(\mathbf{x})$ ie, the generated beam amplitude is the complex conjugate of the signal beam amplitude. Since the imaginary part of the amplitude contains the phase of the beam, this results in the reversal of phase.

Note that the constant of proportionality between the signal and conjugate beams can be greater than 1. This is effectively a mirror with a reflection coefficient greater than 100%, producing an amplified reflection. The power for this comes from the two pump beams, which are depleted by the process. The frequency of the conjugate wave can be different from that of the signal wave. If the pump waves are of frequency $\omega_1 = \omega_2 = \omega$, and the signal wave is higher in frequency such that $\omega_3 = \omega + \Delta\omega$, then the conjugate wave is of frequency $\omega_4 = \omega - \Delta\omega$. This is known as frequency flipping.

11. **Two-photon Absorption (TPA):** The process of two-photon absorption is similar to ordinary single photon absorption. In this process an electron absorbs two photons at approximately the same time (or within less than a nanosecond) and achieves an excited state that corresponds to the sum of the energy of the incident photons. There need not be an intermediate state for the atom to reach before arriving at the final excited state (as if it were moving up two stair steps by stepping one at a time). Instead, the atom is excited to a "virtual state" which need not correspond to any electronic or vibrational energy eigenstate.

Selection rules for these transitions logically follow from the selection rules for one photon transitions. With one photon absorption, an electron may undergo transition only if the change in angular momentum (change in L) is +1 or -1. Since photons have angular momentum of +1 or -1, an electronic state absorbing two photons simultaneously may change angular momentum by +2, 0. Two L =+1 photons cause a change of +2; a photon of L = +1 and L = -1 cause a change of 0.

Through two-photon absorption we can populate high energy levels that are otherwise unreachable by single photon transitions from the ground state. Once electrons have absorbed two photons and are at a high energy level, it takes no more than the absorption of another photon to release the electron and ionize the atom. If there is an intense, monochromatic photon source (such as a high energy laser) used to excite these atoms through two-photon absorption, it is assured that there are ample photons to continue the excitation process and ionize the electron before it radiates back to a lower energy level.

1.1.3   Nonlinear Optical Materials

Nonlinear optical materials are materials in which the intensity of light input, including its frequency, is not related to the intensity of light output by a simple proportionality constant. Because of this nonlinear behavior, an intense light beam propagating through a nonlinear optical material will produce new effects that cannot be seen with weak light beams.

The properties of materials that make them suitable for nonlinear optical applications are not that handled by the traditional material scientist[8]. Familiar properties like elasticity, hardness, etc. of a material may play an indirect role in terms of establishing the life time of a suitable optical material. However, the essence of a good nonlinear optical material lies in the magnitude of

the so-called "nonlinear optical response function" or "nonlinear dielectric sus-
ceptibility," which provides a measure of how the material reacts to modify an
incoming light beam. The latter quality can be partitioned somewhat arbitrar-
ily into a resonant and nonresonant optical response. Resonant optical response
can involve either light absorption or amplification due to coupling to the dipole
oscillators making up the material. A nonresonant optical response involves es-
sentially non modification to the amplitude of the impinging light signal but,
rather, induces an intensity dependent phase change. Hence the refractive in-
dex of the material gets modified. In reality both absorption/amplification and
refraction changes occur simultaneously but one or the other can be enhanced
depending on the requirement.

There is little doubt that nonlinear optics, whether realized in an all-optical
or a hybrid electro-optical mode, will have an increasingly important impact on
modern technology. The search for suitable materials to satisfy future technol-
ogy needs is an ongoing challenge.

1. Inorganic nonlinear Optical Materials

    In the early days of nonlinear optics, studies mainly concentrated on in-
    organic materials such as quartz; KDP; and semiconductors such as cad-
    mium sulfide, selenium, and tellurium. These materials were first studied
    because they were found to give population inversion necessary for laser
    research. Later, inorganic materials such as KTP and BBO became promi-
    nent due to high efficiency and widespread use for harmonic generation or
    other device applications.

2. Organic nonlinear Optical Materials

    Organic compounds with delocalized conjugated π-electrons have gained
    much attention because of their large non-linear optical properties and
    quick response. Polydiacetylene and one-dimensional metal complexes
    exhibit excellent non-linear optical properties. Some examples are por-
    phyrins and phthalocyanines. This will be discussed in detail in subse-
    quent chapters.

3. Semiconductors

    Semiconductor nanoparticle suspensions are used as NLO media and these
    are usually prepared by laser ablation technique. The local field enhance-
    ment of nanoparticles in colloidal suspensions and considerable nonlinear
    optical susceptibilities of chalcogenide structures make these semiconduc-
    tor nanoparticles interesting materials. Aqueous colloidal suspensions of

As_2S_3 and CdS nanoparticles are examples. The semiconductor chalcogenide structures show promise for applications in information processing systems due to such properties as high nonlinearities, high transparency in the infrared range, and easy processing. Among other potential applications of amorphous chalcogenides are wave conjugation, optical image processing, optical switching, integral optical devices, and holographic optical elements. Chalcogenide films such as As_2S_3, $As_{20}S_{80}$, $2As_2S_3/As_2Se_3$, and $3As_2S_3/As_2Se_3$ can be prepared by the evaporation of chalcogenide glass components (for example, As_2S_3, $As_{20}S_{80}$, As_2Se_3) onto the surfaces of BK7 glass substrates.

1.2   Measurement Techniques for NLO Properties

Some of the commonly used measurement techniques for nonlinear optical properties are discussed below.

1.2.1   Degenerate Four Wave Mixing (DFWM)

Frequency mixing represents one of the most general but nonetheless important phenomena in nonlinear optics. In this process, two or more waves interact in a nonlinear medium to produce an output at various sum or difference frequencies. Four-wave mixing can take place in any material. It refers to the interaction of four waves via the third order nonlinear polarization. When all waves have the same frequency, the process is called degenerate, although their wave vectors are different. This process results from the nonlinear index of refraction. Degenerate four-wave mixing (DFWM) can yield phase conjugation and is useful, for example, for correcting aberrations by using a phase conjugate mirror (PCM).

As a technique, DFWM is one of those most heavily employed in characterizing third order nonlinear materials. In all the configurations for DFWM, the working principle is that two beams interfere to form some type of grating (e.g. intensity grating) and a third beam scatters off this grating, generating the fourth beam named the conjugate or signal beam. The most frequently used DFWM configuration is the phase-conjugate geometry as given in Figure 1.7. Two common DFWM experimental geometries are given in this Figure. Three beams with wavevectors k_1, k_2, and k_3 interact in a sample to generate a fourth beam with wavevector k_4. The interacting beams and the sample are drawn in the x-y plane in the first line, and the coordinates of the beam wavevectors
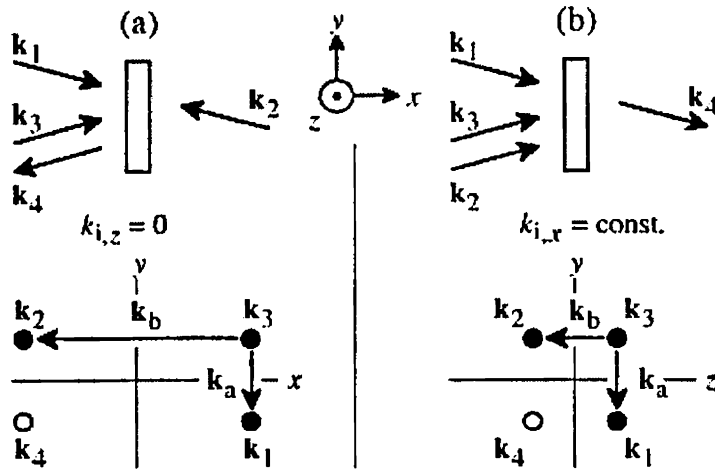
Figure 1.7: Two most commonly used DFWM experimental configurations.

are plotted in the second line. For clarity, the x and y axes are not in scale. (a) Beams 1 and 2, and beams 4 (signal) and 3, are counterpropagating . (b) All input input beams travel towards the positive x direction. The beams are distinguished by a slightly different z direction.

1.2.2 Nearly Degenerate Four-Wave Mixing

Nearly degenerate four-wave mixing (NDFWM)can be demonstrated by simultaneously injecting two waves of slightly different frequencies in the same direction. A new frequency wave at an expected frequency for NDFWM is observed with the same order of output as that of the injected light. The output power ratio of the three beams is strongly dependent on the sign of the frequency detuning. Theoretical analysis can be done by considering the carrier rate equation coupled with nonlinear Maxwell's equations. The procedure will ultimately yield the value of n_2.

1.2.3 Ellipse Rotation

These types of measurements depend on an estimate of the beam profile, for a focused beam. The experimental set up can be calibrated by measuring the ellipse rotation for CS_2 whose $\alpha + 2\beta$ values can be obtained from other techniques. Strong enough focussing of the beam into the sample will ensure that the

entire ellipse rotation takes place within the sample volume[9]. The laser source
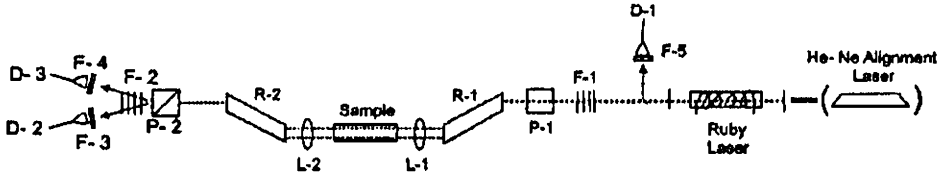
Figure 1.8: Experimental set up for ellipse rotation measurements: courtesy Adelbert[9]

in the given example is a ruby laser, giving 20 ns pulses. The Rochon prism P1 determines the plane of polarization prior to introduction into the Fresnel Rhomb R1 which produces an elliptically polarized input. R2 is oriented parallel to R1 so as to produce a linearly polarized output in the absence of ellipse rotation. This is followed by Wollaston prism P2, which directs the maximum "transmitted" signal into D3 and the minimum "nulled" signal into D2, when there is no ellipse rotation. With suitable light intensity, the polarization ellipse will rotate and this will be revealed as a relative increase in the "nulled" signal. By performing some detailed calculations one can obtain the value of nonlinear index of refraction n_2.

1.2.4   Beam Distortion Measurements

This is a pump probe technique which allows one to investigate non-degenerate components of the nonlinearity[10]. Figure 1.9 shows the principle of the method. A pump beam is used to introduce a 'phase object' in the sample. In the simplest case the object may be just the circular spot created by suitably focussing the pump beam. A probe beam crosses the sample and acquires the phase distortion via XPM. Free propagation of this beam converts this phase distortion into amplitude variations in the far field. Since the pump beam is chopped at some frequency, relatively small amplitude modulation can be readily detected using a lock-in amplifier. Modulation of the local intensity of the probe beam will appear when either a phase distortion (due to the real part of $\chi^{(3)}$) or an amplitude distortion (due to the imaginary part of $\chi^{(3)}$) occurs. However, the presence of a phase distortion can be detected only in the far field while the amplitude distortion is detectable at the sample plane itself. Therefore, choosing the position of the imaging lens to image either the sample plane or the far field region onto the detector aperture, one can distinguish between the imaginary and real parts of the nonlinearity.
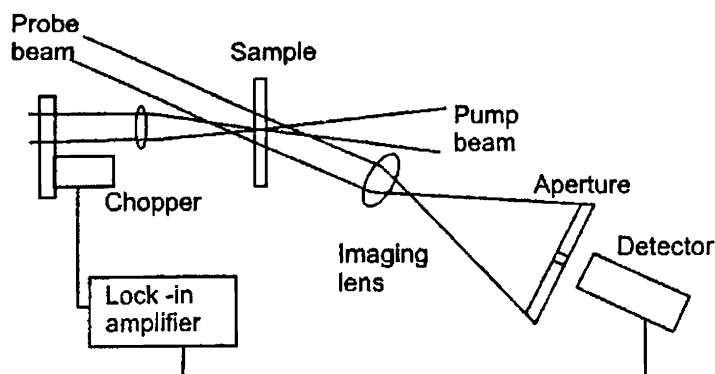
Figure 1.9: The principle of pump-probe phase distortion measurements of third-order nonlinearity. The pump and probe beam may be derived from the same short-pulse source

1.2.5   Photothermal and Photoacoustic Techniques

These techniques are not widely used for the determination of nonlinear optical parameters. However some of them are very interesting [11, 12].

1. Photothermal method

   Optical nonlinearity originating in photothermal effects causes SPM in the medium, and this can be characterized by use of heat-conduction analysis [11]. The refractive-index distributions that are due to the photothermal optical nonlinearity will be determined by two different methods. One method is analytical solution of Kirchhoffs diffraction integral including the higher-order nonlinear phase distribution. Another method is by analytical solution of a heat-conducting equation. The method yields the values of nonlinear refractive index.

2. Photoacoustic method

   One of the method to study nonlinear optical response of a material is the coherent photoacoustic technique for measuring excited-state absorption. The experimental set up is as shown in Figure 1.10. It involves a picosecond pulse sequence with four pulses. The first pulse populates the excited state. Then, a pair of time coincident pulses cross in the sample, making an optical interference pattern and generating an acoustic diffraction grating. The amplitude of the acoustic grating is proportional to the excited-state absorption cross section. The amplitude is measured by the Bragg diffraction of the fourth pulse from the acoustic grating. This method can be readily applied to liquids, glasses or crystals. The results

of ESA measurements from this experiments, are used in addressing the
mechanism for acoustic diffraction of a probe beam nearly resonant with a
strong and narrow ground-state transition, e.g., pentacene in p-terphenyl.
It has been demonstrated by researchers that there is a density wave in-
duced spectral shift contribution to the acoustic grating which results in
greatly increased diffraction efficiency near resonance. For more details
and description of the experimental set up, one can refer [12].

1.2.6   Z-scan

Z-scan is a technique based on the principles of spatial beam distortion, but
offers simplicity as well as very high sensitivity. For many practical cases, non-
linear refraction and its sign can be obtained from a simple linear relationship
between the observed transmittance changes and the induced phase distortion
without the need for performing detailed calculations. This technique has been
employed in investigating the NLO properties of various materials reported in
this thesis. Therefore a detailed description is presented below as a separate
section.

1.3   Z-scan: Experimental Technique and The-
ory

This is a very commonly used experimental configuration to measure the non-
linear absorption and nonlinear refraction of thin sample medium. This was
proposed as a technique with complete theory by Sheik Bahea et al in 1990
[13, 14]. They used an extension to the Gaussian decomposition method sug-
gested by Weaire et al [15].

1.3.1   Experimental Technique

A single Gaussian laser beam in a tight focus geometry is used in this method.
And the the transmittance of the nonlinear medium through a finite aperture
in the far field as a function of the sample position z, is measured with respect
to the focal plane. (see diagram of experimental set up in chapter 2). This is
called the z-scan trace.

   To understand how this z-scan trace is related to the nonlinear refraction
of the sample, consider the following cases. Assume that the material has a
negative nonlinear refractive index and a thickness smaller than the diffraction
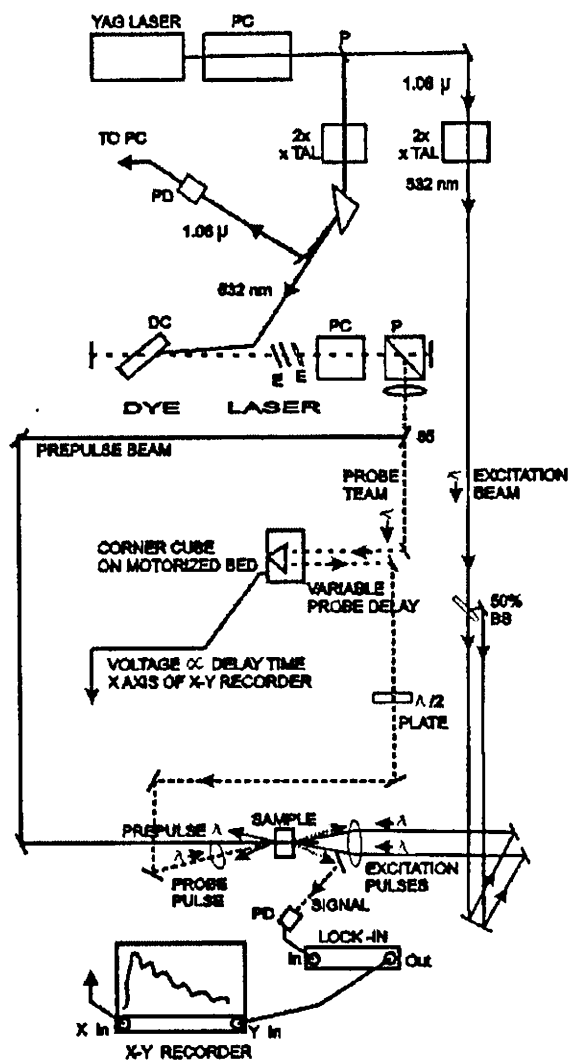
Figure 1.10: Experimental set up for photoacoustic determination of excited state absorption

length of the focused beam. This can be regarded as a thin lens of variable focal length. Starting the scan from a distance far away from the focus (negative z), the beam irradiance is low and negligible nonlinear refraction occurs; hence, the transmittance remains relatively constant. As the sample is brought closer to focus, the beam irradiance increases, leading to self-lensing in the sample. A negative self-lensing prior to focus will tend to collimate the beam, causing a beam narrowing at the aperture which results in an increase in the measured transmittance. As the scan in z continues and the sample passes the focal plane to the right (positive z), the same self-defocussing increases the beam divergence, leading to beam broadening at the aperture, and thus a decrease in transmittance. Therefore the trace will cross the 'zero' point in this process. This is analogous to placing a thin lens at or near the focus, resulting in a minimal change of the far-field pattern of the beam.

Therefore, a negative nonlinear refraction results in peak-valley structure. Positive nonlinear refraction, following the same analogy, gives rise to an opposite valley-peak configuration. It is an extremely useful feature of the z-scan method that the sign of the nonlinear index is immediately obvious from the data, and the magnitude can also be easily estimated using a simple analysis for a thin medium. By suitable modification of the experimental set up, theoretical formalism and detection schemes, it is possible to extract details of nonlinear absorption, nonlinear refraction, excited state absorption etc. from the z-scan signal. Some of these methods are illustrated in the next two chapters, where it is suitably described with the experimental results from metal phthalocyanines. In the next section, the theory to find nonlinear absorption coefficient (β) and nonlinear refraction coefficient (γ) has been briefly explained.

1.3.2   Theory

The nonlinear optical coefficients β and γ are extracted from the z-scan data, as follows. In the case of cubic nonlinearity the index of refraction is given by[28]

$$n = n_0 + \frac{n_2}{2}|E|^2 = n_0 + \gamma I \qquad (1.31)$$

where n_0 is the linear refractive index, I is the intensity of the incident light, expressed in W/m^2, E is the peak electric field (cgs) and γ is the nonlinear refractive index in SI units, expressed in m^2/W and n_2 is the same in CGS esu units. In Equation 1.31 assuming a Gaussian TEM_{00} beam we can write the normalized transmittance when no aperture is kept before the detector, (OA or

linear transmittance, S=1) as

$$T(z, S = 1) = \frac{1}{\sqrt{\pi} q_0(z,0)} \int_{-\infty}^{\infty} ln[1 + q_0(z,0)e^{\tau^2}]dt \qquad (1.32)$$

where $q_0(z,t) = \frac{\beta I_0(t) L_{eff}}{1 + z^2/z_0}$ and $L_{eff} = \frac{(1 - e^{-\alpha L})}{\alpha}$ is the effective sample path length, L the sample length and α is the linear absorption. Thus once an open aperture z-scan is performed, the nonlinear absorption coefficient β can be determined. γ can then be deduced from the z-scan signal, if one keeps an aperture in front of the detector, which is often referred to as closed aperture,(CA) z-scan for which S$\neq$ 1. This is done as follows. For a sample with small nonlinear absorption, the equation for CA transmittance is expressed conveniently as

$$T(z) = 1 - \Delta\phi_0 \frac{4x}{(1 + x^2)(9 + x^2)} \qquad (1.33)$$

where $\Delta\phi_0$ is the on axis nonlinear phase shift at focus, x is the dimensionless sample position $\frac{z}{z_0}$. The nonlinear phase shift is given by $\Delta\phi_0 = k\gamma I_0 L_{eff}$ where $k = \frac{2\pi}{\lambda}$ This equation is used to calculate the value of γ, $\Delta\phi$ being obtained from the CA z-scan fit.

1.3.3 Advantages & Disadvantages of Z-scan over other Techniques

Z-scan is a technique that is particularly useful when the nonlinear refraction is accompanied by nonlinear absorption[17]. One advantage of the technique is that the z-scan signals are linearly related to the nonlinear phase shift, and therefore z-scan results do not suffer from the ambiguity of those methods that measure the modulus of $\chi^{(3)}$. However, the use of z-scan for thin films of polymers is quite difficult because of the need to use relatively high light intensities and large refractive-index changes to obtain a measurable signal on a short propagation path, which often leads to the appearance of permanent refractive-index changes that distort the measurement results. Z-scan is, however, a convenient technique for solution measurements. However, there are certain aspects one needs to take into account while setting up and acquiring the transmittance data from the z-scan experiment. Usually, it is difficult to get any information about the time scale of the refractive-index changes that are being detected. Thus one may be misled by phenomena that occur on a longer time scale than the laser pulses but provide cumulative effects from pulse to pulse. For this careful modification of the experiment and detection schemes should be made.

A few of such techniques are mentioned in the next section.

1.3.4   Possible Variants of the Z-scan Experiment

Depending on the nonlinear mechanisms that we want to study and also the type of laser (repetition rate, pulse width etc.)used for excitation, one should modify the detection schemes and also the theory used to interpret the data. There can be slow and fast components to nonlinearity, cumulative effects etc, which needs careful attention while data handling. Several modification to the previously mentioned experimental set up are used by various researchers. A few of them are,

1. Single beam time resolved z-scan

   In the conventional technique, as explained previously, the measurements are usually carried out with fast 'subnanosecond' response Kerr-like media, in a spectral region where the sample is transparent. The laser frequency will usually be far from any resonance of the medium, the nonlinear susceptibility is fairly small, and its measurement demands a high intensity light, only achieved with Q-switched or modelocked lasers. In the resonance region, the nonlinear susceptibility is large and thus, even a low power CW laser would be suitable for its measurement. Moreover, if the optical nonlinearity arises due to the population of a long-lived electronic state or if it has a thermal origin, the medium will present a slow 'millisecond' response. In this situation, the sensitivity of the z-scan technique can be substantially improved by eliminating any parasitic linear effect by means of a time resolved signal detection.

   The experimental setup is shown in Figure 1.11. The light source is CW. In order to keep the same optical alignment an electro-optical modulator (EOM) is used to change the light intensity. The use of this device is important if the same region of the sample has to be probed at different intensities. A spatial filter (SF) assures a good transverse mode quality. After passing through the spatial filter the beam is focused (lens L1) on the chopper blade that mechanically modulates the radiation, such that the on-off transition time is minimized. Lens L2 recollimates the beam while L3 produces the focus at z = 0. The rest of the diagram is as in the ordinary z-scan set up. For a slow response medium, the use of the chopper and the microcomputer allows the monitoring of the transmittance temporal evolution, which can be used to eliminate linear effects. For more details see reference [7].
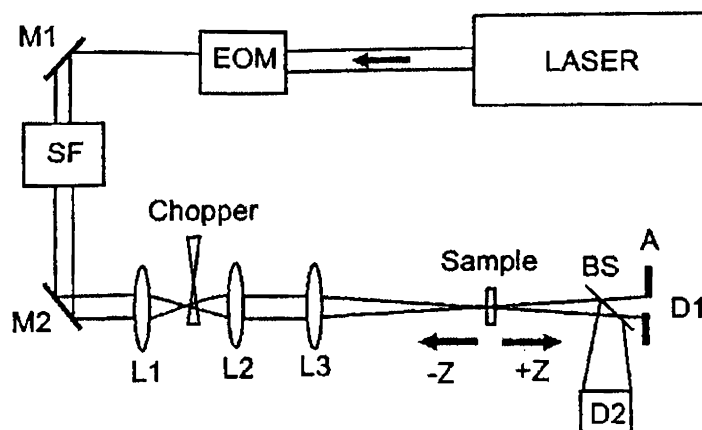
Figure 1.11: Experimental set up for single beam time resolved z-scan.

Immediately after the chopper opens at t=0, there was not enough time for any long-lived excited state to be populated; neither had the sample absorbed enough energy to increase its temperature. Therefore, the transmittance is purely linear at t=0. As the time evolves, the sample heats and/or excited states become populated and nonlinear effects start to manifest themselves. For times much longer than the characteristic relaxation time, the steady state is reached and the final transmittance presents both linear and nonlinear contributions.

2. Reflection z-scan

This technique is suitable for opaque or highly absorbing samples. The incident Gaussian beam propagates along the z axis, with its waist located at z=0 (see Figure 1.12). The distance between the beam waist and the sample surface is z and the aperture plane is placed at the distance d from the beam waist. The terms used in this diagram are common. The application of this method is to measure nonlinear parameters and the surface expansion of highly absorptive materials - even opaque samples. Here also calculation of the far-field pattern of the beam at the aperture plane is by applying the "Gaussian decomposition method." [19]

There are numerous other techniques like eclipsed z -scan, dual beam z-scan etc [20].
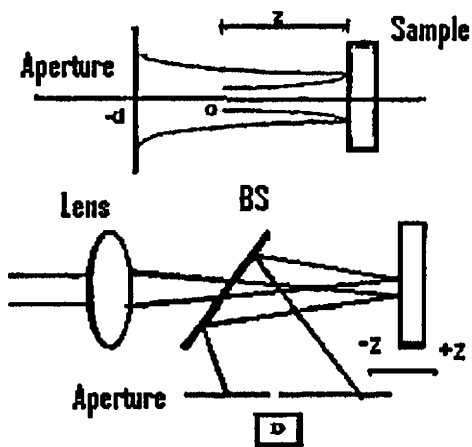
Figure 1.12: Experimental configuration for reflection z-scan.

1.4   Conclusions

There are several experimental techniques for studying the nonlinear optical properties of materials. However, z-scan is one of the simplest method that has been employed by several researchers. In this thesis, the nonlinear optical behavior of certain phthalocyanines are studied using both closed aperture and open aperture z-scan. These are dealt with in detail in the next chapters.

References

[1] Robert W Boyd, *Nonlinear Optics*, Academic Press, San Diego, (1992).

[2] Franken, P.A., Hill, A.E., Peters, C.W., and Weinreich,G., *Phys. Rev. Lett.*, 7, (1961) p.118

[3] B B Laud, *Lasers and Nonlinear Optics/2e*, Wiley Eastern Ltd, India, (1993)

[4] Marlan.O. Scully, M. Suhail Zubairy,*Quantum Optics*, Cambridge University Press, (1997)

[5] Y.Guo, C.K.Kao, E.H.Li and K.S.Chiang *Nonlinear Photonics,* (Springer Verlag, The Chinese University Press., (2002)

[6] E.G Sauter,*Nonlinear Optics,*John Wiley and Sons,Canada, (1996)

[7] T. Brabec, Ch. Spielmann, P. F. Curley, and F Krausz, *Opt. Lett.*, 17,(1992) p.620

[8] Jerome.V.Moloney,(Ed),*Nonlinear optical Materials,*The IMA volumes in Mathermatics and its Applications, vol.101, Springer, UK, (1982)

[9] Adelbert Owyoung et al., *Phy. Rev.B*, 5, (1972) p.628

[10] M.Samoc et al., *Organic Thin Films for Photonic Applications Technical Digest,* 17,Opt.Soc.of America, Washington, D.C. (1993) p.200

[11] H.Ono, Y.Harato., *J.Opt.Soc.Am. B*, 16(12), (1999) p.2195

[12] R.J.Dwayne Miller, Marc Pierre, Todd S.Rose, and M.D. Fayer., *J. Phys. Chem.*, 88 (1984) p.3021

[13] M.Sheik-Bahae, A.A.Said, T.H.Wei, D.J.Hagan and E.W.Van stryland., *IEEE J.Quantum Elect.*, 26(4) (1990) p.760

[14] M. Sheik-Bahae, A. A.Said, and E.W. Van Stryland, *Opt. Lett.*, 14 (1989) p.955

[15] D.Weaire, B.S.Wherrett, D.A.B.Miller, and S.D. Smith, *Opt.Lett.*, 4(10) (1979) p.331

[16] Amnon Yariv, *Quantum Electronics*(3/e), John Wiley & Sons, Inc., (1989)

[17] M.Samoc, A.Samoc, B.L.Davies, *J. Opt. Soc. Am. B*, 15(2) (1998) p.817

[18] L.C.Oliveira and S.C.Zilio., *Appl. Phys. Lett.*, 65(17) (1994) p.2121

[19] D.V.Petrov, A.S.L.Gomes, and Cid B.de Araujo., *Appl. Phys. Lett.*, 65(9) (1994) p.1068

[20] M. Shaobin; Z.Q.Feng, L.W. Hung, *J.Chem.Res.*, 2004(10) (2004) p.714

Chapter 2

Nonlinear Absorption and Nonlinear Refraction in Metal Phthalocyanines

"We can't solve problems by using the same kind of thinking we used when we created them."- Einstein

ABSTRACT

Closed aperture and open aperture z-scan experiments were performed in single metal substituted phthalocyanines of cobalt, nickel, copper and zinc, using the fundamental and second harmonic of the Nd:YAG laser. It has been explained in detail, how the nonlinear refraction and nonlinear absorption coefficients can be calculated from these studies. The nonlinear absorption of these materials at the specified wavelengths is due to a mechanism known as Reverse Saturable Absorption. One of the very important applications of a reverse saturable absorber is in the technique of optical limiting. Details of optical limiting experiments performed in these samples are also described in this chapter.

2.1   Introduction

Third-order nonlinearity is responsible for the variation of refractive and absorptive properties of a medium when an intense laser beam propagates through it. Numerous studies have been carried out on the analysis of these properties, due to the growing interest in the applications of nonlinear optical propagation effects [1]. Z-scan technique is a popular method for measuring optical

nonlinearities using a single laser beam. This includes both nonlinear absorptive and nonlinear refractive measurements. In most cases nonlinear refraction (NLR) is accompanied by nonlinear absorption (NLA). However it is possible in this method to separately evaluate these two nonlinear optical coefficients by performing straightforward measurements [2].

2.2 Porphyrins and Phthalocyanines

Optical second harmonic generation (OSHG) in an organic material was first reported in 1964 (3,4-benzopyrene by Rentzepis and Pao and hexamethylene-traamine crystals by Heilmer et al). An important development occurred in 1970, when Davydov et al reported strong SHG in organic molecules having donor and acceptor groups connected with a benzene ring. This discovery led to an entirely new research effort to engineer new organic materials for SHG studies. Davydov et al concluded that noncentrosymmetric dipolar aromatic molecules possessing an electron donor and acceptor group contribute to large second-order optical nonlinearities arising from the intramolecular charge transfer between the opposite groups through the π conjugated system [3].

In the case of inorganic systems, the NLO response arises from band structure effects, whereas for organic and polymer systems it is due to virtual electron excitations occurring in the individual molecular or polymeric units. The individual molecular unit acts as a dipole, which gets strengthened by an increased number of highly mobile electrons or a large conjugation length to allow for maximum separation of charge. Also, factors such as the nature of the π electron bonding sequence, the dimensionality, and the substitution of alternate atoms into the conjugated structure, affect the dipole moment and optical susceptibility of the molecule. Following the path of second-order nonlinear materials, third-order nonlinear materials also have been shown to be affected by donor-acceptor groups, symmetry, the nature of the π electron bonding sequence, the dimensionality, and the substitution of alternate atoms into the conjugated structure. However, no clear structure-property relationship has been understood. Third-order materials are not constrained to be acentric and, thus, do not require any bulk order. Therefore, all materials, including random media such as liquids and amorphous structures such as glass, exhibit $\chi^{(3)}$.

To have the potential to be used in a practical NLO device, in addition to exhibiting a strong NLO response, a material should possess a combination of photophysical properties such as high laser damage threshold, fast optical response time, wide phase matchable angle, structural flexibility and adaptability,
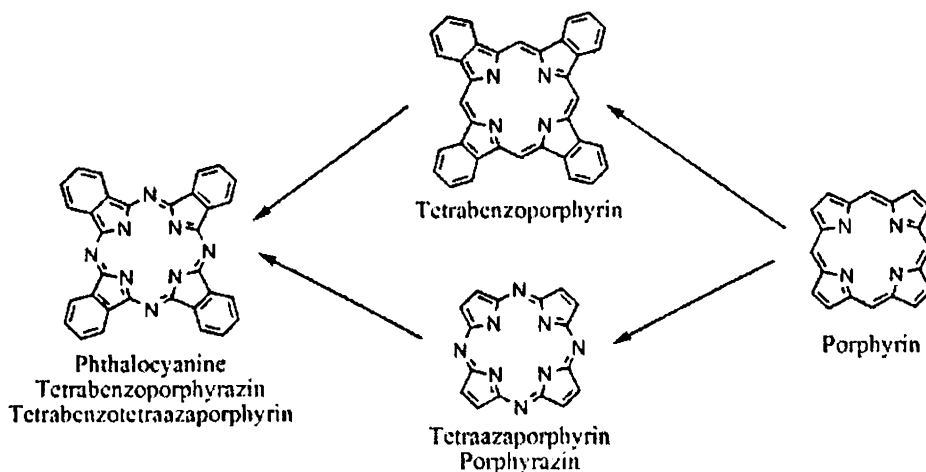
Figure 2.1: Structural relationship between porphyrins and phthalocyanines

optical transparency, ease of fabrication, nontoxicity, high mechanical strength, and environmental and thermal stability. Compared to inorganic materials, organic materials fulfill many of these requirements. However, they typically have shortcomings in environmental and mechanical strength, performance at high and low temperatures, and linear transparency.

Linear organometallics and organometallic macrocycles are some of the most promising third-order nonlinear materials, in part due to their generally high chemical and thermal stability. The insertion of a metal unit into a conjugated structure may significantly influence the π electron behavior in the molecule. Structures containing transition metals offer new properties derived from the richness of the various excited states, possibly due to low-lying d-d transitions present in these systems. Furthermore, the ligand-metal bonding displays large molecular hyperpolarizability due to transfer of electron density between the metal atom and the ligand systems. This transfer causes the electron orbitals of the ligands to tend to overlap with the metal orbitals, thus leading to large intermolecular interactions. Some organometallics that have shown significant frequency doubling responses are π electron systems in which the metal acts to reinforce planarity and to improve π type mixing between donor and acceptor regions. The most common forms of organometallics and pseudo-organometallics are metalloporphyrin (MPP) complexes, metal carbonyl complexes, and metallo phthallocyanine (MPc) complexes.

Metallophthalocyanines are planar π conjugated heterocyclic aromatic system derived from porphyrin. Relationship of the phthalocyanine with the por-

phyrin macrocycle is shown in Figure 2.1. They have useful applications in a variety of fields such as chemical sensors, molecular metals, electrochromic and photovoltaic cells, etc [4]. The desire for stronger NLO response, coordination of larger cations, and increased production of singlet oxygen motivated the development of the so-called expanded porphyrins in 1966. Porphyrins are found in nearly all living organisms and are located primarily in cells and organs that are responsible for energy production, metabolism, and transport functions. These ring-like molecules (or macrocycles) are usually aromatic, with an 18 π electron framework. This aromaticity allows for the ability to absorb visible light, to mediate the conversion of absorbed light to other forms of physical and chemical energy, and to enhance kinetic and thermodynamic stability. Porphyrins have a central cavity that allows for the binding of a wide variety of cations (including transition metals) to the nitrogen atoms contained in ring structure, thus allowing for the formation of planar or nearly planar 1:1 ligand-to-metal complexes. In this chapter, the nonlinear refraction and absorption properties of single metal phthalocyanines of cobalt, nickel, copper and zinc (CoPc, NiPc, CuPc and ZnPc) are discussed.

2.3   Closed Aperture Z-scan to Study Nonlinear Refraction

Nonlinear optical properties of materials have steadily increased in importance since the invention of the laser. Most attention has been focused on the second order nonlinearity, $\chi^{(2)}$, of non centrosymmetric materials because of its applications to harmonic generation and frequency shifting using parametric oscillators. The third order nonlinearity, $\chi^{(3)}$ has also become of increasing interest because of its effect on the optical propagation of intense beams and its rapidly proliferating importance and applications in modern optical technology. There have been many efforts in measuring the third order nonlinearities of optical materials and to relate their nonlinear behavior to their linear refractive index and compositional and structural characteristics. It is generally understood that the third order nonlinearities at optical frequencies far below the optical band gap, increase more or less monotonically with the linear refractive index. This has inspired attempts to empirically relate the third order nonlinearity to linear refractive index . The nonlinear refractive index n_2 is one of the simplest property derived from $\chi^{(3)}$ which is a very complicated quantity in its most general form. n_2 is an important consideration in the design of high
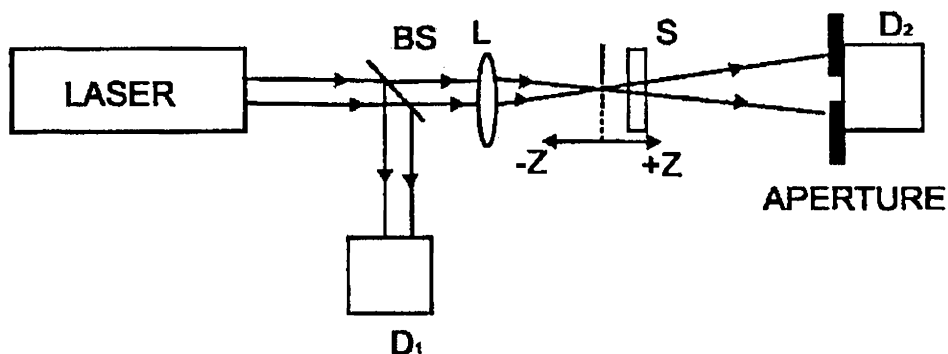
Figure 2.2: Experimental set up for single beam z-scan technique

power lasers and optical systems. It is because the spatial intensity fluctuations in the wave front of a laser beam passing through a medium grow exponentially with the nonlinear phase shift, which is proportional to n_2 [5]. Closed aperture z-scan is one of the easiest method to determine the sign and magnitude of n_2.

2.3.1   Experimental Arrangement

A brief account of z-scan technique was given in the previous chapter. In this section, a detailed account of the nonlinear absorption measurements performed in the four MPc's is presented. The experimental set up is shown schematically in Figure 2.2. The laser source used for this study was a Q switched Nd:YAG, emitting pulses of 8 ns duration (FWHM), at a repetition rate of 10 Hz. A few percent of the output of this laser source was collected, spatially filtered and made to pass through an achromatic convex lens before entering the sample. This lens produces a beam waist of $1/e^2$ radius of 35 μm at 532 nm[1]. The corresponding Rayleigh range (z_0) is 7.59 mm and hence a cuvette of path length 1 mm was used to satisfy thin lens approximation. This is to ensure that the beam dimension does not change at the entrance and exit side of the sample. The sample is translated through the beam waist using a motorized translation stage, and the ratio of transmitted and incident energies were measured using

---

[1]For a focussed Gaussian beam the beam spot radius at the focus is given by

$$w_0 = f\lambda/d$$

where f is the focal length of the convex lens and d is the radius of the unfocussed beam. The Rayleigh range or depth of focus is given by

$$z_0 = \pi w_0^2/\lambda$$
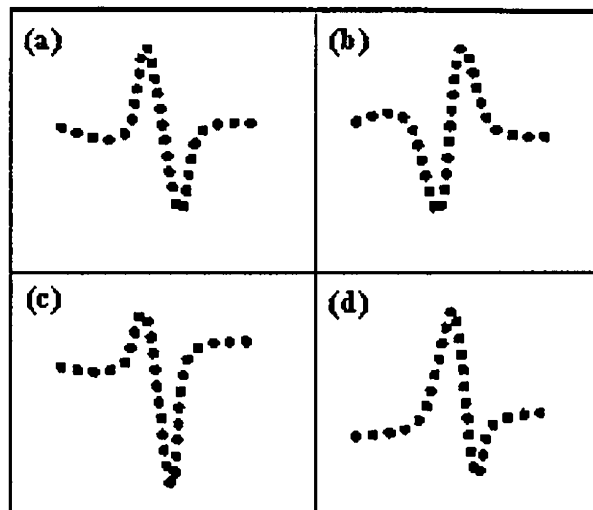
Figure 2.3: Ideal closed aperture z-scan signals. Horizontal axis is sample position along the beam axis and vertical axis is normalized transmittance. (a) negative refractive nonlinearity (b) positive refractive nonlinearity (c) peak suppressed-effect of saturation (d) peak enhanced-effect of induced absorption

energy ratio-meter (Laser probe Inc.) with RjP 735 probes. The complete experimental set up was automated using LabView. A very small aperture kept before the detector in the transmittance arm, enables the detection of phase distortion of the beam due to nonlinear refraction effects in the material. This is the reason why this configuration is called 'closed aperture' or CA z-scan. It is assumed that the focus corresponds to sample position z=0 where the sign of nonlinearity changes; (see Figure 2.3), and z is negative towards left and positive towards right of the focus. Similar type of measurements were made using the fundamental (1064 nm) and second harmonic (532 nm) of the Nd:YAG laser. A 0.5 mM solution of all these phthalocyanines were prepared in dimethyle formamide (DMF) and dimethyle sulphoxide (DMSO) for the study.

One of the very important advantages of z-scan method is that the sign and nature of the nonlinearity is clearly obvious from the transmittance curve. This is illustrated in Figure 2.3, which shows some typical z-scan curves. Y axis is for normalized transmittance, T (with T=1 at large distance from the focus), and x axis is for sample position z. Meaning of all these types of z-scan traces, is mentioned in the figure caption.

2.3.2 Detailed theory for Closed Aperture Z-scan

It is worthwhile to visualize the various processes taking place in the sample, and its effect on the transmitted beam profile, as we scan the sample across the beam focus. While the input energy measured at D1 is kept unchanged, the medium experiences different incident irradiance at different positions, which is decided by the position dependent beam spot size w(z), given by,

$$w^2(z) = w_0^2(1 + \frac{z^2}{z_0^2}).$$ (2.1)

Nonlinear refraction in the medium induces a phase distortion in the beam profile that causes a change in the fraction of light passing through the aperture kept at far field. Therefore the aperture transmittance is a function of the sample position z [6]. In this way of describing z-scan, it is assumed that a purely refractive nonlinearity is present and that there are no absorptive nonlinearities (such as multiphoton or saturation of absorption) in the material. .

While investigating the propagation of intense laser beam inside a nonlinear material and the ensuing self-refraction, for simplicity let us consider a thin nonlinear medium with a third-order nonlinear refraction, where the refractive index n is given by[2]

$$n = n_0 + \gamma I \qquad \text{or} \qquad n = n_0 + \frac{n_2}{2}|E|^2$$ (2.2)

where n_o is the linear index of refraction, E is the peak electric field (cgs), and I denotes the irradiance (MKS) of the laser beam within the sample. (The nonlinear refraction coefficients n_2 (esu), and γ (SI) are related through the conversion formula,

$$n_2(esu) = \frac{cn_o}{40\pi}\gamma(m^2 W^{-1})$$ (2.3)

where c (m/s) is the speed of light in vacuum.

The nonlinear refractive index is determined by several physical mechanisms, acting on a broad range of time scales. It is therefore necessary to be explicit about the contributing mechanisms in a particular experiment. The various

---

[2]There are numerous ways for defining the nonlinear refractive index n_2, and the relationship between $\chi^{(3)}$ and n_2 depends on several factors, which include: whether n_2 is defined in terms of the field amplitude squared or intensity; whether or not a factor of 1/2 is included in the definition of field amplitudes and yet another factor of 1/2 in the definition of n_2 and so on. Actually there are at least 2^5 distinct relationships which can be connected and therefore this is a continuing source of discrepancy and confusion. One should be extremely cautious therefore, while comparing literature values of various NLO parameters and should adhere to uniform notations and usage [7].

contributions to n_2 are

$$n_2 = n_2(\text{electronic}) + n_2(\text{vibrational}) + n_2(\text{electrostriction}) + n_2(\text{thermal}) \quad (2.4)$$

The response times of these various contributions can be estimated from simple arguments. The electronic and vibrational response times can be obtained from the frequencies of optical transitions involving the bound electrons and lattice vibrations; these are 10^{-15} s and 10^{-13} s respectively. The electrostrictive response time is roughly equal to the time required for an acoustic deformation to travel across the diameter of the optical beam which therefore depends on the geometry of the experimental set up, the optics used for creating the beam waist in the laser beam etc. In most experimental conditions using nanosecond pulses, this will be in the range of a few nanoseconds. By suitably choosing the optics and the beam parameters, it is possible to neutralize this effect if one desires so. Thermal diffusion time scales are even longer, and depend on the thermal properties of the medium.

Now let us consider the propagation of an intense laser beam through a material. At high intensities such as at the peak of an ultrashort laser pulse, the refractive index of any medium becomes a function of the incident intensity. Assuming a TEM$_{oo}$ Gaussian beam of beam waist radius w_0 traveling in the +z direction, we can write E as

$$E(z, r, t) = E_0(t) \frac{w_0}{w(z)} \, exp \, (-\frac{r^2}{w^2(z)} - \frac{ikr^2}{2Rz(z)}) \, e^{-i\phi(z,t)} \quad (2.5)$$

where the radius of curvature, R is defined as $R(z) = z(1 + \frac{z_0^2}{z^2})$, z_0 being the Rayleigh range, or depth of focus. As the beam reaches the exit surface of the sample, it suffers a radial variation in its phase given by $\Delta\phi(r)$. For a thin sample, the amplitude and phase of the electric field varies as a function of position inside the sample, z'($\int z' dz$ = sample length) and is given by,

$$\frac{d\Delta\phi}{dz'} = \Delta(I)k \quad \text{and} \quad \frac{dI}{dz'} = -\alpha(I)I \quad (2.6)$$

where $\alpha(I)$ in general, includes linear and nonlinear absorption terms. When the nonlinear absorption is negligible, Equations 2.6 are solved to give the phase shift $\Delta\phi$ at the exit surface of the sample which simply follows the radial variation of the incident irradiance at a given position of the sample z. Thus,

$$\Delta\phi(z, r, t) = \Delta\phi_0(z, t) \, exp \, (-\frac{2r^2}{w^2(z)}) \quad (2.7)$$

with $\Delta \phi_0(z,t) = \Delta \phi_0(t)/(1 + \frac{z^2}{z_0^2})$ where the on-axis phase shift at the focus, $\Delta \phi_0(t)$ is defined as

$$\Delta \phi_0(t) = (2\pi/\lambda) \ (\Delta n_0(t) \ L_{eff}) \tag{2.8}$$

and the effective sample length is given by $L_{eff} = (1 - e^{-\alpha \ L})/\alpha$; α being the linear absorption coefficient, and $\Delta n_0(opt) = \gamma I_0$ with I_0 the on-axis irradiance at focus.

The electric field at the exit surface of the sample now contains the nonlinear phase change and is expressed as,

$$E_e(r,z,t) = E(z,r,t)e^{-\alpha/2}e^{i\Delta\phi(z,r,t)}. \tag{2.9}$$

To find out the field at the detector plane, one uses the Gaussian decomposition method (GD method) adopted by Weaire et al [18]. For this, the nonlinear phase term is expanded as a Taylor series which modifies E_e in equation 2.9 as a sum of infinite number of Gaussian beams. Thus

$$e^{i\Delta\phi(z,r,t)} = \sum_{m=0}^{\infty} \frac{[i\Delta\phi(z,t)]^m}{m!} \ e^{-2mr^2/w^2(z)} \tag{2.10}$$

These Gaussian beams are individually propagated to the aperture plane and then added to get the resultant field, E_a.

$$E_a(r,t) = E(z,r=0,t) \ e^{-\alpha L/2} \sum_{m=0}^{\infty} \frac{[i\Delta\phi(z,t)]^m}{m!} \ \frac{w_{m0}}{w_m} \cdot exp\left(-\frac{r^2}{w_m^2} - \frac{ikr^2}{2R_m} + i\theta_m\right) \tag{2.11}$$

where d is the distance from sample to the aperture plane, $w_{m0}^2 = \frac{w^2}{2m+1}$ and other new terms in the equation are introduced as part of a convenient rearrangement, for which the reader may refer to [15]. The transmitted power through the aperture P_T is obtained by spatially integrating $E_a(r,t)$ upto the aperture radius r_a. Thus,

$$P_T(\Delta\phi_0(t)) = c \ \epsilon_0 \ n_0 \ \pi \ \int_0^{r_a} |E_a(r,t)|^2 \ rdr \tag{2.12}$$

where ϵ_0 is the permittivity of vacuum. Including the pulse temporal variation, the normalized z-scan transmittance T(z) can be calculated as

$$T(z) = \frac{\int_{-\infty}^{\infty} P_T\{\Delta\phi_0(t)\} \ dt}{S \ \int_{-\infty}^{\infty} P_i(t) \ dt} \tag{2.13}$$

where $P_i(t) = \pi w_0^2 I_0(t)/2$ is the instantaneous input power (within the sample) and $S = 1 - exp\left(-2r_a^2/w_a^2\right)$ is the aperture linear transmittance and w_a is the beam radius at the aperture. For a third-order nonlinear response, the nonlinear refractive index is related to the on-axis (r=0), peak (t=0) nonlinear phase shift by [15],

$$\gamma(m^2/W) = \frac{\Delta\phi_0\lambda}{2\pi\ L_{eff}I_0} \qquad (2.14)$$

A fit of the experimental data to Equation 2.13 will give the value of on-axis phase change $\Delta\phi_0$, which can be used with Equation 2.14 to get the nonlinear refractive index n_2. For this we use the relation between $\Delta\phi_0$ and refractive index change Δn_0;

$$\Delta\phi_0(t) = \frac{2\pi}{\lambda}\Delta n_0(t)L_{eff} \qquad (2.15)$$

and the expression for γ in terms of Δn_0, which is,

$$\Delta n_0 = \gamma I_0(t) \qquad (2.16)$$

where I_0 is the irradiance within the sample. The sign of $\Delta\phi_0$ and hence n_2 is determined from the relative position of the peak and valley with z. It is also possible to deduce the values of $\Delta\phi_0$ and n_2 from the measured peak-valley transmittance difference T_{p-v}

$$T_{p-v} = 0.406\ (1-S)^{0.25}|\Delta\phi_0| \quad for \quad |\Delta\phi_0| \le \pi \qquad (2.17)$$

The real part of third order susceptibility $\chi^{(3)}$ is related to γ through the relation,

$$\chi_R^{(3)} = 2n_0^2\ \epsilon_0\ c\ \gamma \qquad (2.18)$$

The unit [3] for $\chi_R^{(3)}$ is m^2V^{-2}(SI).

2.4   Nonlinear Refraction Measurements in Metal Phthalocyanines

Phthalocyanines, porphyrins and related macrocyclic metal-organic complexes are very attractive NLO materials because of their relatively large nonreso-

---

[3]To obtain a convenient unit for $\chi^{(3)}$ it is useful to remember that $volt = joule/coulomb$. This expression gives $\chi^{(3)}$ in units of m^2V^{-2}. However most of the reported values of nonlinear optical constants are in the electro static units (CGS esu unit). We can convert $\chi^{(3)}$ in m^2V^{-2} using the conversion formula, (express lengths in cm and $1volt = (10^8/c)$ esu where c is speed of light in cgs units). $1m^2V^{-2} = 9 \times 10^8 esu$

nant third-order susceptibilities and inherently fast response times. Extensive work has been done on investigation of the third-order susceptibilities and optical limiting performances of phthalocyanines and porphyrins by different techniques, such as third harmonic generation (THG), degenerate four wave mixing (DFWM), and z-scan. In this section the experimental results for refractive nonlinearity in metal phthalocyanines using the z-scan technique are described.
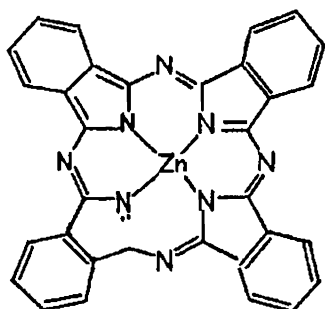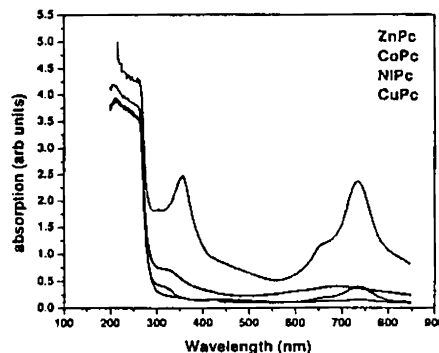
(a)   (b)

Figure 2.4:   (a) Structure of single metal phthalocyanine, (b) Absorption spectra of 0.5 mM solution of CoPc, NiPc, CuPc and ZnPc in DMSO. The labels are marked in the order in which they appear on the spectrum.

The structure of single metal phthalocyanine is as given in Figure 2.4(a) which is ZnPc. The central metallic nucleus will be replaced with Co, Ni or Cu as the case may be for the rest of the materials used in this study. The absorption spectra of all of them at a concentration of 0.5 mM in DMSO is shown in Figure 2.4(b). There is not much variation in the characteristics of the spectrum when the solvent is DMF. To optimize the experiment, z-scan was performed using a test sample at various aperture transmittance, S, keeping all the other conditions identical. A partially closed aperture was placed before the detector, and the detector output is monitored as the position of the sample, z, is varied along the axis relative to the focal plane of the input lens (z=0). The results are shown in Figure 2.5, and it can be seen that S=28% gives a good signal. Therefore the corresponding aperture size was used for the entire measurements. When S is 37% the valley is wider than the peak and hence it was not selected.
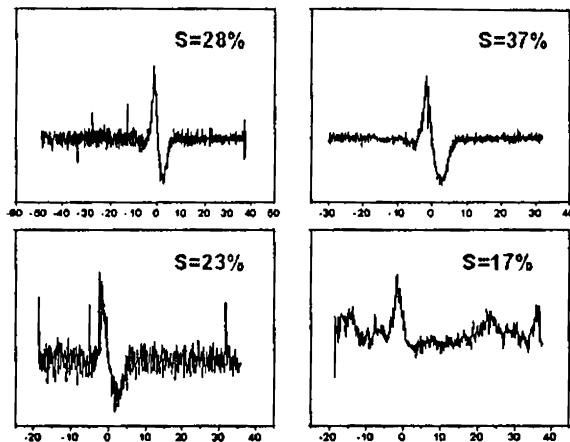
Figure 2.5: Shape of CA z-scan curves obtained with various aperture linear transmittance, S. Un-normalized transmittance is plotted on Y-axis and sample position in mm along x-axis. All plots are to the same scale. Aperture transmittance 28% gives comparatively better signal to noise ratio.

2.4.1 Nonlinear Refraction Coefficient

Typical CA- z-scan traces obtained for all the four MPc's dissolved in DMSO is shown in Figure 2.6 for identical experimental conditions. To obtain these z-scan results, special care was taken to avoid stray scattering which significantly affects z-scan data particularly for n_2 measurements requiring an aperture in the far field. Such stray scattering is a probable source of error in the sign determination of n_2. Theoretical fit of the experimental data to Equation 2.13 gives the value of $\Delta\phi_0$ which in turn gives the value of nonlinear refractive index as explained earlier. Example of the theoretical fitting is illustrated in Figure 2.7.

The observed peak-valley structure is the sign of negative nonlinearity which is either electronic or thermal in origin. Therefore the value of nonlinear refraction coefficient γ is due to the combined effect of these two mechanisms and is calculated using Equations 2.15, 2.16 and 2.17. One can get n_2 using relation 2.3. The results are shown in Table 2.1.[4] For ZnPc the CA transmittance signal

---

[4]Some authors use n_2 for nonlinear refractive index in both esu and SI systems; both being distinguished by explicit specification of system of units in braces; for example $n_2(SI)$ and $n_2(esu)$. However in this thesis γ is used for $n_2(SI)$ and just n_2 for $n_2(esu)$. Conversion from one system of unit to another is done by the use of equation 2.3
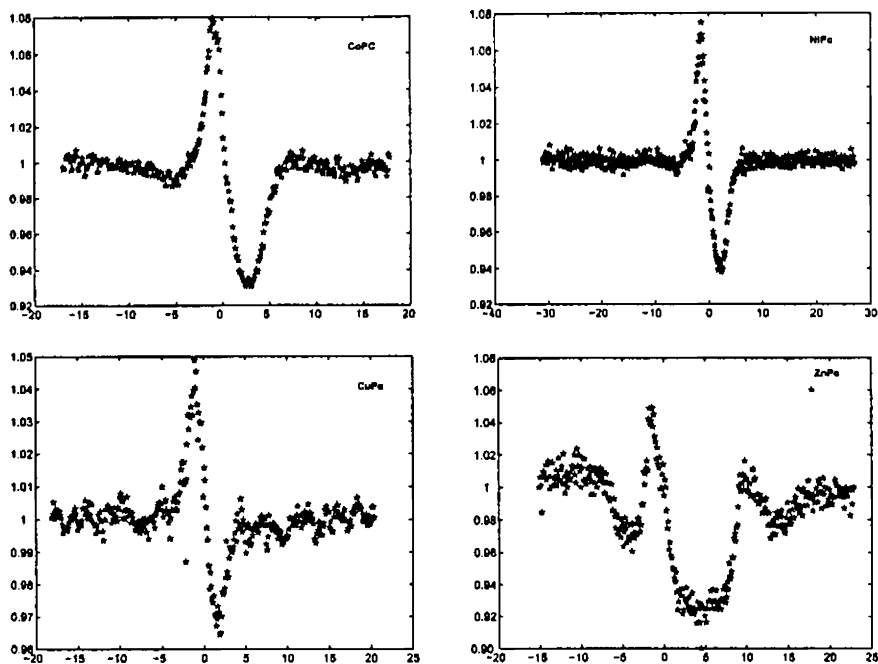
Figure 2.6: Experimental results for CA z-scan with DMSO as solvent. (a) CoPc, (b) NiPc, (c) CuPc and (d) ZnPc. Normalized transmittance is taken along Y-axis and sample position in mm along the X-axis.
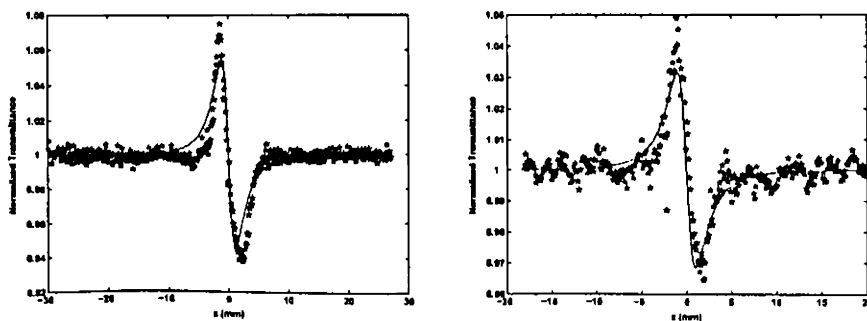
Figure 2.7: Theoretical fit to equation 2.13 for the CA-z-scan experimental data obtained for (a) NiPc and (b) CuPc in DMSO at 532 nm. I_0=0.3 GW/cm^2

obtained was very irregular in appearance at 532 nm excitation. (Figure 2.8).
It shows comparison of the shapes of the closed aperture data with ZnPc at
the fundamental and second harmonic of the Nd:YAG laser. The axes in the
graphs are not normalized. The purpose is only to show the difference in the
peak-valley structures in both the cases, when all other experimental conditions
are identical, including the pulse energy measured at D1.

Sample used	$\gamma(\times 10^{-5})\ cm^2\ GW^{-1}$			
	532 nm		1064 nm	
	DMF	DMSO	DMF	DMSO
NiPc	10.51	9.33	5.81	3.27
CoPC	12.44	13.81	10.32	9.81
ZnPC	–	–	0.88	1.26
CuPC	11.87	10.07	1.42	0.31

Table 2.1: Measured values of γ for the four MPc's at the fundamental and second harmonic
of the Nd:YAG laser. Samples were 0.5 mM solutions in DMF and DMSO.

The reasons for the multiple peaks and valley at 532 nm may be due to
the comparatively higher linear absorption of the material as can be seen from
the absorption spectrum in Figure 2.4(b). However, further investigations are
necessary to account for this behavior. The nonlinear refraction measurements
were therefore not done at this wavelength for ZnPc. Extensive nonlinear ab-
sorption studies were carried out in this material and the results are presented
in the next chapter.
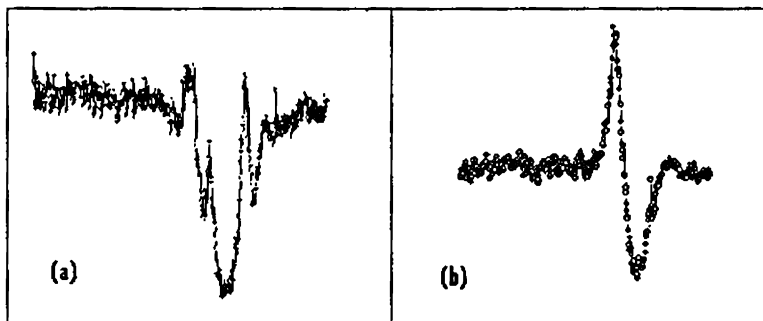
Figure 2.8: Comparison of the shapes of CA-z-scan curves obtained for ZnPc in DMF at
(a) 532 nm and (b) 1064 nm of the Nd:YAG laser under identical experimental conditions

2.4.2   Significance of Nonlinear Refraction

As mentioned earlier, a high intensity laser beam propagating through a material will modify its refractive index as given in Equation 2.2 which is referred to as optical Kerr effect [10]. In certain materials like fused silica, the nonlinear refractive index is very small, $\sim 3 \times 10^{-16} cm^2 W^{-1}$. A laser pulse with center frequency ω traveling through a medium of length L will acquire an optical phase $\omega L n/c$ and therefore the effects of the nonlinear refractive index will become important when this phase factor becomes equivalent to that of 1 λ. As an example, consider the propagation of femtosecond pulses through an optical fibre. With a 9μm fibre-core diameter (typical for communications-grade fibre), 10-nJ pulse energy and 100-fs pulse width, the peak power is 100 kW, corresponding to a power density of $1.5 \times 10^{11} W/cm^2$. If the length of the fibre is 1 cm, the optical path length changes by $L n_2 I$ which is approximately half a wavelength used for typical optical fiber communication systems. From this calculation, it can be seen that the optical Kerr effect can have a significant effect on a femtosecond pulse traveling through a medium. For pulses with energies of the order of millijoules or higher, even the nonlinear refractive index of air becomes important.

To understand how the optical Kerr effect can modify the spectral properties of an ultrashort pulse, one has to consider how the nonlinear refractive index modifies the optical phase of the pulse. The electric field of a laser pulse traveling in the x direction can be written as $E(t)cos(\omega t - kx)$. Since the wave number k depends on the (nonlinear) refractive index of the medium, the pulse will acquire a time-dependent phase induced by the Kerr effect. Inserting equation $k = \omega n/c$ into the expression for electric field and performing a Taylor expansion around the peak of the ultrashort pulse, one finds that the field modifies to $E(t)cos(\omega + xit)\, t - kx)$ where E depends on the nonlinear refractive index, the pulse width, peak power, and the distance traveled. Consequently, the nonlinear refractive index induces an approximately linear frequency sweep (or chirp) on the pulse. In other words, the spectrum of the pulse gets broadened due to the nonlinear interaction. If a single pulse modifies its own characteristics this way, the effect is often referred to as self phase modulation. If one pulse modifies the effective refractive index causing a second pulse to change its characteristics, this is referred to as cross phase modulation.

The spectral broadening induced by the nonlinear refractive index is extremely useful in spectroscopic applications. For example, an 800-nm femtosecond pulse can be sent through a short length of fibre or through a few millimeters of glass or sapphire to produce a broadband output pulse. Often there will be

significant power at wavelengths ranging from 400 nm to 1.6μm. For this reason, such spectrally broadened pulses are referred to as white-light continuum pulses. The white-light continuum generated in a fibre has been used to generate some of the world's shortest pulses of around 5 fs. A white-light continuum pulse is an ideal seed for an optical parametric amplifier.

An implication of the nonlinear refractive index is self-focusing or defocusing. due to Kerr effect. Self-focusing can become a run-away process leading to beam distortion and catastrophic damage to optical components. In white-light generation, self-focusing can result in the beam breaking up into multiple filaments that make the white-light output extremely unstable. It is therefore of utmost importance to choose the incident power such that white-light is generated without producing multiple filaments. For a 100-fs pulse, this usually means that the pulse energy should be limited to approximately 1μJ.

A negative value for the sign of n_2 was clearly established at 1064 nm and 532 nm for all these materials. We varied the incident fluence from 0.1 to 0.6 GW/cm^2 and repeated the experiments for the entire samples but did not observe any reversal of sign in refractive nonlinearity. Calculation of the γ values were done after dividing the CA z-scan data with the corresponding OA z-scan data to cancel the effect of absorptive nonlinearity, which will be discussed in detail in the next section. There was not any systematic variation of the measured values of γ with change in excitation wavelength or with change in the solvent. However, 1064 nm gives a smaller value of γ than what we obtained at 532 nm. The large magnitude of the off resonant γ of these materials should have a wide range of applications in ultrafast pico and femtosecond all-optical switching, and pulse compression. These measured values of γ or n_2 can be used to calculate the real part of third order susceptibility $\chi^{(3)}$ through the expression [11],

$$\chi_R^{(3)} = 2\gamma \, n_0^2 \, \epsilon_0^2 \, c \qquad (2.19)$$

2.4.3 Nonlinear Refraction Cross-section

In this section a brief account of how nonlinear refraction cross-section can be calculated from the CA z-scan data is presented. Some researchers believe that the nonlinear refractive coefficient, n_2, may not be the best description for cumulative nonlinearities that occur, for example, in reverse saturable absorbing (RSA) dyes. In such dyes, linear absorption is followed by excited-state absorption (ESA) where the excited-state absorption cross section is larger than the ground state absorption cross section. In these systems, the resulting change in

refractive index, due to population redistribution, is better described by refractive cross section σ_r than by n_2. In the case of phthalocyanines also, at 1064 and 532 nm, the material exhibits RSA behavior. Therefore it will be worthwhile to calculate σ_r at these wavelengths. σ_r is related to the on-axis phase distortion at focus, $\Delta\phi_0$ by the expression, [12].

$$\Delta\phi_0 = \frac{\alpha}{2\,h\nu}\sigma_r F_0 L_{eff} \qquad (2.20)$$

2.5 Open aperture Z-scan to Study Nonlinear Absorption

Large refractive nonlinearities in materials are commonly associated with a resonant transition which may be of single or multiphoton nature. The nonlinear absorption in such materials arising from either direct multiphoton absorption, saturation of the single photon absorption, or dynamic free-carrier absorption have strong effects on the measurements of nonlinear refraction using the z-scan technique. Z-scan traces with no aperture are expected to be symmetric with respect to the focus (z=0) where they have a minimum transmittance (e.g., multiphoton absorption) or maximum transmittance (e.g., saturation of absorption). In fact, the coefficients of nonlinear absorption can be easily calculated from such transmittance curves. The experimental set up for this study is as given in Figure 2.2, with a slight modification. The aperture in front of detector D2 is not necessary in induced absorption measurements, because we need to collect the entire transmitted beam. This is the reason why it is called 'open aperture' or OA z-scan.

2.5.1 Detailed theory for Open Aperture Z-scan

To derive an expression for transmittance in this case, let us briefly re-examine some important aspects of the CA experiment. The normalized transmittance T(CA) in the far field is as shown in Figure 2.7 for a small aperture (S=0.28). They exhibit a peak-valley structure indicating negative nonlinearity. For a given $\Delta\phi_0$, the magnitude and shape of T(CA) do not depend on the wavelength or geometry as long as the far-field condition for the aperture plane, $(d \gg z_0)$, is satisfied. The aperture size S, however, is an important parameter since a large aperture reduces the variations in T(CA). This reduction is more prominent in the peak where beam narrowing occurs and can result in a peak transmittance which cannot exceed (1-S). Moreover, for very large aperture or no aperture (S

=1 or 'Open aperture'), the effect vanishes and T(OA)=1 for all z and $\Delta\phi_0$. However, when nonlinear absorbtion is present, it will affect the z-scan signal, giving it either a peak or dip at the z=0 position, depending on the nature of the absorptive nonlinearity.

In the low excitation regimes, where free carrier effects are negligible, the set of equations 2.6 can be modified to derive T(OA) after the substitution,

$$\alpha(I) = \alpha_0 + \beta I. \tag{2.21}$$

This modifies the irradiance distribution and phase shift of the beam at the exit surface of the sample as

$$I_e(z, r, t) = \frac{I(z, r, t)e^{-\alpha L}}{1 + q(z, r, t)} \tag{2.22}$$

and

$$\Delta\phi(z, r, t) = \frac{k\gamma}{\beta} ln[1 + q(z, r, t)] \tag{2.23}$$

where $q(z, r, t) = \beta I(z, r, t)L_{eff}$, (z being the sample position). Combining 2.22 and 2.23, we obtain the complex field at the exit surface of the sample to be

$$E_e = E(z, r, t)e^{-\alpha L/2}(1 + q)^{(ik(\gamma/\beta) - (1/2))}. \tag{2.24}$$

Equation 2.24 reduces to Equation 2.9 in the limit of no nonlinear absorption, β. In general, a zeroth-order Hankel transform of Equation 2.24 will give the field distribution at the aperture which can then be used in Equations 2.13 to yield the transmittance. For $|q| \ll 1$, following a binomial series expansion in powers of 'q', Equation 2.24 can be expressed as an infinite sum of Gaussian beams similar to the purely refractive case described earlier.

$$E_e = E(z, r, t)e^{-\alpha L/2} \sum_{m=0}^{\infty} \frac{q(z, r, t)^m}{m!} \cdot [\prod_{n=0} (ik\gamma/\beta - 1/2 - n + 1)] \tag{2.25}$$

where the Gaussian spatial profiles are implicit in q(z,r,t) and E(z,r,t). The complex field pattern at the aperture plane can be obtained in the same manner as done for CA experiment. The result can again be represented by Equation 2.11 if we substitute the $(i\Delta\phi_0(z, t))^m/m!$ terms in the sum by

$$f_m = \frac{(i\Delta\phi_0(z, t))^m}{m!} \prod_{n=0}^{m} (1 + i(2n - 1)\frac{\beta}{2k\gamma}) \tag{2.26}$$

with $f_0=1$. Here the coupling factor $\beta/2k\gamma$ is the ratio of the imaginary to real parts of the third-order nonlinear susceptibility $\chi^{(3)}$.

The z-scan transmittance variations can be calculated following the same procedure as described previously. The absorptive and refractive contributions to the far-field beam profile and hence to the z-scan transmittance are coupled. When the aperture is removed, however, the z-scan transmittance is insensitive to beam distortion and is only a function of the nonlinear absorption. The total transmitted fluence in that case (S =1) can be obtained by spatially integrating Equation 2.22 without having to include the free-space propagation process. Thus we obtain the transmitted power P(z,t) as follows,

$$P(z,t) = P_i(t)e^{-\alpha L}\frac{ln[1+q_0(z,t)]}{q_0(z,t)} \tag{2.27}$$

where

$$q_0(z,t) = \beta I_0(t) \ L_{eff}/(1+(z^2/z_0^2)) \tag{2.28}$$

and $P_i(t)$ is the same as defined for CA situation.

For a temporally Gaussian pulse, Equation 2.27 can be time integrated to give the normalized energy transmittance

$$T(z,S=1) = \frac{1}{\sqrt{\pi} \ q_0(z,0)} \cdot \int_{-\infty}^{\infty} ln[1+q_0(z,0)e^{-\tau^2}]d\tau. \tag{2.29}$$

For $|q_0| < 1$, this transmittance can be expressed in terms of the peak irradiance in a summation form as,

$$T(z,S=1) = \sum_{m=0}^{\infty} \frac{[-q_0(z,0)]^m}{(m+1)^{3/2}}. \tag{2.30}$$

Thus, in cases where both nonlinear absorption and nonlinear refraction are present, an open aperture (S=1) z-scan gives the value of nonlinear absorption coefficient β.

2.6   Nonlinear Absorption Measurements in Metal Phthalocyanines

One of the advantages of the z-scan technique is the possibility of defining the contribution of several nonlinearities when they are present simultaneously. In general, when both nonlinear refraction and absorption are present, the normal-

ized transmittance T will be the resultant of transmittance due to both these effects [13]. An example of the OA z-scan trace obtained for ZnPc using 532 nm and 1064 nm excitation is shown in Figure 2.9.
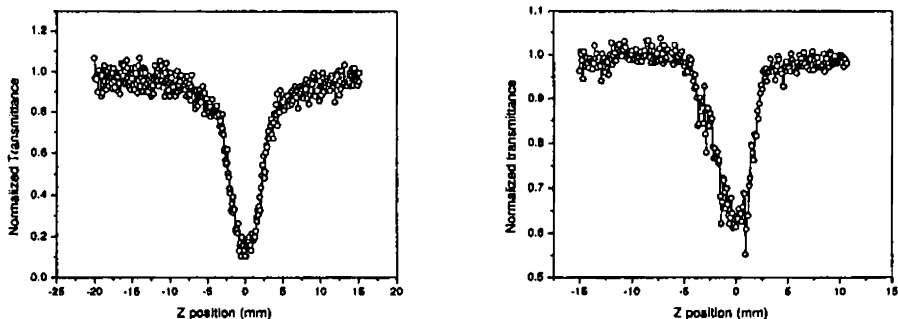
Figure 2.9: Example of OA z-scan curves obtained for ZnPc in DMF at (a) 1064 nm and (b) 532 nm of the Nd:YAG laser under identical experimental conditions

2.6.1 Induced Absorption in Pc's - Reverse Saturable Absorption

The physical processes leading to the type of OA z-scan trace as shown in Figure 2.9 is referred to as reverse saturable absorption or induced absorption. There are various processes leading to this phenomenon like excited state absorption (singlet and triplet), multi-photon absorption etc. Which of these processes dominate in a certain situation, will be determined by several aspects like, the life times of various excited states of the molecules, triplet cross-over time, the pulse duration of the laser used for excitation etc. A detailed account of the reasons for induced absorption in metal Pc's is given in Chapter 3. In general, when the incident energy is low, (far away from z=0 on either side of the OA z-scan trace) the material has linear response to the incoming optical beam, and hence transmittance follows the Beer's law. Normalized transmittance does not show any variation in this regime (T=1), because the linear response is very much inconspicuous compared to the extremely large power densities available as the sample moves over to the focus, z=0. Around the focus, the large power density induces nonlinear response in the material, which results in either further absorption from the excited state to higher levels, or simultaneous absorption of two or more photons etc, which results in decreased transmittance. This results

in a dip of the curve at this region.

2.6.2   Nonlinear Absorption Coefficient
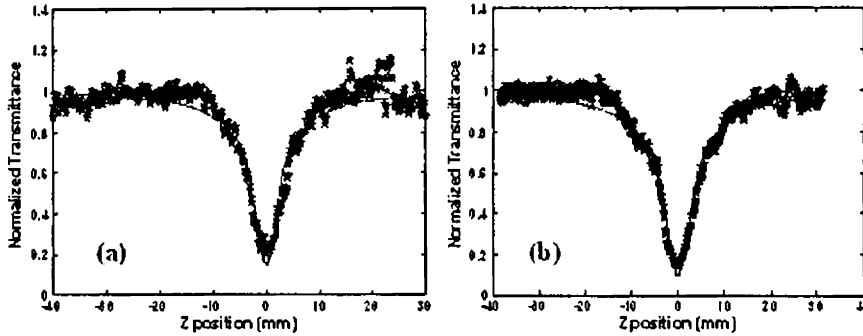
Figure 2.10: Open aperture z-scan curves and theoretical fit for the case of 0.35 mM solution of (a) CoPc and (b) CuPc in DMF at 532 nm of Nd:YAG

The values of nonlinear absorption coefficient β can be extracted from the OA z-scan data by giving it a theoretical fit to equation 2.29. Examples are shown in Figure 2.10. The constant q_0 can be used as a fit parameter and with the known values of I_0, z_0 and L_{eff} one can directly calculate the value of nonlinear absorption coefficient β from Equation 2.28. Experiments were performed at various possible energy densities and it was observed the nonlinear mechanism is RSA at all these fluence levels. The calculated values of β is given in Table 2.2.

| Sample used | β (cm/GW) | | | |
| | 532 nm | | 1064 nm | |
	DMF	DMSO	DMF	DMSO
NiPc	5.66	3.14	6.54	2.37
CoPC	6.14	5.23	3.25	9.57
ZnPC	6.46	6.38	7.36	9.87
CuPC	5.84	1.26	7.68	6.39

Table 2.2: Measured values of β for the four MPc's at the fundamental and second harmonic of the Nd:YAG laser. Samples were 0.35 mM solutions in DMF and DMSO.

2.7   Optical Limiting in RSA Materials

The need for passive optical limiters to protect human eyes and sensors from intense optical beams has generated much interest in the development of optical limiting materials [14]. Metallo-phthalocyanines and metallo-naphthalocyanines are among the most promising molecular materials for use in these devices because of their relatively low linear absorption and high ratios of excited-state to ground-state absorption cross sections (σ_e/σ_g) in the 450 - 600 nm region. The use of these complexes is limited, however, by their relatively high linear absorption outside of the 450 - 600 nm region and, in some cases, by the low quantum yields of their triplet excited states.

The nonlinear absorption studies that was have carried out, revealed that the MPc's have large third-order nonlinear optical susceptibilities at both 532 nm and 1064 nm and that they have a strong reverse saturable absorption (RSA), for nanosecond pulses at these wavelengths. In addition, photolysis studies done by earlier workers revealed that these complexes exhibit high intersystem crossing rates and high quantum yields of triplet excited states. These preliminary results are extremely promising, Here we will examine the optical limiting performance of these materials.

2.7.1   Experimental set up

The z-scan set up shown previously can be used for the optical limiting studies also. The sample should be kept slightly away from the focus, to avoid damage, and at a fixed sample position, the incident energy (or fluence) at detector D1 and the transmitted energy (or fluence) at detector D2 should be measured as a function of input fluence. This gives the optical limiting response as described in the next section. It is also possible to extract this graph from the OA z-scan data [15, 16].

2.7.2   Optical Limiting Performance of ZnPc

One consideration in evaluating materials for optical limiting applications is the bandwidth over which the limiting performance is effective. An ideal RSA molecule should have a large ratio of excited state absorption cross section to ground state cross section over a wide spectral range. The linear absorption spectrum shown in Figure 2.4(b), reveals a strong Q(0,0) band centered at 730 nm and a B band centered at 350 nm. Hence, a relatively wide optical window is formed in the 480 - 660 nm region. This suggests that reverse saturable

absorption will occur over the 480 - 660 nm spectral range for nanosecond or longer pulses duration, up to the limit imposed by the triplet excited state lifetime.

The optical limiting (OL) studies were done on ZnPc using the above experimental set up. The wavelengths used for this study were 532 and 1064 nm of the Nd:YAG laser. The results are shown in Figure 2.11(a). The material can act as an RSA based optical limiter at these wavelengths. Since saturable absorption behavior begins to dominate at resonant wavelengths, it will be very attractive if the B band and the Q band are well separated in wavelength. Wenfang et al had demonstrated that this can be achieved by modifying the side chains in porphyrin like complexes [21].

(a)   (b)
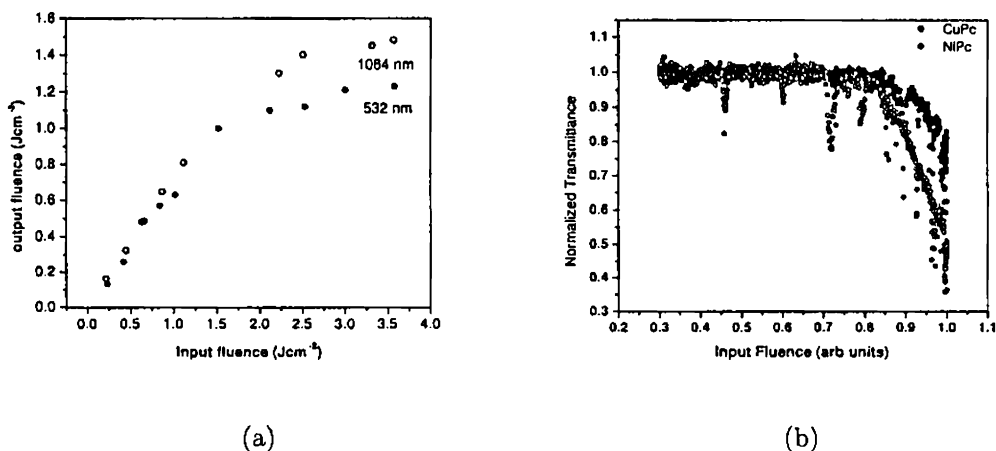
Figure 2.11: (a) Optical limiting performance of ZnPc at 532 and 1064 nm of Nd:YAG (b) Information about Optical limiting obtained from the OA z-scan data

The low intensity transmission for ZnPc at 532 nm and 1064 nm are 67% and 81% respectively. The limiting threshold, which is the input intensity at which the absorption in the material increases to two times its low absorption value, is approximately 2.5 Jcm^{-2} for 532 nm and 2.2 Jcm^{-2} for 1064 nm excitation. The limiting throughput defined as the constant value of output fluence obtained beyond the limiting threshold of input fluence, is about 1.44 Jcm^{-2} and 1.2 Jcm^{-2} respectively at 1064 nm and 532 nm wavelengths. This means that the optical limiting device does not allow the output fluence to rise beyond this value. There are observations that heavy metal substitution results in enhanced optical limiting in Pc's. Shirk etal reported OL studies in lead phthalocyanine

at 532 nm which showed limiting behavior for input energies as low as 10 nJ. They obtained a threshold for limiting of 8 nJ for a linear transmission of 68%. They also demonstrated that the limiting threshold and throughput depends on the 'f' number of the collection optics [22]. OL results are also available for derivatized fullerines in reference [23]. The throughput value they obtained at 532 nm are nearly $2.55 Jcm^{-2}$ for 50% linear transmission.

2.7.3 Optical Limiting Curves and Open Aperture Z-scan Data

It is also possible to obtain information about the optical limiting performance of an RSA based limiter, from the OA z-scan data. It is because while the sample is translated through the focus of the Gaussian beam, the sample experiences variation in the incident fluence levels, and the corresponding transmittance is what we measure at the output. By converting the x axis value (which is sample position in the OA traces) to the corresponding fluence, by incorporating the position dependent beam spot size via equation, $w^2(z) = w_0^2(1 + \frac{z^2}{z_0^2})$, we can obtain the nature of the limiting performance of the material. Examples are shown in Figure 2.11(b) with CuPc and NiPc. While calculating the fluence at the sample surface, the values of w_0 and z_0 and energy (measured at D1) are taken as unity. Therefore the maximum fluence at the sample surface will also be unity. Data points only from -z to z=0 from the OA transmittance curve is necessary to produce the OL curve. However if one desires to find the values of through put and the threshold of optical limiting, the exact values may be used in the calculations.

2.8   Conclusions

Z-scan is ideally suited to measure the nonlinear absorption and nonlinear refraction of material media. This has been demonstrated using solutions of some metal phthalocyanines. The nonlinear absorption coefficient β and nonlinear refraction coefficient γ are measured for these materials using the open aperture and closed aperture schemes respectively. It has also been found out that these materials display very good optical limiting behavior at 532 and 1064 nm input wavelengths. The limiting threshold and the throughput values are also measured at these wavelengths. The method to obtain information about the nature of optical limiting from the open aperture z-scan data is also discussed.

References

[1] R.A.Ganeev, *J. Opt. A: Pure Appl. Opt.*, 7 (2005) p.717

[2] Sheng-Li Guo, Jun Yan, Li Xu1, BingGu, Xi-Zhi Fan, Hui-Tian Wang, and N B Ming., *J. Opt. A: Pure Appl. Opt.*, 4 (2002) p.504

[3] P. Mouroulis, M. McKerns, *Opt. Eng.*, 39, (2000) p.808,

[4] C. C. Leznoff and A. B. P. Lever, *Phthalocyanines- Properties and Applications* VCH, New York, Vols. 1-4 (1989, 1993, 1996)

[5] Robert Adair, L. L. Chase, S.A.Payne, *Phy.Rev.B*, 39, (5), (1989), p.3337

[6] W. P.Zang, J.G.Tian, Z.B.Liu, W.Y.Zhou, F.S.Chun Zhang, and J.J.Xu., *J. Opt. Soc. Am. B*, 21 (2),(2004), p.349

[7] P. N. Butcher and D. Cotter, *The elements of Nonlinear optics*, Cambridge University Press, (1990), p.307

[8] D. Weaire, B. S. Wherrett, D. A. B. Miller, and S. D. Smith, *Opt. Lett.*, 4, (10) (1979) p.331

[9] M.Sheik-Bahae, A.A.Said, T.H.Wei, D.J.Hagan and E.W.Van stryland., *IEEE J.Quantum Elect.*, 26(4) (1990) p.760

[10] W. H. Knox. R. L. Fork, M. C. Downer, R. H. Stolen, and C. V. Shank, *Appl. Phys. Lett.*, 46 (1985) p.1120

[11] G.B.Jonathan, D.D.Dlott,L.K.Iwaki,S.M.Kirkpatrick and T.B.Rauchfuss, *J.Phys.Chem. A.*, 103 (1999) p.6930

[12] E.W.V. Stryland, M. Sheikbahae, A.A. Said, and D.J. Hagan, *Proc. SPIE*, 1852 (1993) p.135

[13] X. Lui, S. Guo, H. Wang, and L. Hou, *Opt. Commun.*, 197, (2001) p.431

[14] W.Sun, C.C.Byeon, M.McKerns, and C.M.Lawson, *Appl.Phys.Lett.*, 73(9) (1998) p.1167

[15] Binoy Paul, *Investigations of Nonlinear optical properties of certain organic photonic materials using z-scan and DFWM techniques* (PhD thesis), International school of Photonics, CUSAT, (2004)

[16] K.P.Unnikrishnan, *Z-scan and DFWM techniques in certain photonic materials* (PhD thesis), International school of Photonics, CUSAT, (2003)

[17] Wenfang Sun, Clare Byeon, Micheal McKerns and Chris Lawson, *App.Phy.Lett.*, 73(9), (1998) p.1167

[18] James. S. Shirk, Richard. G. S. Pong, F. J. Bartoli and Arthur. W. Snow, *App.Phy.Lett.*, 63(14), (1993) p.1880

[19] L. Smilowitz et al, *Opt.Lett.*, 21(13), (1996) p.922

Chapter 3

Excited State Absorption Spectrum Using Z-scan

"What we have to learn to do, we learn by doing."- Aristotle

ABSTRACT

Wavelength dependence of saturable and reverse saturable absorption (SA and RSA) of zinc phthalocyanine (ZnPc) is studied using 10 Hz, 8 ns pulses from an OPO in the wavelength range from 520-686 nm, which includes the rising edge of the Q-band in the electronic absorption spectrum. The nonlinear response is wavelength dependent and switching from RSA to SA has been observed as the excitation wavelength changes from the low absorption window region to higher absorption regime near the Q-band. The SA again changes back to RSA when we further move over to the infrared region. Values of the imaginary part of third order susceptibility, $Im \; \chi^{(3)}$, are calculated for various wavelengths in this range. This study is important in identifying the spectral range over which the nonlinear material acts as RSA based optical limiter. A five level energy diagram is used to account for the spectral dependence of nonlinear absorption.

3.1   Introduction

In the previous chapter the nonlinear absorption and refraction measurements of four metal phthalocyanines were discussed. It was seen that the material ZnPc behaves slightly different from the rest of the MPc's and also has very prominent peaks in the absorption spectrum compared to other materials. Therefore its nonlinear absorption studies were conducted in little more detail and has been presented in this chapter. The wavelength dependence of nonlinear (NL) absorption of ZnPc dissolved in dimethyl formamide (DMF) under nanosecond

excitation, has been studied and made use of in recording the excited state absorption spectrum. The studies of nonlinear processes in photonic materials are significant in the context of their technological applications, especially in areas like passive optical power limiting, in optical switching and in the design of logic gates. Optical limiting occurs when the absolute transmittance of a material decreases with increase in input fluence.

Metallophthalocyanine (MPc's) molecules are widely researched because of their strong reverse saturable absorption (RSA). One mechanism for optical limiting (OL) is provided by RSA, in which the excited state absorption cross-section is higher than the ground state absorption cross-section. It is also known that the substitution of heavy metal dopants significantly improve the limiting performance of Pc's at 532 nm.

3.2   Nonlinear Absorption

As discussed in the previous chapter, nonlinear absorption can be studied using the open aperture z-scan technique. Two important situations are encountered here, namely, saturable and reverse saturable absorption (SA and RSA).

3.2.1   Reverse Saturable Absorption (RSA)

Reverse saturable absorption is defined as the situation when absorption by suitable photons excite molecules into a higher-lying energy state, whereby the excited-state species absorb photons at a rate that is greater than the ground-state species. It is this situation that leads to strong optical limiting. In the open aperture z-scan experiment, this will be manifested as a dip at the z=0 position. In the literature RSA dyes are defined as those materials having a larger excited-state absorption cross section σ_e than the ground-state absorption cross section σ_g [1, 4]. It has therefore been common to define the critical condition for the achievement of RSA to be $R > 1$, where $R = \sigma_e/\sigma_g$. This criterion originates from taking a steady-state model for the classic RSA five-level energy scheme which will be discussed later in this chapter. One can see that the RSA medium will become opaque for high intense optical radiation.

3.2.2   Saturable Absorption (SA)

A saturable absorber exhibits reduced absorption coefficient at high input intensities. In the open aperture z-scan, this will result in a peak at the z=0 position. SA can occur in a medium with absorbing species, when a strong

optical intensity leads to depletion of the ground state of these ions. Similar effects can occur in semiconductors. These materials find application in passive Q switching or mode locking of lasers. Particularly for passive mode locking, semiconductor saturable absorber mirrors (also called SESAMs) are often used. Other saturable absorbers for mode locking are based on quantum dots (e.g. lead sulfide (PbS) suspended in glasses). For passive Q switching of solid state lasers, Cr4+:YAG crystals are most popular. They are also used as gain media.

3.3   Measurement of Nonlinear Absorption in the Presence of RSA and SA

Z-scan method is widely used for studying self refraction in nonlinear materials [15, 6]. As discussed earlier, it enables the determination of nonlinear properties of solids, ordinary liquids, and liquid crystals. In the z-scan experiment, the intensity dependence of refractive index and absorption are reflected as a position dependent transmission variation of the material which in turn can be made use of in extracting various nonlinear optical parameters like real and imaginary part of susceptibility, cross sections of nonlinear absorption and nonlinear refraction etc. However, we are mainly focussing on the wavelength dependence of nonlinear absorption studies in a 0.5 mM solution of ZnPc in DMF with particular emphasize on the RSA and SA properties.

The experimental set up for nonlinear absorption measurements consists of a wavelength tunable OPO (Quanta Ray) emitting pulses of 8 ns (FWHM) duration at a repetition rate of 10 Hz. A portion of the output of this laser was made to pass through an achromatic convex lens before entering the sample. An aperture was placed before the convex lens to obtain required beam size. The intensity dependent transmission of the sample for a number of wavelengths in the range from 520-686 nm was measured. For this, it is necessary to move the sample through the beam waist of the laser which was done using a motorized translation stage. Apart from the excitation source, other details of the experimental arrangement is more or less similar to that discussed in the previous chapter. However, some of the important optical parameters in this configuration is as follows. The focussing lens produces a beam waist of $1/e^2$ radius in the range 35-45 μm for these wavelengths. The corresponding Rayleigh range is 7.59 - 9.25 mm in this configuration. The transmitted and incident energies were measured using energy ratio-meter (Laser probe Inc.) with RjP 735 probes.

Chemical structure of ZnPc was given in the previous chapter. Its electronic

absorption characteristics (Figure 3.1) shows a B band around 350 nm and a Q band around 730 nm. A somewhat wide optical window is formed between these two bands. Most Pc's have been described with a 5-level energy diagram consisting of three singlets and two triplets as in Figure 3.2 [7].
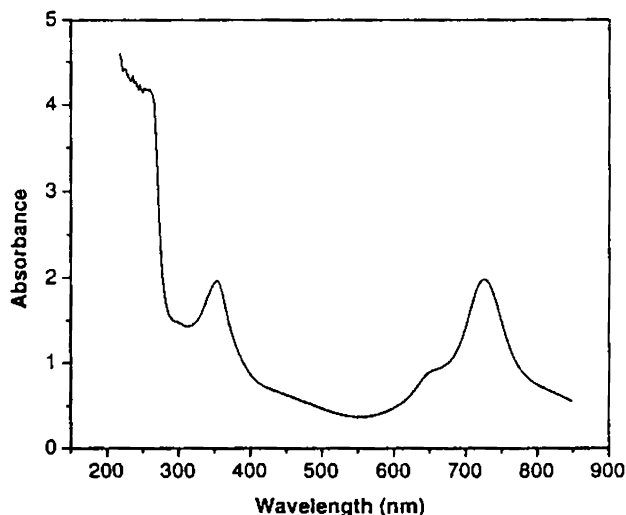
Figure 3.1: Absorption spectrum of ZnPc dissolved in DMF. The bands at 350 and 730 nm are designated as B band and Q band respectively.

In this diagram, S stands for singlet states with the suffix 0 for ground state and 1 and 2 for first and second electronic excited states. σ are the absorption cross sections. If the molecules at S_1 are excited to S_2 (with cross-section σ_{12}), and then relaxes to the state S_0, losing energy by radiation and/or by some radiationless process, it is characterized by a constant $k_{10} = 1/\tau_3$. If it suffers intersystem crossing to the triplet state $T_1(k_{ISC} = 1/t_{ISC})$, then it is possible for the molecule to go to T_2 with the corresponding triplet absorption cross section, σ_T. The efficiency of the T_1 formation is called triplet quantum yield ϕ. Porphyrins have rather high quantum yield for the triplet formation [8].

3.3.1   Theory

Saturable absorption is characterized by transmittance increase with the increase of the energy input, whereas the opposite happens in RSA. Here, we
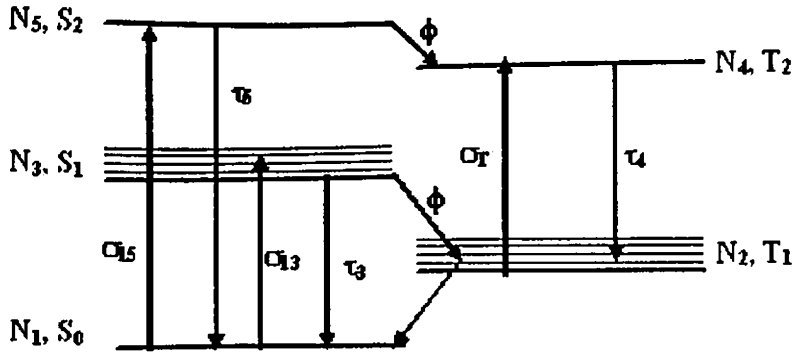
Figure 3.2: Schematic energy level diagram of ZnPc. The various symbols are, N - number density of molecules in each level, S- singlet states, T- triplet states, σ-absorption cross sections between the corresponding levels, τ- the life times of the decaying levels, ϕ -quantum yield for triplet formation.

have to consider the transmittance of the sample under two situations: 1) in the presence of RSA and 2) in the presence of SA. RSA is also referred to as induced absorption and there are various mechanisms leading to this process. In the presence of RSA the optical nonlinearity is described by the equation, [9]

$$\alpha(I) = \alpha_0 + \beta I \qquad (3.1)$$

α_0 is the linear absorption coefficient (in cm^{-1}) corresponding to transition from S_0 to S_1 and β is the nonlinear absorption cross section (mW^{-1}). The parameter β is related to the imaginary part of susceptibility by the relation,

$$Im(\chi^3) = \frac{\lambda \epsilon_0 n_0^2 c \beta}{4\pi} \qquad (3.2)$$

where λ is the excitation wavelength, ϵ_0 permittivity (Farad/m or coulomb/Vm), n_0 is the linear refractive index of the sample, and c is speed of light. For obtaining a convenient unit for $Im(\chi^{(3)})$ it is useful to remember that $volt = joule/coulomb$. This expression gives $\chi^{(3)}$ in units of m^2V^{-2}. However, most of the reported values of nonlinear optical constants are in the electro static units (CGS esu unit).

$$1m^2V^{-2} = 9 \times 10^8 esu \qquad (3.3)$$

The spatial variation of the intensity of the laser beam as it propagates through the sample is given by the relation,

$$\frac{dI}{dz} = -\alpha(I)I \tag{3.4}$$

Solving Equation 3.4 by integrating between limits I_0 to I, (the intensities at the entrance and exit surface of the sample, respectively) and putting transmission, $T = I/I_0$, we get,

$$T = \frac{e^{-\alpha_0 L}}{1 + \beta I_0 L_{eff}} \tag{3.5}$$

where

$$L_{eff} = \frac{1 - e^{-\alpha_0 L}}{\alpha_0} \tag{3.6}$$

This equation can be used to fit the experimental data of the open aperture z-scan trace, treating I_0 as the position dependent intensity. This is because of the presence of the focussing lens before the sample. The position dependence in intensity should be incorporated into the expression by considering the variation of beam size on either side of the focus ($\omega(z)$). The equation is $\omega(z)^2 = \omega_0^2(1 + \frac{z^2}{z_0^2})$ where $z = 0$ is the focus and $z_0 = \pi\omega^2/\lambda$ is referred to as Rayleigh range or diffraction length of the beam. β can be treated as an adjustable parameter. From the value of β we can calculate $Im\chi^{(3)}$ using Equation 3.2 in SI units.

In the presence of SA, Equation 3.1 modifies to [10]

$$\alpha(I) = \frac{\alpha_0}{1 + \frac{I}{I_s}} \tag{3.7}$$

Substituting this in Equation 3.4 and integrating between the limits I_0 to I gives

$$ln\frac{I}{I_0} = -\alpha_0 L - (\frac{I - I_0}{I_0}) \tag{3.8}$$

This can be solved numerically to get the transmission characteristics of the sample. If excitation intensity I_0 is less than I_s, we can consider SA as a third order process and in such cases $\frac{-\alpha_0}{I_s}$ is equivalent to nonlinear absorption coefficient β which will then give $Im\chi^{(3)}$.

3.4   Cross-over from RSA to SA

We have observed that the nature of NL absorption in ZnPc is dependent on the wavelength of the excitation beam. It was seen that the material exhibits RSA for wavelengths within 527 nm to 576 nm after which the NL response decreases and stops completely at 596 nm. This means that the material does not exhibit any sign of absorptive nonlinearity at this wavelength. As we move farther from 596 nm the behavior gradually changes to SA and reaches a maximum at 668 nm which is close to the resonance peak of 724 nm. This interesting feature is illustrated in Figure 3.3. At 650 nm the material has a small peak in the absorption spectrum. We were not able to explore the regions from 670 to 1064 nm due to the limitations of frequency mixing in OPO. However it can be concluded that the nonlinear absorption changes from RSA to SA when the excitation wavelength changes from off-resonant to near-resonant regions. At 1064 nm also the material exhibits RSA behavior. From the graph it can be seen that the value of nonlinear absorption is positive (RSA),when the linear absorption for the corresponding excitation wavelength is very small. The magnitude of NL absorption gradually decreases and becomes negative (SA) as the excitation shifts to near resonant wavelengths. The absolute value of this absorption increases as the excitation gets closer to the resonant peaks. When 1064 nm excitation wavelength from Nd:YAG was used, RSA was observed, with a large nonlinear susceptibility of $0.3313 \times 10^{-17} m^2 V^{-2}$ which is an order of magnitude higher than what we obtained at other wavelengths.

3.4.1   Explanations for the RSA Behavior in ZnPc

In general, induced absorption or RSA, can occur due to a variety of processes. However, which of them dominates is decided by factors like duration of the excitation pulse, life times of excited singlet and triplet states and intersystem crossing time, crossing yield etc. Nonlinear absorption can occur through the transitions $S_n \leftarrow S_0$ by instantaneous two photon absorption (TPA) or through $S_n \leftarrow S_1 \leftarrow S_0$ which is sequential TPA. This is an irradiance dependent process [11]. If the molecules undergo vibrational relaxation in S_1 and then reaches S_n by further absorption, it is referred to as singlet excited state absorption (SESA). Unlike TPA, ESA is a fluence dependent process. This means that the same fluence for two different pulse widths, will give the same nonlinear absorption if the mechanism is ESA. Singlet ESA is more likely to happen when the excitation pulse duration is pico seconds or shorter. For longer pulses usually triplet excited state absorption (TESA), $T_2 \leftarrow T_1$ dominates.
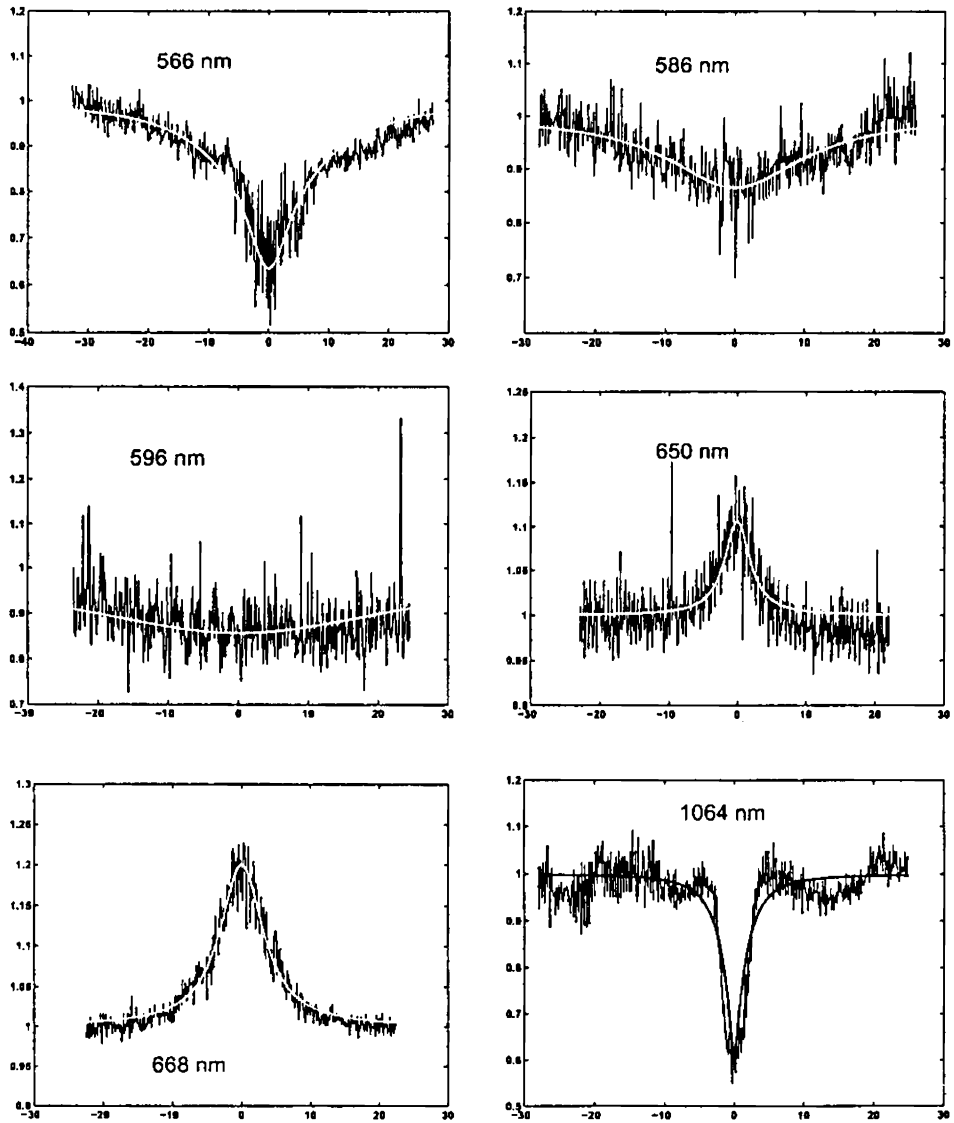
Figure 3.3: Open aperture trace of ZnPc for various wavelengths of excitation and its theoretical fit. All plots are in the same scale. On Y axis, the normalized transmittance and on X axis, the value of z, distance of the sample are given.

Moreover, in MPc's, the S_n life times are of the order of a few picoseconds and the triplet cross over time is a few hundred pico seconds. For ZnPc the singlet excited state S_n have a life time of 9 ps and the triplet states are longer lived [12]. The vibrational relaxation in singlet states takes place very fast, (in ps time scales). Joseph et al reported that the reverse saturable absorption and the optical-limiting of metal phthalocyanines can be enhanced by use of the heavy-atom effect [19]. They demonstrated this with Pc's containing heavy-metal atoms, such as In, Sn, and Pb. The enhancement in the ratio of effective excited-state to ground-state absorption cross sections compared with those containing lighter atoms, such as Al and Si was nearly two times. The fluorescence quantum yield for ZnPc is small, approximately 0.16 - 0.28 [14]. Considering all these factors and also that we used ns excitation pulses, it is reasonable to assume that TESA is one important factor contributing to induced absorption in our sample. It is possible to confirm whether TESA or TPA dominates in contributing to induced absorption, by measuring the nonlinear absorption for various pulse durations. As a rule, transmittance change ΔT at a fixed pulse energy will be independent of pulse width if the mechanism is TESA but will depend on pulse width if it is TPA. Since in our case the inter system crossing is very fast compared to the duration of the pulse, T_1 state gets populated. Therefore the observed nonlinear absorption is directly related to the product $(\phi \sigma_T)/\sigma_0$, where ϕ is the triplet yield. Certain metal ions can influence the inter system crossing rate to increase ϕ significantly. Zinc being a transition metal with partially filled d states, it enhances the intersystem crossing efficiency through spin orbit coupling leading to enhanced RSA behavior than other light metal phthalocyanines.

3.4.2   Figure of Merit for RSA materials, σ_e/σ_g

All RSA materials possess a higher absorption cross-section of excited states(σ_e) compared to that of the ground state (σ_g) at the excitation radiation wavelength [15]. Interestingly they will also give a positive value for the imaginary part of susceptibility $Im(\chi^{(3)})$ which is actually a measure of the induced absorption. On the other hand a saturable absorber has a negative value for $Im(\chi^{(3)})$. The most important application of these materials is in optical limiting. However, they also act as saturable absorbers at certain excitation wavelengths. Since these properties are spectral dependent, it is more common to use a figure of merit, $\frac{\sigma_e}{\sigma_g}$ which is the ratio of excited to ground state absorption cross-section. The value of σ_g can be obtained from the linear absorption spectrum using the

Beer's law. To evaluate σ_e we need to analyze the z-scan signal in a different manner, for example as followed by Wei et al [11].

3.4.3   Calculation of Exited State Absorption Cross-section

In analyzing the ESA spectrum from the z-scan trace, we neglected all excitations to singlet states higher than the first singlet excitation and assumed that the inter system crossing rate is fast compared with the pulse duration, (it is actually of the order of hundreds of pico seconds, [16]) and that all of the initially excited molecules are in the lowest triplet state. Excitation from the first triplet state then leads to ESA. The equations governing the spatial variation of absorption through the medium are[17],

$$\frac{dI}{dz} = -\alpha I - \sigma_e N(t)I \qquad (3.9)$$

$$\frac{dN}{dt} = \frac{\alpha I}{\hbar\omega} \qquad (3.10)$$

where I is the intensity, σ_{es} is the excited-state absorption cross section, N is the number density of species in the excited state, and ω is the angular frequency of the laser pump beam. Equations 3.9 and 3.10 can be combined to yield

$$\frac{dI}{dz} = -\alpha I - \frac{\sigma_{es}\alpha I}{\hbar\omega} \int_{-\infty}^{t} I(t')dt' \qquad (3.11)$$

Solving this equation for the fluence and integrating over the spatial extent of the beam, we may write the normalized energy transmission T as

$$T = ln(1 + \frac{q_0}{1 + x^2})/(\frac{q_0}{1 + x^2}) \qquad (3.12)$$

where $q_0 = (\sigma_{es}F_0(r = 0)L_{eff})/(2\hbar\omega)$, $x = z/z_0$ and $L_{eff} = \frac{(1-e^{-\alpha L})}{\alpha}$ is the effective sample path length. The experiment was performed as explained previously and the ratio of the transmitted intensity and the incident intensity was recorded for each pulse, using the energy ratio meter, and averaged to obtain the open aperture z-scan trace. Equation 3.12 was used to fit this experimental trace and this yields the value of q_0. The value of q_0 will then give the excited state absorption cross section, σ_{es}. The ground state absorption cross section can be calculated from the linear absorption spectrum, using Beer's law. This is plotted in Figure 3.4(a).

(a)   (b)
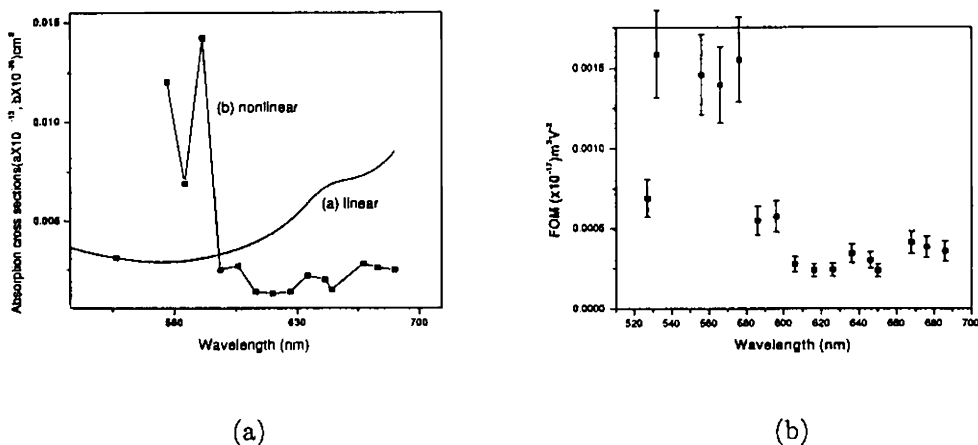
Figure 3.4: (a) Comparison of Excited state and ground state absorption cross sections (b) Figure of merit for $Im\chi^{(3)}$

3.5 Spectrum of Third Order Susceptibility

The calculated values of $Im\chi^{(3)}$ (this is the bulk third order susceptibility) as a function of wavelength is shown in Figure 3.5(a). The depth of the normalized z scan trace varies as shown in Figure 3.5(b). These values are within an error of 17% contributed mainly by the uncertainty in intensity measurements in the sample and the fitting error. $\chi^{(2)}$ and $\chi^{(4)}$ vanish in liquids and higher order odd terms such as $\chi^{(5)}$ will be very small compared to $\chi^{(3)}$. One should be very careful while comparing the susceptibility values available in literature. These values vary to a great extent depending on the excitation wavelength, pulse duration, experimental technique, concentration of the molecular species in the sample etc. K.P.Unnikrishnan et al have reported $Im\chi^{(3)}$ values of $Sm(Pc)_2$ and $Eu(Pc)_2$ dissolved in DMF at various wavelengths using the same technique [18]. $Sm(Pc)_2$ and $Eu(Pc)_2$ have a different structure compared to ZnPc. However, in the SA regions, their reported values are in the range from $(-3.2$ to $-0.07) \times 10^{-18} m^2 V^{-2}$ for $Eu(Pc)_2$ and from $(-4.0$ to $-0.14) \times 10^{-18} m^2 V^{-2}$ for $Sm(Pc)_2$ which are of the same order of magnitude as we obtained. Gema et al gives an extensive review of nonlinear optical studies in porphyrins and phthalocyanines and lists the values of $\chi^{(2)}$, $\chi^{(3)}$ and also the molecular hyper-polarizability values obtained using various techniques [7]. However, the value of $Im\chi^{(3)}$ of ZnPc is not mentioned. Diaz-Garcia reported the magnitude of $\chi^{(3)}$ of Langmuir−Blodgett films of octasubstituted MPc's using THG experiments,

(a)   (b)
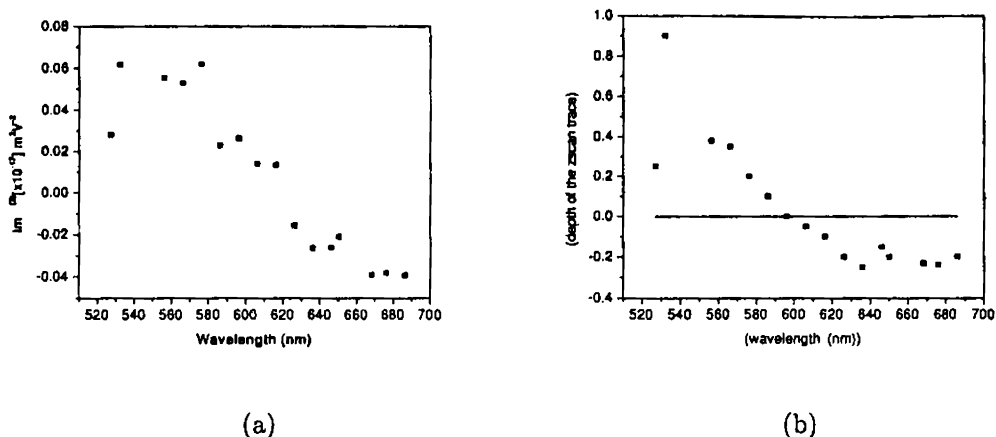
Figure 3.5: (a) Calculated values of $\mathrm{Im}\chi^{(3)}$ for various wavelengths (b) Depth of the zscan trace as a function of wavelength

at 1064 nm. These values are in the range 3.4 to 5.7×10^{-13} esu [19].

3.5.1 Effective Nonlinear Absorption Coefficient

The measured values of β_{eff} for those wavelengths at which the material shows induced absorption are given in Table 3.1. Considering the possibility of sequential and/or pure TPA and TESA, it is more appropriate to assume that an effective nonlinear absorption coefficient is what we can measure from the z-scan data, which we denote as β_{eff} instead of β. When it is a saturable absorber, a more useful parameter to extract from the transmission measurements is the saturation intensity I_s, which is also given in the table. The corresponding linear absorptions are also shown. It can also be assumed that for a saturable absorber $\frac{-\alpha_0}{I_s}$ is equivalent to β_{eff} of an RSA material. Henari et al used the same technique to find out the nonlinear optical parameters of certain group IV metal phthalocyanines using 665 nm, picosecond laser [20]. The absolute values of β_{eff} they obtained are nearly of the same order of magnitude as we calculated. However, they report I_s values that are at least two orders of magnitude higher than what we observed. We attribute these differences to the type of laser excitation and to the differences in sample properties.

$\lambda(nm)$	$\alpha_0(cm^{-1})$	$\beta_{eff}(cmGW^{-1})$	$I_s(GWcm^{-2})$
527	0.405	22.09	-
532	0.394	47.74	-
556	0.376	40.92	-
566	0.384	38.43	-
576	0.400	44.22	-
586	0.426	16.21	-
596	0.461	18.27	-
606	0.506	9.5	-
616	0.568	9.03	-
626	0.653	-	0.0637
636	0.766	-	0.0454
646	0.867	-	0.0523
650	0.892	-	0.0672
668	0.950	-	0.0469
676	0.998	-	0.0431
686	1.106	-	0.0397

Table 3.1: The linear (α_0) and nonlinear (β_{eff}) absorption coefficients, and saturation intensity (I_s) of ZnPc in DMF, for various wavelengths of excitation. The material acts as saturable absorber for wavelengths at which I_s is given. β_{eff} is mentioned only for the case of RSA.

3.5.2   Figure of Merit for $Im\chi^{(3)}$

As the wavelength of excitation approaches the wavelength of resonant absorption, α_0 increases and the nonlinear absorption gradually changes to SA. It will be useful to define a figure of merit 'FOM' for this type of materials as the ratio $\frac{|Im\chi^{(3)}|}{\alpha_0}$, which specifies the magnitude of nonlinear absorption for unit value of linear absorption loss (Figure 3.4(b)). FOM is larger by a small amount in the valley region between 500 nm and 600 nm in the absorption spectrum. The value FOM helps in comparing the absorptive nonlinearities at various excitation wavelengths.

3.6   Five-level Model for $Im\chi^{(3)}$

To account for the spectral dependence of $Im(\chi^{(3)})$ we have developed a theoretical formalism, using a 5 level model for energy transfer mechanism in the ZnPc molecules. It is depicted in Figure 3.2 and the notations are explained earlier. The resulting rate equations should be properly solved to get the population dynamics and the expressions for susceptibility. The details are given below.

3.6.1   Rate Equations for Five-level Model

To clearly understand the mechanisms for RSA, we need to solve the coupled rate equations for non steady state (time dependent) in Pc's, assuming a 5 level model for the energy levels. This gives a picture of the population transients in various levels[16]. This should be compared with the duration of the pump beam, and we will get a clear idea of various possible transitions that can take place while the pulse lasts inside the sample. The result of this simulation is shown in Figure 3.6(a) where two-photon absorption (TPA) is not taken into account.

(a)   (b)
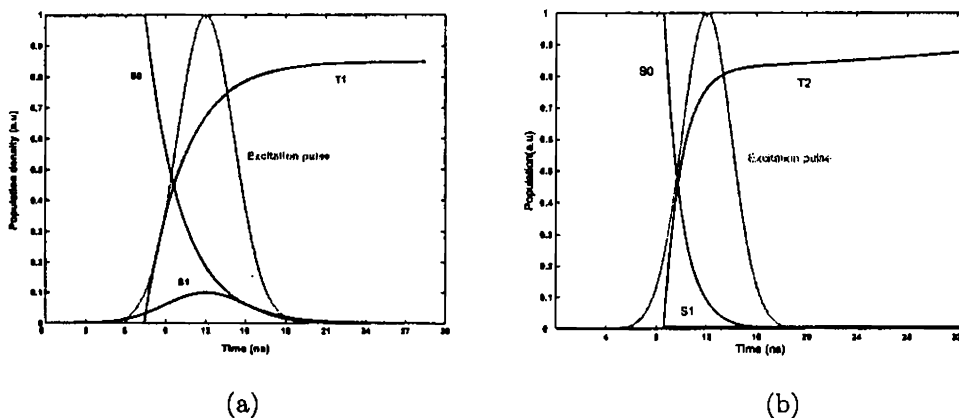
Figure 3.6: (a) Calculated population densities of S_0, S_1 and T_1 when TPA is absent (b) Calculated population densities of S_0, S_1 and T_2 when TPA is present

This means that when the excitation wavelength does not favor multiphoton processes, the triplet to triplet excited state absorption is the dominant mechanism for RSA. However, if we consider the possibility of two photon absorption, the rate equation should be modified, taking into account, the variation of population of ground state as proportional to p^2 (p being the fluence) and the TPA cross section obtained from the theoretical fit to OA z-scan trace. Then the first term on the right hand side of equation 3.13(c) can be neglected, which is due to one photon absorption, and the first term in the Equation 3.13(e) will be modified as, $(N_1 - N_5)\beta p^2$. The modified plot of time dependent population is given in Figure 3.6. The pulse duration of the laser used for this study is 8 ns. It can be assumed that within this time, most of the molecules were excited through TPA, and hence the population in S_1 and T_1 will be very negligible [21, 13]. The coupled rate equations implied by the energy level diagram given

in Figure 3.2 (considering only the relevant terms) are as follows,

$$N_1 + N_2 + N_3 + N_4 + N_5 = N_0 \tag{3.13a}$$

$$\frac{dN_2}{dt} = \frac{N_3\phi_{32}}{\tau_3} + \frac{N_4}{\tau_4} \tag{3.13b}$$

$$\frac{dN_3}{dt} = (N_1 - N_3)\sigma_{13}p - \frac{N_3\phi_{32}}{\tau_3} - \frac{N_3(1-\phi_{32})}{\tau_3} \tag{3.13c}$$

$$\frac{dN_4}{dt} = (N_2 - N_4)\sigma_T p - \frac{N_4}{\tau_4} + \frac{N_5\phi_{54}}{\tau_5} \tag{3.13d}$$

$$\frac{dN_5}{dt} = (N_1 - N_5)\sigma_{15}p - \frac{N_5(1-\phi_{54})}{\tau_5} - \frac{N_5\phi_{54}}{\tau_5} + (N_3 - N_5)\sigma_{35}p \tag{3.13e}$$

where ϕ are the intersystem crossing yields, σ are the absorption coefficients, and τ are the life time of the energy levels. β can be obtained from the OA signal as described in the previous chapter.

3.6.2   Rate Equations in the Transient Regime - Excited State Dynamics

It can be assumed that during the rising part of the excitation pulse, the population in various levels undergo a change due to all possible excitation and de-excitation processes in the molecular system. The solution of the governing rate equations as given by the above set of Equations 3.13, keeping the time dependent terms, will therefore give the excited state dynamics of the system. This is what is plotted in Figure 3.6, under two conditions, viz, with and without the presence of two photon absorption. Such calculations will help in determining the exact nature of the induced absorption processes. For example in the system under our investigation, it is the triplet to triplet absorption that leads to RSA [14, 27].

3.6.3   Rate Equations in the Steady state Regime - Evaluation of $\chi^{(3)}$

When the system attains steady state, one can equate the dN/dt terms in the rate equations to zero, and solve them and by a proper rearrangement of the terms it will finally lead to expressions for the real and imaginary part of susceptibility. Since only the nonlinear absorption studies were carried out, the focus is mainly on the derivation for $\text{Im}\chi^{(3)}$ as a function of wavelength of excitation

Vibrational relaxation	10^{-12} - 10^{-10}s
Fluorescence	10^{-9} - 10^{-5} s
External conversion	10^{-12} - 10^{-7} s
Electronic excitation	10^{-15} - 10^{-14}s
Phosphorescence	10^{-4} - 10^{-6} s
Internal conversion	10^{-12} - 10^{-7} s
Intersystem crossing	10^{-12} - 10^{-7} s

Table 3.2: Time scales for various excitation and relaxation processes in metal phthalicyanines

and the linear absorption coefficient. This will give a theoretical model for the excited state absorption spectrum .

To develop this model, the following steps are taken:

1. Identify the various processes that can take place in a time of $\sim$ 10 ns, which is the pulse duration of the laser used.

2. Write down the rate equations for 5 level system, incorporating all these possible transitions

3. Solve for steady state, neglecting processes that take more than 10 ns to take place.

4. Substitute the results into the expression for susceptibility obtained from the density matrix formalism and simplify.

5. Compare the results with the experimentally obtained values given in the previous sections.

In the case of ZnPc, and other common metal Pc's the time scales of various electronic excitation and de-excitation processes are given in Table 3.2. From these data it is reasonable to assume that, the system attains steady state during the time in which one pulse lasts in the medium, provided we neglect fluorescence and phosphorescence.

To derive a general expression for susceptibility, we can use the density matrix formalism adopted in refrence [28]. For example, considering a simple two level system, the corresponding density matrix is written as

$$\begin{pmatrix} \rho_{11} & \rho_{12} \\ \rho_{21} & \rho_{22} \end{pmatrix}$$

When light interacts with this system (Electric field E), it is represented by the interaction Hamiltonian,

$$H'(t) = -\mu E(t) \qquad (3.14)$$

where μ is the component of the dipole operator along the direction of the field, and the diagonal elements of $H'(t)$ are taken as zeroes. As appropriate to the transitions between states of definite parity, one can also put

$$\mu_{11} = \mu_{22} = 0 \qquad (3.15a)$$

$$\mu_{21} = \mu_{12} = \mu \qquad (3.15b)$$

and the total Hamiltonian is

$$H = H_0 + H' \qquad (3.16)$$

and

$$E = \begin{pmatrix} E_1 & 0 \\ 0 & E_2 \end{pmatrix}$$

The ensemble average of the dipole moment is $\langle \mu \rangle$ and we should solve for $\langle \mu \rangle$ of the atom that is induced by field E(t).

$$\langle \mu \rangle = trace\langle \rho\mu \rangle = tr \begin{pmatrix} \rho_{11} & \rho_{12} \\ \rho_{21} & \rho_{22} \end{pmatrix} \begin{pmatrix} 0 & \mu \\ \mu & 0 \end{pmatrix} = \mu(\rho_{12} + \rho_{21}) \qquad (3.17)$$

Using the relations

$$\frac{d\rho_{21}}{dt} = \frac{-i}{\hbar} (H \ \rho)_{21}$$

and using the equation 3.16, one gets the sets of equations,

$$\begin{aligned} \frac{d\rho_{21}}{dt} &= -\frac{i}{\hbar} [H'_{21}(\rho_{11} - \rho_{22}) + (E_2 - E_1)\rho_{21}] \\ &= \frac{i\mu}{\hbar} E(t)(\rho_{11} - \rho_{22}) - i\omega_0\rho_{21} \end{aligned} \qquad (3.18)$$

and

$$\begin{aligned} \frac{d\rho_{22}}{dt} &= -\frac{i\mu}{\hbar} E(t)(\rho_{12} - \rho_{21}) \\ &= -\frac{i\mu}{\hbar} E(t)(\rho_{21} - \rho_{21}^*) \end{aligned} \qquad (3.19)$$

The normalization condition is

$$\rho_{11} + \rho_{22} = 1$$

and therefore we get,

$$\frac{d}{dt}(\rho_{11} - \rho_{22}) = \frac{2i\mu}{\hbar}E(t)(\rho_{21} - \rho_{21}^*) \tag{3.20}$$

Equation 3.18 can be modified to include the collision terms as

$$\frac{d\rho_{21}}{dt} = \frac{i\mu}{\hbar}E(t)(\rho_{11} - \rho_{22}) - i\omega_0\rho_{21} - \frac{\rho_{21}}{T_2} \tag{3.21}$$

Here ρ_{ii} is the probability of finding the atom in the ith state. If N is the density of atoms, $N(\rho_{11} - \rho_{22}) \equiv \Delta N$ is the average density of the population difference between the two levels. Let the equilibrium value of (ie at $E(t) = 0$), $\rho_{11} - \rho_{22}$ is $(\rho_{11} - \rho_{22})_0$ and when E(t) is turned off, ΔN relaxes towards its equilibrium value $N(\rho_{11} - \rho_{22})_0$ with a time constant τ. Therefore Equations 3.18 and 3.19 becomes,

$$\begin{aligned}\frac{d}{dt}(\rho_{11} - \rho_{22}) &= \frac{2i\mu E(t)}{\hbar}(\rho_{21} - \rho_{21}^*) \\ &\quad - \frac{(\rho_{11} - \rho_{22}) - (\rho_{11} - \rho_{22})_0}{\tau}\end{aligned} \tag{3.22}$$

The perturbing field can be written as

$$E(t) = E_0\cos\omega t \tag{3.23}$$

and when it is zero, Equation 3.21 becomes

$$\frac{d\rho_{21}}{dt} = -i\omega_0\rho_{21} - \frac{\rho_{21}}{T_2}$$

so that when $\omega \approx \omega_0$ we can define a quantity σ_{21} as

$$\rho_{21}(t) = \sigma_{21}(t)e^{-i\omega t} \tag{3.24a}$$

$$\rho_{12}(t) = \sigma_{12}(t)e^{-i\omega t} = \rho_{21}^* \tag{3.24b}$$

Using Equations 3.23 and 3.24 in Equations 3.21 and 3.20 we get

$$\begin{aligned}
\frac{d\sigma_{21}}{dt} &= \frac{d}{dt}\left(\rho_{21}e^{i\omega t}\right) \\
&= i(\omega - \omega_0)\sigma_{21} + \frac{i\mu E_0}{2\hbar}(\rho_{11} - \rho_{22}) - \frac{\sigma_{21}}{T_2}
\end{aligned} \qquad (3.25)$$

and

$$\frac{d}{dt}(\rho_{11} - \rho_{22}) = \frac{i\mu E_0}{2\hbar}(\sigma_{21} - \sigma_{21}^*) - \frac{(\rho_{11} - \rho_{22}) - (\rho_{11} - \rho_{22})_0}{\tau} \qquad (3.26)$$

using these Equations 3.17 leads to the expectation value of the density matrix as

$$\langle \mu \rangle = 2\mu \left[Re\sigma_{21}(t)cos\omega t + Im\sigma_{21}(t)sin\omega t\right] \qquad (3.27)$$

To obtain steady state solutions, equate the Equations 3.25 and 3.26 to zero. Thus we get the absolute value of σ_{21} as a complex number. Its real and imaginary parts are,

$$Im\ \sigma_{21} = \frac{\Omega T_2(\rho_{11} - \rho_{22})_0}{1 + (\omega - \omega_0)^2\ T_2^2\ + 4\Omega^2 T_2 \tau} \qquad (3.28a)$$

$$Re\ \sigma_{21} = \frac{(\omega_0 - \omega)\Omega\ T_2^2(\rho_{11} - \rho_{22})_0}{1 + (\omega - \omega_0)^2\ T_2^2\ + 4\Omega^2 T_2 \tau} \qquad (3.28b)$$

where $\Omega = \mu E_0/2\hbar$ is the precession frequency. To obtain the expression for $\chi^{(3)}$ we need to use the relation $P = N\langle\mu\rangle$. Here P is the macroscopic polarization and use the Equation 3.27 to obtain P and then compare it with the standard relation

$$P(t) = E_0 \left(\epsilon_0 Re(\chi^{(3)})cos\omega t + \epsilon_0 Im(\chi^{(3)})sin\omega t\right). \qquad (3.29)$$

This leads to

$$Re\chi^{(3)}(\omega) = \frac{\mu^2(\omega_0 - \omega)T_2}{2\epsilon_0 \hbar}\Delta N g(\nu) \qquad (3.30a)$$

$$Im\chi^{(3)}(\omega) = \frac{\mu^2}{2\epsilon_0 \hbar}\Delta N g(\nu) \qquad (3.30b)$$

where the normalized line shape function is

$$g(\nu) = \frac{\Delta\nu/2\pi}{(\nu - \nu_0)^2 + (\Delta\nu/2)^2} \qquad (3.31)$$

and $\Delta\nu$ is the full width at half maximum is also the inverse of the dephasing time T_2.

This is extended to 5 level model to obtain the nonlinear susceptibility. To reduce the complexity in calculations, the rate equations given earlier are reformulated as follows, considering only the important and relevant terms.[1]

$$N_5 R_{52} + N_3 R_{32} + \frac{N_4}{\tau_{42}} = 0 \tag{3.32a}$$

$$(N_1 - N_3)\sigma_{13}p + \frac{N_5}{\tau_{53}} = N_3 R_{32} + \frac{N_3}{\tau_{31}} \tag{3.32b}$$

$$(N_2 - N_4)\sigma_{T42}p + N_5 R_{54} = \frac{N_4}{\tau_{42}} \tag{3.32c}$$

$$(N_1 - N_5)\sigma_{15}p + (N_3 - N_5)\sigma_{35}p = \frac{N_5}{\tau_{53}} + \frac{N_5}{\tau_{51}} + N_5 R_{54} + N_5 R_{52} \tag{3.32d}$$

$$N_1 + N_2 + N_3 + N_4 + N_5 = N_0 \tag{3.32e}$$

The solution gives values of N_1, N_2, N_3, N_4 and N_5. Substitute these values into the equation for imaginary part of susceptibility to give,

$$Im\chi^{(3)}(\omega) = \frac{n_0 c}{\omega}[(N_1 - N_3)\sigma_{13} + (N_2 - N_4)\sigma_{T42} + (N_1 - N_5)\sigma_{15} + (N_3 - N_5)\sigma_{35}] \tag{3.33}$$

and use the approximation $R_{52} \cong 0$ and assuming there is no decay from level 5 to level 3. This gives,

$$Im\chi_{eff}(\omega) = \frac{n_0 c}{\omega}\{\frac{-N_0 \sigma_{T42}(\sigma_{13} + \sigma_{15})}{B}\} \tag{3.34}$$

where B is defined as
$(R_{32}\tau_{31}(\sigma_{13} + \sigma_{15}) + \sigma_{T42}(-1 - 2p\sigma_{13}\tau_{31} - p\sigma_{15}\tau_{31} + p\sigma_{35}\tau_{31} + R_{32}\tau_{31}(-1 + 2p\sigma_{13}\tau_{42} + 2p\sigma_{15}\tau_{42})))$
Now this should be expanded in terms of flux density 'p'($= I/\hbar\omega$) and compared with the expression

$$\chi_{eff} = \chi^{(1)} + \chi^{(3)}|E|^2 = \chi^{(1)} + \chi^{(3)}\frac{2I_0}{\epsilon_0 n_0 c} \tag{3.35}$$

Thus the spectral dependence for $Im\chi^{(3)}$ can be written as

$$Im\chi^{(3)} = k1.k2 \left(k3[4\mu_{13}^6 g_{31}^3 + 2\mu_{15}^6 g_{51}^3 \tau_{31}] - k4[\mu_{13}^4 g_{31}^2 + \mu_{15}^2 g_{51}^2]\right) \tag{3.36}$$

To get the nature of the excited state absorption spectrum, the dependence of

---

[1]For a numerical solution of these coupled equations, one can use the command A=Solve[{Equation1, Equation2...Equation$n$}(in the form LHS==RHS), $\{N_1, N_2...N_n\}$]

$Im\chi^{(3)}$ as given above is sufficient. Values of g's defined in equation 3.31 are obtained from the linear absorption spectrum, by giving a Lorentzian fit to the absorption peaks. The inclusion of the term 'g' contains a detuning factor $\delta\nu$, that effectively incorporates the spectral dependence in susceptibility.

3.7 Conclusion

We have studied the nonlinear optical properties of ZnPc dissolved in DMF over a wide wavelength range. It has been observed that the nonlinear response shifts from RSA to SA when the excitation wavelength changes from off resonant to near resonant regions. The wavelength dependence of nonlinear absorption coefficient, imaginary part of the third order nonlinear susceptibility and also the figure of merit are calculated. We conclude that the RSA behavior is due to the combined effect of TPA and triplet ESA. The material can act as an RSA based optical limiter in the wavelength range from 527 to 576 nm and also at 1064 nm. When the excitation wavelength approaches the Q band, the nonlinear mechanism changes to SA. In the SA region we observed approximately 50% enhancement in $Im\chi^{(3)}$ for a wavelength change from 656 to 686 nm towards the resonant peak.

References

[1] Y. B. Band, in Proceedings of the Fritz Harz International Symposium , Plenum, New York (1985) p. 23

[2] Y. B. Band, *Chem. Phys. Lett.*, 127 (1986) p.381

[3] W. Blau, H. Byrne, W. M. Dennis, and J. Kelly, *Opt. Commun.*, 56 (1993) p.1985

[4] T. H. Wei, D. J. Hagan, M. J. Sence, E. W. Van Stryland, J. W. Perry, and D. R. Coulter, *Appl. Phys. B*, 54 (1992) p.46

[5] M. Sheik-Bahae, A. A . Said and E. W .Van Stryland, *Opt.Lett.*, 14, (1989) p.955

[6] A. Santhi,V. N. Vinu, *Proc. SPIE*, Nonlinear Frequency Generation and Conversion: Materials,Devices and ApplicationsIV. 5710 (2005) p. 91

[7] Gema de la Torre, Purificacin Vzquez, F. Agull-Lpez and Toms Torres, *Chem Rev.* 104, (2004) p.3723

[8] Marta Pineiro, Ana. L. Carvalho, Mariette. M. Pereira, A. M. Rocha Gonsalves, Lus. G. Arnaut, Sebastio. J. Formosinho, *Chemistry-A European journal.* 4(11), (1998) p.2299

[9] M. Sheik-Bahae, *IEEE Journal of Quantum Electronics.*, 26(4) (1990) p.760

[10] Rangel Rojo,S.Yamada,H.Matsuda, *J. Opt.Soc.America,B.*, 15(12), (1998) p.2937

[11] T. H. Wei etal, *App.Phy.B.*, 54, (1992) p.46

[12] I. Rckmann, A. Zeug, R. Herter, and B. Rder, *Phot.Chem.and Phot.Bio..* 66(5), (1997) p.576

[13] Joseph. W. Perry etal, *Opt.Lett.*, 19(9), (1994) p.625

[14] Inés Scalise and Edgardo N.Durantini,7th International Electronic Conference on Synthetic Organic Chemistry(ECSOC-7),1 (2003)

[15] P. J. Gonalves, I. E. Borissevitch, L. de Boni, N. M. Barbosa Neto, J. J. Rodrigues Jr, S. C. Zlio Av.Bandeirantes, XXVI ENFMC - *Annals of Optics*, 5, (2003) p.1

[16] Feng Li, Yinglin Song, Kun Yang, Shoutian Liu, Chunfei Li, *Appl. Phys,Lett.*, 71(15), (1997) p.2073

[17] Gary L. Wood, Mary J. Miller, and Andrew G. Mott, *Opt. Lett.*, 20(9) (1995) p.1

[18] K.P.Unnikrishnan, *Opt. Comm.*, 217 (2003) p.269

[19] M. A. Diaz Garcia, *App. Phys. Lett.*, 69(3), (1996) p.293

[20] F. Z. Henari, J. Callaghan, W. J. Blau, P. Haisch and M. Hanack, *Pure Appl. Opt.*, 6, (1997) p.741,

[21] Wenfang Sun, Clare Byeon, Micheal McKerns and Chris Lawson, *App.Phy.Lett.*, 73(9), (1998) p.1167

[22] James. S. Shirk, Richard. G. S. Pong, F. J. Bartoli and Arthur. W. Snow, *App.Phy.Lett.*, 63(14), (1993) p.1880

[23] L. Smilowitz et al, *Opt.Lett.*, 21(13), (1996) p.922

[24] Wei-Ping Zang, Jian-Guo Tian, Zhi-Bo Liu, Wen-Yuan Zhou, Feng Song, Chun-Ping Zhang, and Jing-Jun Xu, *J. Opt. Soc. Am. B*, 21(2), (2004) p.349

[25] Lina Yang, R Dorsinville, Q Z Wang,P X Ye, R R Alfano, *Opt,Lett.*, 17(5), (1992) p.323

[26] Christine A Carter and Joel M Harris, *Appl. Opt.*, 23(3), (1994) p.476

[27] K Kandasamy, K Divakar Rao, Rekha Deshpande, P N Puntambekar, Bhanu P Sing, Shankar J Shetty, T S Srivastava, *Appl. Phy, B*, 64, (1997) p.479

[28] Amnon Yariv, Quantum Electronics(3/e), John Wiley & Sons, Inc., (1989)

Part II

Thermal Lens technique

Chapter 4

Photo thermal Methods for Material Characterization

"But in science the credit goes to the man who convinces the world, and not to the man to whom the idea first occurs."- Francis Darwin

ABSTRACT

Photothermal techniques generally include the areas of photothermal spectroscopy, imaging and velocimetry. Photo thermal spectroscopy is generally defined as the field in which the nature of the matter is probed using optical excitation of a medium and probing of the thermal energy which results from this excitation. Normally both pumping and probing are done using lasers and detection can be in the form of deflection, diffraction, refraction, displacement and lensing. This chapter classifies some of the usual photothermal detection methods and provides an overview of the theory for photothermal lensing technique which is generally used for investigations related to the samples under studies.

4.1 Photothermal Spectroscopy

4.1.1 Introduction

Photothermal (PT) generation refers to heating of the sample due to absorption of electromagnetic radiation. Effects similar to PT generation can be produced by other types of excitation beams like electrons, protons, ions etc. PT generation has in general three kinds of applications (a) PT material probing (b) PT material processing (c) PT material destruction. Type (a) applications cause no sample modifications, type (b) causes sample to change to another useful
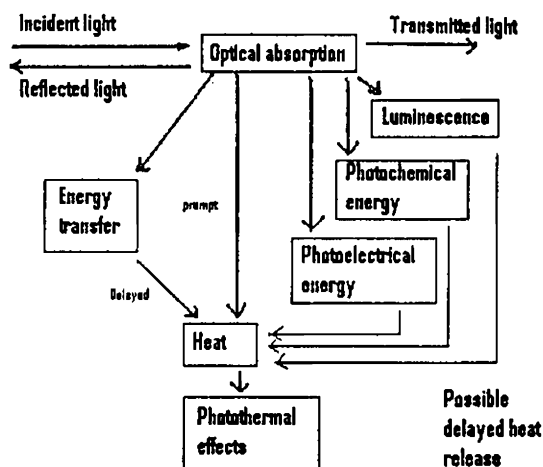
Figure 4.1: Block diagram to indicate the possible consequences of optical absorption leading to "prompt" or "delayed" heat production in competition with other de-excitation channels.

form, and type (c) makes the sample useless. The temperatures involved also generally increases in this order [6, 2].

The photothermal probing of material is based on the idea given in Figure 4.1. Optical excitation of the sample can result in the production of several forms of energy: heat, luminescence, chemical energy or electrical energy. The heat can be produced at various time delays arising due to energy transfer mechanisms. All these resulting energy forms add up to equal the absorbed optical energy, which makes the de-excitation branches shown in Figure 4.1 complementary.

PT heating of the sample in air will produce temperature rise, photo acoustic waves, and refractive index changes in the sample and in the adjacent air, infra red thermal radiation changes etc., at the same time. Thus the choice of a suitable PT effect for probing will depend on the material, the sample environment, the light source used, the purpose of the detection etc.

4.2   Photo Thermal Detection and Applications

Detection methods for various PT effects are summarized in Table 4.1. These detection methods can either be applied to the sample itself or the coupling fluid adjacent to the sample giving the 'direct' or 'indirect' PT detection schemes re-

Photothermal effects	Detection methods (applicable to sample S or adjacent fluid F)
Temperature rise	Laser calorimetry (S or F)
Pressure change	Direct photoacoustic detection (S) Indirect photoacoustic detection (F)
Refractive index change (Thermal or acoustic)	Probe-beam refraction (S or F) Probe-beam diffraction (S or F) Other optical probes (S or F)
Surface deformation (Thermal or acoustic)	Probe-beam deflection (S) Optical interference (S)
Thermal emission change	Photothermal radiometry (S)
Reflectivity or absorptivity change	Transient thermal reflectance (S) Transient piezo reflectance (S) Optical transmission monitoring (S or F)

Table 4.1: The heating of a sample due to optical absorption can result in various PT effects. The corresponding detection techniques are given.

spectively. All the PT detection schemes require a modulation for the excitation light. Such a modulation can be in the form of short intense pulses separated by long dark periods (referred to as pulsed PT detection) or continuous train of pulses at about 50% duty cycle (referred to as continuous modulated PT detection). The former detection is typically in the time domain, where the PT signal magnitude and shape after the pulse excitation are recorded, whereas the latter detection scheme is in the frequency domain where the PT signal magnitude and phase are recorded by lock-in detection with respect to excitation. Various PT detection methods are detailed below.

4.2.1 Temperature Rise

To detect PT heating one can monitor the rise in temperature; this is called laser calorimetry. To detect the temperature rise, thermo couples, pyro electric detectors or thermistors can be used. The advantage in directly measuring the rise in temperature is that absolute calibration is readily available, ie., the directly measured temperature rise can be related to physical parameters like absorption coefficients. But the disadvantage is that the response is slow, sensitivity

is relatively low compared to other methods.

4.2.2   Pressure Change

Pressure variation due to the absorption of light by a sample is usually called "photoacoustic" (PA) generation. PA generation mechanisms include electrostriction, thermo elastic expansion, volume changes due to photochemistry, gas evolution, boiling or ablation and dielectric breakdown, with the PA generation efficiency η (i.e acoustic energy generated /light energy absorbed) generally increasing in this order. For electrostriction and thermal expansion mechanisms, η is small, whereas for breakdown mechanisms η can be very large. To get a qualitative spectrum of a sample, the wavelength of the excitation beam is scanned and the corresponding magnitude of the acoustic signal, normalized by the excitation pulse energy, is measured to provide a PA spectrum.

PA generation can be classified as either direct or indirect. In direct PA generation the acoustic wave is produced in the sample where the excitation beam is absorbed. In indirect PA generation the acoustic wave is generated in a coupling medium adjacent to the sample, usually due to heat leakage and sometimes also due to acoustic transmission from the sample.

4.2.3   Refractive Index Gradient

PT heating of the sample can produce a refractive index gradient (RIG) in the sample (direct effect) or in an adjacent coupling fluid (indirect effect). Also there are two types of RIG produced by the PT heating of the sample, namely, a "thermal RIG" and an "acoustic RIG". The thermal RIG is produced by the decreased intensity of the medium, caused by the local temperature rise, decays in time following the diffusional decay of the temperature profile, and remains near the initial optically excited region. The acoustic RIG is associated with the density fluctuations of the medium caused by propagation of the PA wave, decays in propagation distance following the attenuation of the PA wave, and travels at the acoustics velocity away from the initial optically excited region. Thermal and Acoustic RIG are related and can be used to measure similar parameters, like optical absorption coefficients, temperature or flow velocity of the sample etc. However, thermal diffusivity can only be measured by the time evolution of the thermal RIG, and acoustic velocity and attenuation can only be measured by the spatial dependence of the Acoustic RIG. Also at distances farther from several thermal diffusion lengths from the excitation region, only acoustic RIG can be detected. In general, thermal RIG provides a larger signal

compared to acoustic RIG, which, however, can have a narrower temporal profile and be detectable far away from the excitation region.

1. Thermal RIG

   The thermal refractive index gradient generated by the excitation beam affects the propagation of an optical beam in its vicinity, including its own propagation, resulting in self-defocusing or "thermal blooming." Self-defocusing generally occurs instead of self focussing because the derivative of refractive index with respect to temperature is usually negative so that the temperature gradient results in a negative lens. The thermal RIG also affects the propagation of another probe beam in the vicinity of the excitation beam. Thus thermal RIG can be detected either by self-defocusing or by probe beam refraction (PBR).

   The PBR technique for probing the refractive index gradient can employ collinear beams giving rise to thermal lens effect. Probe beam can also be parallel to, but displaced from the excitation beam. By choosing appropriate displacements this configuration can give higher sensitivity than thermal lens spectroscopy. The most appropriate displacement of the probe beam from the pump beam position should be selected so as to have maximum refractive index gradient. This distance is approximately one beam radius from the axis of the excitation beam.

2. Acoustic RIG

   Similar to the optical probing of thermal RIG one can also detect the RIG associated with the PA pulse. This method is called the optical probing of the acoustic refractive index gradient. It is applicable for "direct detection" inside a material that is transparent to the probe beam or to "indirect detection" in a transparent coupling media. Here the transient deflection of the probe due to the traversal of the PA pulse is detected. By using two or more probe beams at different displacements and at different times, acoustic velocity and attenuation can be detected.

3. Other detection Schemes for RIG by PT generation

   To detect photothermal generated refractive index variations there are some other methods in use like phase fluctuation, heterodyne interferometry and Moire deflectometry [3]. Some researchers have also used two intersecting coherent pump beams for photothermal generation of a thermal refractive index grating in the sample and a probe beam diffraction scheme to measure the decay of this grating. It is also possible to use a
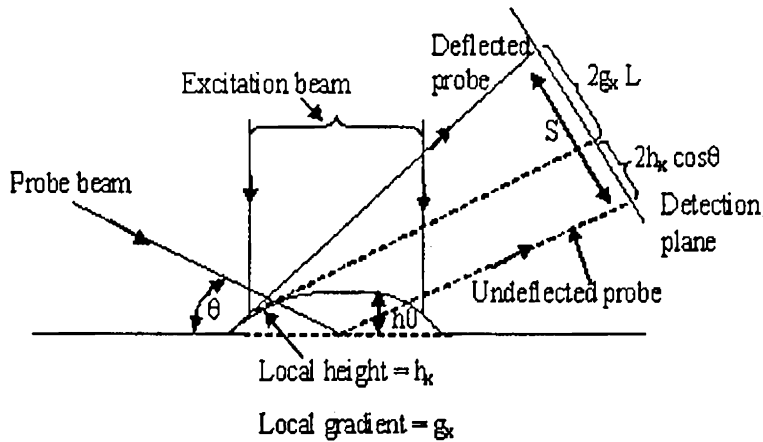
Figure 4.2: The probe beam incident at the displaced surface gets deflected, and the displacement at the detection plane is $2h_x cos\theta + 2g_x L$

high frequency ($\sim$ 1GHz) train of short laser pulses to irradiate an opaque sample giving back scattering of a probe beam due to the modulated refractive index. This is applicable to gas and liquid samples.

4.2.4   Surface Deformation

As for the case of RIG, the deformation of a sample surface due to PT excitation can be of two types, thermal and acoustic. Although these two deformations are related, the thermal one decays in time as thermal diffusion, whereas the acoustic one propagates into the sample bulk and also along the sample surface as bulk and surface acoustic waves, respectively.

1. Thermal Surface Deformation

   The PT heating of a surface causes distortions due to thermal expansion which can be as small as $10^{-3}\text{\AA}$. Detection of these deformations have sensitive spectroscopic applications giving rise to the field of PT displacement spectroscopy (PTDS). The technique of PTDS is shown in Figure 4.2 which indicates the case when a laser beam of power P and area A chopped at frequency f is incident on a solid. Assume that a thin coating of thickness l and absorption coefficient α on a transparent substrate absorbs the laser beam. Then the modulated heating is spread through a thermal diffusion length μ given by,

$$\mu = \left[\frac{D}{\pi f}\right]^{1/2} \tag{4.1}$$

where D is the thermal diffusivity of the solid. The average temperature rise ΔT in this thermal diffusion volume can be estimated as

$$\Delta T = \frac{\alpha \, lP}{2f\rho \, C \, \mu \, A} \tag{4.2}$$

where $P/2f$ is approximately the incident energy in one cycle, $\alpha \, l$ is the fraction of the heat absorbed, ρ is the density, and C is the specific heat of the solid. The magnitude of the maximum surface displacement h_0 is estimated as

$$h_0 = \beta\mu\Delta T = \frac{\beta\alpha lP}{2f \, \rho \, CA} \tag{4.3}$$

where β is the linear thermal expansion coefficient of the solid. Since h_0 is proportional to the coating absorption coefficient α, PTDS provides absorption spectroscopy of the coating by monitoring the deformation as a function of excitation wavelength.

2. Acousic Surface Deformation

   Noncontact optical probing of surface movement due to acoustic waves is important in material probing applications. The probe beam deflection measurement of surface acoustic deformation is similar to the method of optical detection of PT surface distortion described above. It is based on the deflection of a probe beam reflected from the surface. The difference between PT distortion and PA distortion is that, the former is associated with thermal expansion due to local temperature rise, follows the temperature decay via diffusion, and remains close to the excitation region. The latter on the other hand, propagates at a sound speed away from the excitation region. Only PA monitoring can provide values of sound speed and attenuation.

4.2.5   PT Radiometry

The photothermal radiometry (PTR) is a well-established technique used for the determination of the thermophysical properties, like thermal diffusivity and effusivity of various materials [4]. This technique is based on the detection of the

modulated thermal (blackbody) radiation emitted from a material surface after photothermal excitation by a modulated light source, usually a laser beam. The measurement procedures involve the analysis of the PTR signal as a function of the modulation frequency. In order to eliminate the instrumental frequency dependence, a calibration procedure is generally used: the signal for the sample is normalized to the one obtained with a reference sample. An alternative procedure is based on the signal ratio for front and rear surface experimental configurations. The thermophysical parameters are then obtained using multiparameter optimization algorithms to fit the PTR experimental data. The theory basically makes use of the Stefan-Boltzmann law

$$W = \epsilon \sigma T^4 \qquad (4.4)$$

where σ is the Stefan-Boltzmann constant and ϵ the emissivity. Suppose a body is irradiated by an optical pulse of energy E at wavelength λ that is absorbed by the body with an absorption coefficient $\alpha(\lambda)$, resulting in a temperature rise $\partial T(E, \alpha)$. Then the total radiant energy is increased by

$$\partial W(E, \alpha) = 4 \epsilon \sigma T^3 \; \partial T(E, \alpha) \qquad (4.5)$$

If $\partial T(E, \alpha)$ varies linearly with αE, then the normalized PTR signal can be defined as

$$S(\alpha) = \partial W(E, \alpha)/E \qquad (4.6)$$

The PTR spectrum can be monitored by measuring S for various values of λ.

4.3   Thermal lens spectrometry

The thermal lens was the first of the modern photo thermal phenomena to be described. The effect was observed quite by accident when Porto and associates at Bell Laboratories attempted to enhance the intensity of laser Raman scattering from benzene by placing a 1 cm sample cell of the liquid inside the resonator of the He-Ne laser in order to take advantage of the higher circulating intra cavity laser power (0.8 W). With sample cell in place, the laser exhibited power build up and decay transients with a time constant of a few seconds. When steady state was achieved the beam spot size at the laser mirror changed, as if a diverging lens of approximately 1 m focal length had been formed in the sample. The scientists concluded that a 'thermal lens' is produced by the

heating action of the Gaussian laser beam and their analysis forms the basis of the theory of thermal lens effects. The creation of the thermal lens by a laser beam with Gaussian intensity profile is easy to understand. Near the center of the laser beam, the power profile of the laser and hence the temperature profile of the heated sample are nearly parabolic. With a negative value of dn/dT, the refractive index profile very closely approximates to that of a high quality diverging lens [5].

In the thermal lens technique the sample is illuminated using radiation from a TEM_{00} or Gaussian intensity profile laser beam. Some of the radiation is absorbed by the sample or by chromophores within the sample. Excited states formed in this way may either lose energy radiatively, e.g., fluorescence or phosphorescence or by non-radiative routes, e.g., internal conversion or by interaction with other molecules in the sample which results in the generation of heat. These are often competing mechanisms. However, in nearly all situations where the quantum efficiency of fluorescence is less than, e.g., 0.95, some heat is evolved. Even if the quantum efficiency for fluorescence was unity, some heat would be evolved as a consequence of the Stokes' shift. The flow of heat from the region illuminated by the laser results in a thermal gradient proportional to the beam intensity profile in the sample which may be a solution, solid or gas. Heating is stronger at the center of the beam profile than in the wings and hence the thermal gradient in turn establishes a refractive index gradient. The coefficient of refractive index with temperature, dn/dT, varies for different materials, but is normally negative for gases and liquids and positive for solids. In the case of gases and liquids the refractive index gradient established by absorption and subsequent heating of the fluid in effect presents a graded index lens to the beam. As the beam passes through the fluid it progressively diverges and the degree of divergence depends on the power of the laser beam and the absorption coefficient of the sample. From this it is easy to see how the thermal lens effect can be used as an indirect method to determine absorbance and hence its potential as an analytical spectrometric technique.

4.3.1   Focal Length of the Thermal Lens

Fang and Swafford in 1983 [6] showed how to calculate the effective focal length of the index of refraction distribution brought about by thermal lens. This can be easily understood with the aid of the Figure 4.3.

Consider a medium of length l with refractive index n(r) that increases radially. It is assumed that l is less than the TL focal length, f. The optical ray
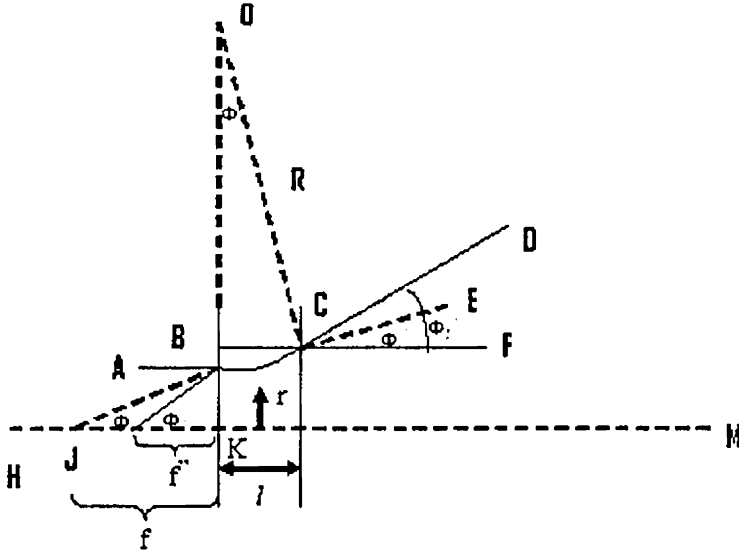
Figure 4.3: Diagram showing the focal length of the thermal lens

AB incident on the medium takes the curved trajectory BC inside the material. BC has a radius of curvature R. ϕ_1 is the angle with which the ray arrives at the right interface, but due to refraction it takes an angle ϕ_2 while moving out of the sample. The effective focal length of the medium is f. From geometry,

$$\phi_1 = \frac{BC}{R} = \frac{l}{R}$$

Therefore,

$$f' = -\frac{r}{\phi_1} = -\frac{rR}{l} \qquad (4.7)$$

but

$$\frac{f}{f'} = \frac{\phi_1}{\phi_2} = \frac{1}{n} \qquad (4.8)$$

combining these two, we get,

$$f = -\frac{rR}{nl}. \qquad (4.9)$$

The index or refraction of the cylindrically symmetric distribution can be written as a Maclaurin series in the radial displacement from the center of the

distribution,

$$n(r) = n(0) + r\left(\frac{\partial n}{\partial r}\right)_{r=0} + \frac{1}{2}r^2\left(\frac{\partial^2 n}{\partial r^2}\right)_{r=0} + \ldots \ldots \tag{4.10}$$

Such a derivative has vanishing first derivative at r=0. The radius of curvature R is given by

$$\frac{1}{R} = \frac{1}{n_0}\frac{\partial n(r)}{\partial r} = \frac{r}{n_0}\left(\frac{\partial^2 n}{\partial r^2}\right)_{r=0} \tag{4.11}$$

The focal length can now be obtained by using Equation 4.11 in Equation 4.9. Thus

$$\frac{1}{f} = -l\left(\frac{\partial^2 n}{\partial r^2}\right)_{r=0} \tag{4.12}$$

Incorporating the radial temperature variation, it can also be written as

$$f = -\left[l\left(\frac{\partial n}{\partial T}\right)\left(\frac{\partial^2 T}{\partial r^2}\right)_{r=0}\right]^{-1} \tag{4.13}$$

Thus the strength of the thermal lens depends on the temperature distribution in the sample. Usually both $\left(\frac{\partial n}{\partial T}\right)$ and $\left(\frac{\partial^2 T}{\partial r^2}\right)$ are negative in the case of liquid samples so that the thermal lens is divergent. ($f < 0$)

4.3.2 Restrictions imposed by the thermal lens model

There are several important restrictions implicit in the development of the thin lens approximation, the most crucial being on the path length of the sample cell. The model described earlier, assumed an index of refraction distribution which remains constant along the beam path through the cell, requiring that the laser beam remains reasonably well collimated over this distance. For this, the sample length should be a fraction of the confocal length of the incident beam. The depth of focus or Rayleigh range of a laser beam is related to the focal spot size ω_0 and the wavelength λ by

$$z_0 = \frac{k\omega_0^2}{2} \tag{4.14}$$

the parameter z_0, also called the confocal length, is the distance to which the beam expands from its minimum size to a radius $\sqrt{2}\omega_0$ [7] .

4.3.3 Continuous Wave Thermal Lens Spectrometry

For most analytical applications the preferred mode of operation is continuous wave (CW) and therefore the theoretical treatment given below relates to that mode. However, there are reports of the use of pulsed lasers as an excitation source (mostly in gas-phase work). It should be remembered that in both cases when a dual beam system is used the probe laser is always of CW. type. Similarly there are several reports of time-resolved CW- TLS in which the CW beam is periodically interrupted. This mode of operation enables the history of the thermal lens to be determined as it propagates through the sample and fundamental thermo-optical parameters of the sample to be determined, e.g., thermal diffusivity and conductivity. Perhaps this mode of operation is a good compromise between pulsed and CW operation for many applications, with the exception of those that require any short exposure times, e,g., absorption and luminescence lifetime studies. Some of these techniques are discussed here [10].

Thermal lensing, led to the observation of build-up and decay transients, mode changes, and relaxation oscillations, all with time constants of the order of seconds. The resulting investigation of this effect predicted that the most important application would be for the measurement of small absorbances. Using this intra-cavity set-up, Leite etal calculated the absorption coefficients for pure liquids, from the focal length of the induced thermal lens. Values ranged from $2.3 \times 10^{-4} cm^{-1} for CCl_4$ to $5.9 \times 10^{-4} cm^{-1}$ for CS_2. Solimini [11] measured the absorption coefficients of several pure organic liquids using the same technique as Leite and later published a comprehensive report on the accuracy and sensitivity of this method for measuring small absorption coefficients.

The biggest problem associated with the intra-cavity experiments was with the reproducibility of the results. This was due to the difficulty in controlling the parameters of such an experimental set-up. The first extra-cavity thermal lens was generated by Rieckhoff [12] who described the self-induced divergence of a CW He-Ne laser beam. However, the effect was explained in terms of non-linear absorption, without considering the possibility of weak linear absorption in a 'transparent' liquid. Although it is easier to place the sample cell outside the laser resonator, the power is much lower outside the laser cavity than inside. Hu and Whinnery [4] however, recognized that the greatest divergence of the laser beam could be attained for a given lens by positioning that lens at the point of minimum radius of curvature of the beam wave fronts, i.e., at a distance of one confocal length (z_0) from the minimum beam waist, ω_0 of the laser. The degree of divergence could be monitored by noting the transient changes in intensity at the beam center, using a pinhole positioned on the beam axis, in front of the

photodetector.

In its simplest form a single CW TEM_{00} laser beam with a Gaussian intensity cross-section passes through an absorbing medium. A part of this laser beam energy is absorbed by the sample which subsequently produces a thermal lens. The steady-state focal length of the induced lens, in the parabolic approximation, is given by equation,

$$f_\omega = \frac{\pi k\, \omega_e^2}{2.303\, P_e \left(\frac{dn}{dT}\right) A} \tag{4.15}$$

where k is the thermal conductivity of the sample, P_e is the laser excitation power and A is the absorbance of the sample. Thus as P_e, dn/dT, and 'A' get larger, the focal length of the lens gets shorter and the beam divergence increases. In a typical experimental set up, the divergence of a single beam passing through the solution can be measured simply by placing a pinhole over the photo detector in the far field at the center of the diverged beam. As the beam energy is spread over a larger area, the photo detector signal falls. Alternatively a linear array photo detector array may be employed to image a cross-section of the beam or the entire area. Analysis of Equation 4.15 shows that the sensitivity of the thermal lens technique is directly proportional to the excitation laser power and on the thermo-optical properties of the solvent. Thus in principle higher sensitivity can be obtained by increasing the power of the excitation laser and by choosing an appropriate solvent. Indeed, trace analysis has been carried out on solutions with an absorption coefficient of $10^{-7} cm^{-1}$, which is three to four orders of magnitude better than what can be achieved with conventional UV/VIS spectrophotometry. This enhancement is not always available, however, as competing energy loss mechanisms, e.g., fluorescence, photochemical reactions and convection effects are often seen. In addition, in many spectrophotometric systems with high reagent blank absorption, the noise associated with the excitation laser can degrade signal-to-noise ratios. When comparing TLS in the UV/VIS region with UV/VIS spectrophotometry, we can consider the basic equations that describe the analytical signal response. Thus in UV/VIS spectrometry the absorbance, A, of a solution is given by Beer's Law [14]

$$I = I_0 e^{-A} \tag{4.16}$$

where I is the initial intensity and A = eCl, where e is the molar absorption coefficient, C is the concentration of the solution and l is the path length of the absorbing cell. For a weakly absorbing solution the relative change in signal,

ΔI, can be written as

$$\Delta I = I_0 A$$

or

$$S_A = \frac{\Delta I}{I_0} = A.$$

In TLS the thermal gradient established after optical absorption and thermal relaxation of the sample results in a change in intensity at the beam centre owing to the induced beam divergence. Thus the time dependent I(t) signal can be written as

$$I(t) = I_0 \left[1 + \frac{S_{TL}}{(1 + t_c/t)} \right] \tag{4.17}$$

where t_c, is a characteristic time constant and S_{TL} is the relative change in signal measured at t = 0 and for $t \gg t_c$ and

$$S_{TL} = \frac{\Delta I}{I} = \frac{P_e(dn/dT)A}{\lambda_p k} \tag{4.18}$$

where P, is the power of the excitation laser (in W), dn/dT is the refractive index temperature coefficient, λ is the wavelength of the probe laser (or excitation laser in a single-beam system) and k is the thermal conductivity of the solvent. This is often referred to as the enhancement factor (E) over absorbance, i,e.,

$$E = \frac{\Delta I}{I} = \frac{P_e(dn/dT)}{\lambda_p k}. \tag{4.19}$$

Generally non-polar solvents (e.g., benzene, carbon tetrachloride) are the best media for sensitive thermal lens measurements owing to their high values of dn/dT and low k values. For benzene dn/dT is $-6.4 \times 10^{-4} K^{-1}$ and k is $14.42 \times 10^{-4} W cm^{-1} K^{-1}$, whereas for water, the most useful and widely encountered solvent, these values are $-0.8 \times 10^{-4} K^{-1}$ and $59.45 \times 10^{-4} W cm^{-1} K^{-1}$, respectively. In terms of thermal lens spectrometry water is not an ideal solvent. Therefore a typical value of E for water is 0.22 mW^{-1} determined using the Ar ion line at 514.5 nm. Thus to achieve a ten-fold theoretical enhancement in sensitivity over UV/VIS spectrometry, one would require an excitation beam power of 45 mW. The parabolic approximation summarized above makes several assumptions that are justifiable for single-beam experiments or for two-beam experiments. The two beam experiments utilize a pump laser for excitation and a different lower-powered laser to probe the thermal lens formed by the pump laser. Usually, the probe laser is arranged to be coaxial with the pump laser in the absorption cell [8, 9]. It is assumed that no appreciable convection takes

place in the cell and that radial heat conduction dominates until a steady-state
temperature gradient is established under these conditions. It is also assumed
that the probe beam diameter does not exceed the pump beam diameter in the
sample cell interaction volume and therefore the Gaussian beam near its axis
can be approximated to be parabolic. This approximation in fact holds until r,
the radial distance from the beam center equals the beam radius ω_0, defined as
the position where the intensity has fallen to $1/e^2$ of its peak value at the beam
center. When r = ω_0, (r/w = 1) 87% of the light energy is included in this radius
and the resultant lens shows little spherical aberration. The parabolic model is
not completely quantitative. The remaining 13% of energy that lies outside r =
ω_0 causes aberrant effects, especially in the wings of the beam profile. Sheldon
et al. were the first to consider the aberrant nature of the thermally-induced
lens. Rather than defining an expression for the focal length of the induced lens
these authors used diffraction theory to find the intensity at the beam centre in
the far-field after it had passed through the sample. Evaluation of the appro-
priate diffraction integrals leads to an expression for the relative change in the
beam centre intensity [10].

$$\frac{I(\theta) - I(\infty)}{I(\infty)} = \frac{1}{1 - \theta \, tan^{-1}\left(\frac{2\zeta}{3+\zeta^2}\right)} - 1 \qquad (4.20)$$

where ζ is a geometrical factor such that when $\zeta = \sqrt{3}$ the cell is located at
$\sqrt{3}$ times the confocal distance in front or behind the beam waist. Sheldon
concluded that at this position the thermal lens effect is optimized. In this
expression θ is proportional to

$$\frac{P_e \, (dn/dT)A}{\lambda \, k}.$$

The parabolic and aberrant lens models were both derived for single-beam sit-
uations and are therefore only useful in single-beam experiments or coaxial
two-beam experiments in which the probe beam and pump beam radii are the
same in the sample cell. In practice greater sensitivity can be achieved using
two-beam configurations in which the focal points (or beam waists) of the pump
and probe beam are displaced. Fang and Swofford postulated that mismatched
waists in a two-beam system (i.e., probe and pump beam waists noncoincident)
would offer enhanced sensitivity but failed to carry out any systematic study
into the potential of such a geometry [15]. Berthoud et al. however, under-
took such an investigation and derived a theoretical, though semi quantitative,

model to describe experimental data produced by a mode-mismatched investigation. In practice the result of these studies is that maximum sensitivity is also obtained in the two-beam configuration when the excitation or pump beam is focused in the sample and the beam waist of the probe beam is arranged to be at a distance of z_0, before that point, where z_0, is the confocal distance for the probe.

4.4   Conclusions

Thermal lens spectroscopy can provide sensitive analytical measurements of absorbing species in a wide range of sample types. In addition, the technique provides method for measurement of certain absolute values of optothermal properties such as absorption coefficients, quantum efficiencies of luminescence and thermal processes as well as thermal properties of materials. The use of TLS as a diagnostic tool for these purposes is extremely important owing to the simplicity of construction of the instrumentation and ease of use of theoretical treatments. Clearly, for analytical purposes, the key to successful exploitation of the technique is provision of cheap, robust, tunable lasers in the visible spectrum with good beam quality. As yet diode lasers seem to offer the best hope for such a source.

References

[1] Fang. H and Swofford. R.L, In *Ultrasensitive Laser Spectroscopy*(D.S.Kliger Ed), (1983), Academic Press, New York

[2] A.C.Tam in *Photothermal Investigations of Solids and Fluids*, Ed Jeffrey A. Sell, Academic Press, Inc., New York, (1989)

[3] Nijmeijer M.J.P., Bakker A.F. and Bruin C., *J. Chem. Phys.*, 89, (1988) p.3789

[4] M. Depriester, P. Hus, S. Delenclos, and A. Hadj Sahraoui, *Rev. Sci. Instrum.*, 76, (2005) p.074902

[5] Dovichi, N. J., *CRC Crit. Rev. Anal. Chem.*, 17, (1987) p.357

[6] H. L. Fang and R. L. Swafford, "*The Thermal Lens in Absorption Spectroscopy,*" in Ultrasensitive Laser Spectroscopy, D. S. Kliger, Ed. (Academic, New York, 1983), Chap. 3, p. 175

[7] Gordon, J. P., Leite, R. C. C., Moore, R. S., Porto, S. P. S., and Whinnery, J. R., *Appl. Phys.*, 36, (1965), p.3

[8] Aihua Xie,Lex van der Meer,Wouter Hoff,Robert H. Austin, *Phy. Rev. Lett,*, 84(23),(2000) p.5435

[9] D. H. Hurley and K. L. Telschow, *Phy. Rev. B*, 66, (2002) p.153

[10] Sheldon, S. J., Knight, L. V., and Thorne, J. M., *Appl. Opt.*, 21, (1982) p.1663

[11] Baesso, M. L., Shen, J., and Snook, R. D., *J. Appl. Phys.*, 75(8), (1994) p.3732

[12] K. E. Rieckhoff, *Appl.Phys. Lett.*, 9, (1966) p.87

[13] C. Hu, J.R. Whinnery, *Applied Optics*, 12, (1973) p.72

[14] Fang, H. L., Gustafson, T. L., and Swofford, R. L., *J. Chem. Phys.*, 78, (1983) p.1663.

[15] Georges, J., *Spectrochim. Acta Rev.*, 15, (1993) p.39

Chapter 5

Thermal Lens Technique for Calculation of Fluorescence Quantum Yield

"No great discovery was ever made without a bold guess."- Isaac Newton

ABSTRACT

Application of dual beam thermal lens technique to determine the fluorescence quantum yield of certain materials is described in this chapter. A chemical schiff base and rhodamine 6G dye in silver sol environment are used as examples. Extensive fluorescence studies were carried out in the schiff base and the results are presented in detail. The determination of the effect of silver sol on both the absolute fluorescence quantum yield and the thermal lens signal intensity, and its reasons are explained.

5.1 Introduction

Fluorescence quantum yield (Q_f) is one of the most important properties of fluorescent materials. It is a measure of the rate of nonradiative transitions that compete with the emission of light. From both theoretical and practical points of view, fluorescence quantum yield values are important. For example, they provide information on radiationless processes in molecules and in the assignment of electronic transitions. It is also of use in fluorescence studies of materials, for determining their purity, and for judging their suitability as wavelength shifters and laser media. Its significance is well recognized in the studies of organic

laser dyes because the knowledge of Q_f of such dyes and their concentration dependence are essential for selecting efficient laser media. It is well known that the conventional measurements of Q_f require the use of accurate luminescence standard samples and comparison of the given sample with such a standard, for which the fluorescence yield is known [1]. However, the reliability of such relative determinations is limited both by the accuracy of the standard yield value and by the confidence that can be placed on the comparison technique. Even after making various corrections for system geometry, re-absorption, polarization, etc., the accuracy of the quantum-yield values obtained from photometric measurements is rather poor. Effectiveness of a material to use as a laser medium depends on the knowledge of absolute fluorescence efficiency rather than relative values. In order to evaluate absolute quantum efficiency, we have to consider both the radiative and nonradiative processes taking place in the medium. As the contribution from nonradiative processes is not directly measurable using the traditional optical detection methods, thermo-optic techniques such as photoacoustic and thermal lens methods have been adopted for this purpose [2, 3]. Measurements based on photothermal effects are capable of giving fluorescence yields of highly fluorescent solutions as well as solids with high accuracy and reproducibility.

5.2   Evaluation of Fluorescence Quantum Yield Using Thermal Lens Technique

It was Hu and Whinnery who pointed out that when combined with conventional transmission data, a thermal blooming measurement permits calculation of luminescence quantum yield [4]. Brannon and Magde presented a detailed theory for the calculation of the luminescence quantum yield and reported successful results with experiments on fluorescein [5]. However, these were all essentially single-beam thermal lens methods, where an auxiliary lens of suitable focal length was used to create a beam waist in the laser beam. Usually the sample cell is centered one confocal distance past the lens focus, where the laser-beam size is $\omega = 2\sqrt{\omega_0}$, where ω_0 is the minimum beam-waist radius. At this point the fractional change in the radius of curvature of the laser beam is largest, for a given lens. The formation of a thermal lens will expand the beam radius, which can be detected at the far field as a corresponding reduction in the detected power. The thermal lens signal is given by the fractional change in the detected power at the far field or in terms of the change in the beam area

[6].

In the case of experiments where we have to change the excitation wave-length, the detector should be carefully chosen and corrected taking into account its wavelength response. The above problem can be overcome by the dual-beam technique [7, 8]. The advantage is that the detection optics and the detectors can be optimized for a single convenient probe wavelength. This is particularly useful in recording thermal lens absorption spectra. The dual-beam thermal lens method has been used by various researchers for the determination of fluorescence quantum yield, to detect small absorption, to record the thermal lens spectra, and for the determination of various thermo-optic parameters like thermal diffusivity, temperature coefficient of refractive index etc. [9, 10, 11]

5.2.1   Theory

The theory is developed based on the fundamental and simple concept of energy conservation [12, 13, 14]. If P_0 is the power of the incident excitation beam and P_t, the power of the transmitted beam, the absorbed power is the sum of the luminescence emission power P_f and the thermal power degraded to heat P_{th}, provided that no photochemical reaction is present. Hence,

$$P_0 = P_t + P_f + P_{th}. \tag{5.1}$$

In the case of a completely fluorescence quenched sample, we can consider the entire excitation energy to be converted into nonradiative relaxation process and hence, the fluorescence quantum yield Q_f is given by,

$$Q_f = \frac{P_f}{AP_0} \frac{\lambda_f}{\lambda} = \left(1 - \frac{P_{th}}{P_\alpha}\right) \frac{\lambda_f}{\lambda} \tag{5.2}$$

where $P_\alpha = AP_0$, A being the absorbance of the sample and the ratio of the peak fluorescence wavelength λ_f to the excitation wavelength λ takes account of the Stokes shift. P_{th} is directly proportional to the TL signal η and P_α is proportional to TL signal η_α corresponding to the concentration at which the fluorescence intensity is quenched completely. The quantum efficiency can be calculated by the equation

$$Q_f = \frac{\lambda_f}{\lambda} \left(1 - \frac{\eta}{\eta_\alpha}\right). \tag{5.3}$$

Thus by performing thermal lens experiment at various concentration of the sample, one can calculate the value of Q_f using the above equation. The same
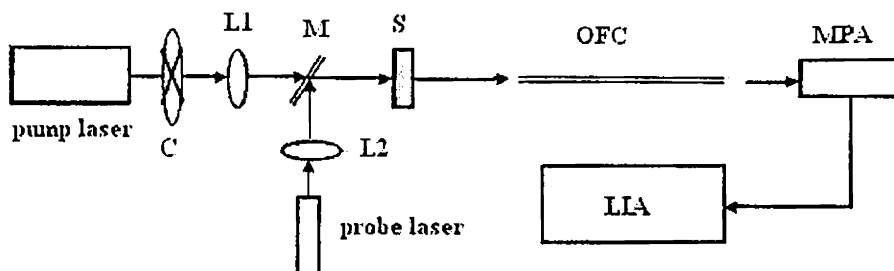
Figure 5.1: Experimental set up for dual beam thermal lens technique

sample at a higher concentration is used as the reference material for quenched sample that gives the values of η_α. This is described in detail in the subsequent sections.

5.2.2 Experimental Set up

Figure 5.1 shows the experimental set up of the pump-probe thermal lens experiment [15]. Two different excitation sources (pump laser) were used for these studies; one a continuous wave (CW) Diode Pumped Solid State laser (DPSS, $NdYVO_4$) that generates the pump field in the wavelength region of 532 nm with average power 50 mW and another Ar-ion laser (CW) with emission wavelengths in the range of 457 nm to 514 nm with average power of around 300 mW. The pump beam passes through a chopper C operating at low frequency (8 Hz). It is focused using an achromatic lens L1 of focal length 35 cm. The probe beam is a CW 1 mW He-Ne laser operating at 6328 Å. Using the dichroic mirror M and lens L2 the probe beam is focused into the sample cell. The dichroic mirror is used to make the two beams collinear. After propagation through the sample, the probe beam is directed to the detector. The thermal lens is detected by sampling the intensity at the center of the probe beam by coupling it to the detector system by an optical fibre, OFC. It also acts as a small aperture and makes the experimental system more flexible. If the pump beam is not completely absorbed by the sample, it will also reach the detection system and this is eliminated by the use of a monochromator which is set to detect the wavelength 6328 Å of the probe. The detection system consists of a Monochromator PMT assembly, MPA, (McPherson 275 with the model 789 A controller) and a lock-in amplifier, LIA, (SR 850 DSP). For fluorescence studies the front surface emission is collected and focused by a convex lens of focal length 10 cm and

coupled to the same detection system. The fluorescence emission is wavelength scanned in the region from 520 nm to 570 nm.

5.3 Measurements of Q_f in Hydroxy Phenyl Iminomethyl Phenol (HPIMP)

Characteristics of ligands and schiff bases in chemical complexes are important in understanding the nature and structure of compounds. This will also be of much use in understanding some of the finer aspects of light - matter interactions. One of the tools in such studies is the optical absorption spectroscopy. Some of the ligands or the schiff bases are fluorescing. In such cases, study of fluorescence emission will provide some valuable information such as using the sample as laser media. Photothermal lensing spectroscopy (PTLS) is a sensitive technique to evaluate fluorescence quantum yields of such potential laser media. It is an important tool in non-destructive studies of various materials. In PTLS, absorption of a laser beam results in an increase in temperature of the irradiated region. It is normally accompanied by a decrease in refractive index of the medium. This gradient in refractive index $\partial n(r,t)/\partial t$ follows the spatial profile of the pump beam, which is Gaussian. This non-uniform refractive index produces a lensing effect, which can be detected using another laser acting as a probe beam. When the probe laser source which is amplitude modulated at frequency ω is used, we can make phase sensitive detection, i.e. the signal at frequency ω having a definite phase with respect to the source can be detected. When radiative de-excitation mechanisms are absent, the absorbed light will produce an increase in temperature, due to thermal energy transfer. However, when fluorescence is present, it will be complementary to the photothermal relaxation processes and therefore PTLS along with fluorescence measurements helps in the determination of the absolute fluorescence quantum yield, Q_f.

5.3.1   Preparation and Chemical Characterization

The schiff base 2-hydroxyphenyl imino methyl phenol (HPIMP) was synthesized using aminophenol and salicylaldehyde. Salicylaldehyde (1mM) in methanol was refluxed with o-amino phenol (1mM) for 2 hours. The reaction mixture was cooled, filtered, collected and recrystallized from methanol. Its chemical structure is shown in Figure 5.2(a). An energy level diagram as mentioned chapter 3, with five levels S_0, S_1, S_2, T_1 and T_2 can be used in this case also, to account for the two peaks in the absorption spectrum. The sample was dissolved
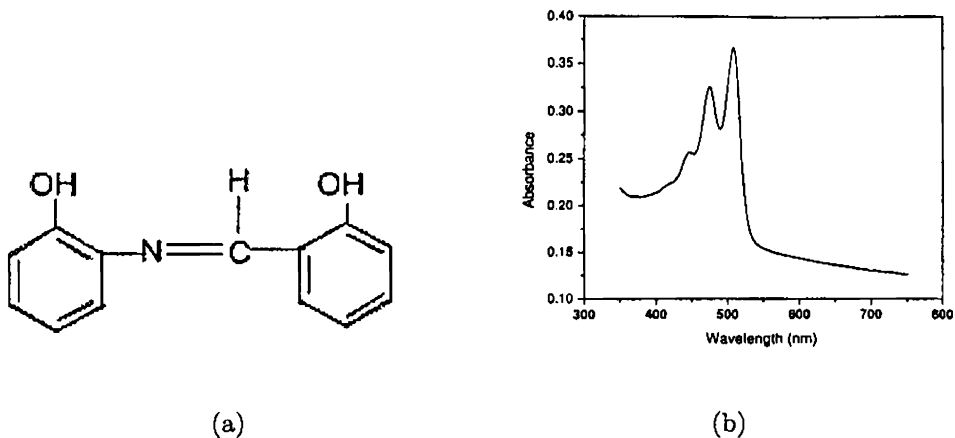
Figure 5.2: (a) Chemical structure of 2-hydroxyphenyl imino methyl phenol(HPIMP) (b) Absorption spectrum of HPIMP

in chloroform and filtered carefully to get the stock solution.

There are schiff bases having important applications in medicine and biotechnology. For example, a thiosemicarbazone possessing antitumor activity against L1210 leukaemia in mice was reported [16]. In addition, 2-acetylpyridine thiosemicarbazone is a class of compounds that has shown a broad spectrum of chemotherapeutic properties, including antimalarial and antitumor activity as well as antibacterial, antitrypanosomal, and antiviral activities. The therapeutic application of the compounds are not explored in the studies presented in this thesis, instead, more emphasize is given to photonic-based applications. The sample for the TL and fluorescence studies was prepared by diluting the stock solution to the required concentration. The absorption spectrum shown in Figure 5.2(b) was taken using a Jasco V570 UV-VIS spectrophotometer. The most important characteristics of the sample is that it is extremely stable in its optical and physical properties. Apart from its highly fluorescing nature, there is not much degradation in its fluorescence intensity with time. Its suitability as a laser dye can be assessed by carrying out photostability and gain studies.

5.3.2   Fluorescence Studies in HPIMP

Fluorescence is the emission of photons, which results from the transition of the molecule from electronically excited singlet state to the ground state. Such transitions are quantum mechanically allowed and have a typical emissive rate
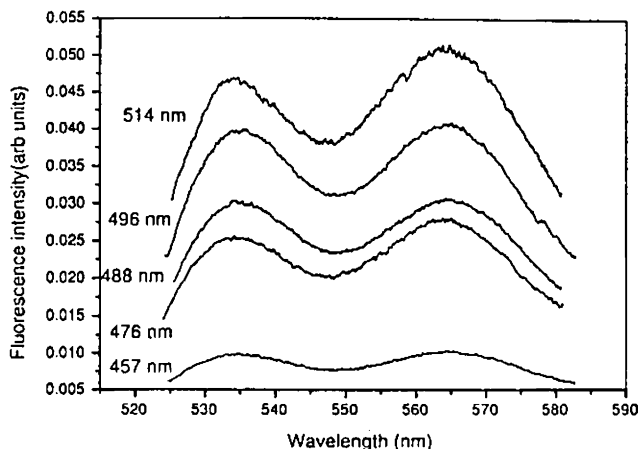
Figure 5.3: Fluorescence spectrum of HPIMP using five wavelengths of excitation from the Ar-ion laser

of 10^8 s^{-1}. Fluorescence quenching is the process which decreases the fluorescence intensity of a given substance. This obviously increases the non-radiative transition [17]. Fluorescence measurements were carried out using an Ar-ion laser.

Typical fluorescence spectra obtained by excitation with five wavelengths from the Ar laser are shown in Figure 5.3. The spectrum is invariant with respect to excitation wavelength, with the exception that the relative intensities reflect the wavelength dependence of the absorption coefficient. The excitation spectrum clearly explains this observation. Under the same conditions, the fluorescence-emission spectrum is independent of the excitation wavelength, due to the partial dissipation of excitation energy during the excited-state lifetime. The emission intensity is proportional to the strength of the absorption at the excitation wavelength. When an aromatic chromophore in solution, such as a dye, is excited by visible light, the transition will be to various vibronic levels of the first excited singlet state S_1. Molecules in the higher vibronic levels of S_1 will decay through nonradiative relaxation to lower vibronic levels of S_1. This means, for every excited state of energy $E(S_{\nu'})$, that fraction of the energy corresponding to $(E(S_{\nu'}) - E(S_{\nu''}))/E(S_{\nu'})$ will immediately appear as heat coming from the sample. Radiative relaxation from $S_{1\nu''}$ to one of the vibronic levels of S_0 will result in fluorescence emission. Fluorescence emission is affected by a variety of environmental factors, like interactions between the

Concentration (μM)	514 nm	496 nm	488 nm	479 nm	457 nm
17.8	528.2	528.2	528.2	528.1	528.1
49.7	532.2	532.2	532.2	532.7	532.5
70.9	532.0	532.2	532.0	532.0	532.0
128	534.5	534.5	534.8	534.5	534.5
159.5	535.9	536.1	535.9	535.5	535.6
212.6	538.3	538.2	538.0	538.4	538.0
319	539.3	539.4	539.2	539.2	539.2

Table 5.1: Variation of peak fluorescence wavelengths of HPIMP at various excitation wavelengths

fluorophore and surrounding solvent molecules (dictated by solvent polarity), other dissolved inorganic and organic compounds, temperature, pH, and the localized concentration of the fluorescent species. There is an important parameter in the fluorescence studies, namely the Stokes shift, which represents the energy lost while the molecule was in the excited state. It is important for many reasons but, from a practical point of view, it allows the emitted fluorescence photons to be easily distinguished from the excitation photons, leading to the possibility of very low backgrounds in fluorescence studies. A high value of polarity of the solvent molecules will increase the Stokes shift, usually by several tens of nanometers. The relative polarity of chloroform, which has been used as a solvent in our case, is only 0.259, which is rather too low to have any appreciable effect on this shift. It was also observed that there is a concentration quenching of fluorescence. The variation of peak fluorescence wavelength with concentration is shown in Table 5.1. For all the excitation wavelengths that we have considered, the change in Stokes shift is almost 11 nm in the concentration range in which the study was conducted. The effects of the environmental parameters on fluorescence vary widely from one fluorophore to another. The absorption and emission spectra, as well as the quantum yields, can be heavily influenced by environmental variables. In fact, the high degree of sensitivity in fluorescence is primarily due to interactions that occur in the local environment during the excited-state lifetime. A fraction, $1 - Q_f$, of all the energy absorbed by $S_1 \leftarrow S_0$ transitions will appear as heat. The photothermal lensing signal will be proportional to the total heat emitted by the sample excited to the S_1 state.

The fluorescence and thermal lens measurements of HPIMP were carried out for various concentrations using the method described earlier. The fluo-
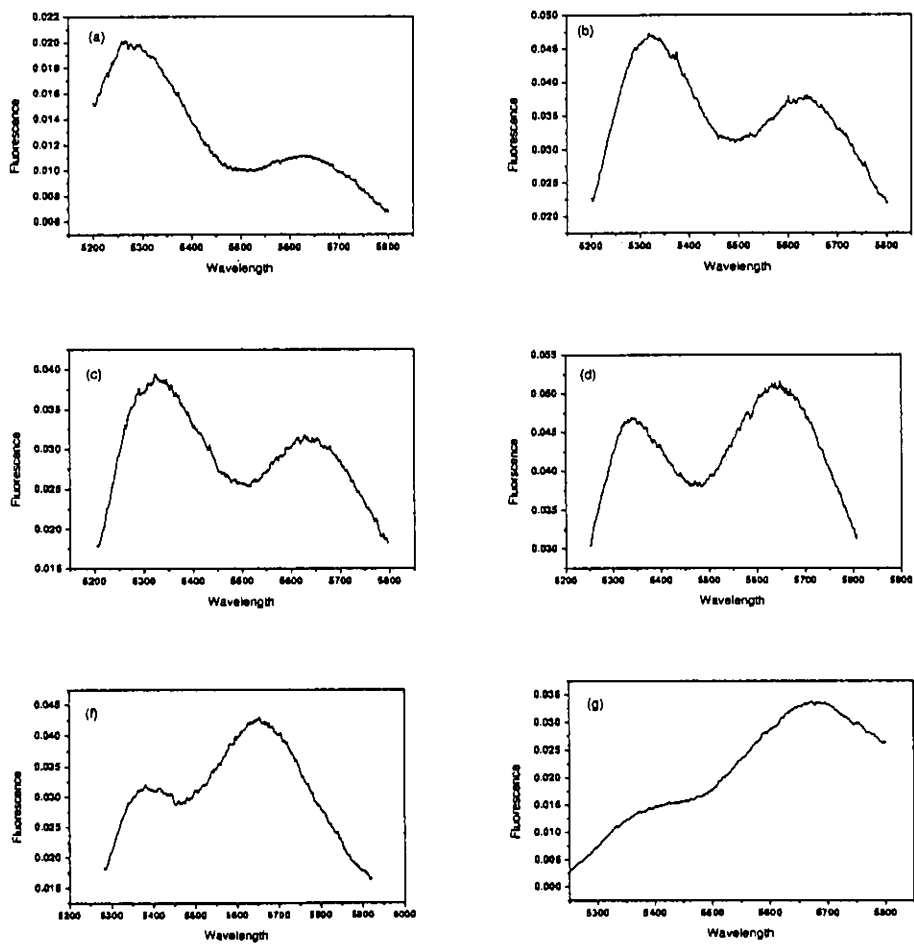
Figure 5.4: Concentration dependence of fluorescence spectrum of HPIMP using 514 nm excitation (a) 0.3775 g/lit (b) 1.059 g/lit (c) 1.51 g/lit (d) 2.72 g/lit (e) 3.4 g/lit (f) 4.53 g/lit

rescence spectra shows a very interesting characteristic, with dual peak, one centered around 530 nm (SE) and the other one at 560 nm (LE). The relative intensities are concentration dependent, the SE band weakens and the LE band gets stronger with concentration. (Figure 5.4). Usually, an essential role in the formation of LE band is played by two different processes [18]: dielectric relaxation of the solvent polar molecules around the fluorophore and the twisted intramolecular charge transfer, which can occur only in liquid samples. The usual concentration quenching of fluorescence is observed in this case also as seen in the Figure 5.5. This is plotted for the wavelength 514 nm and 496 nm of the Ar laser, showing the decay of both the SE (538 nm) and the LE (565 nm) emissions.
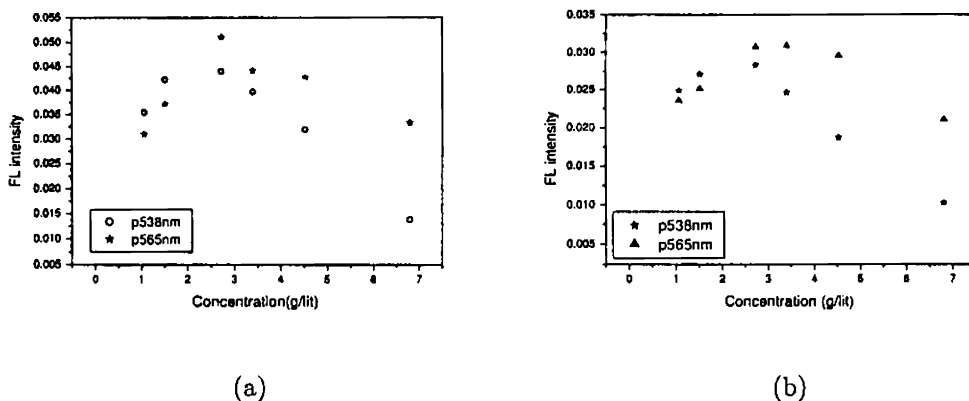

(a)   (b)

Figure 5.5: Concentration dependence of peak fluorescence intensity at (a) 514 nm and (b) 496 nm.

5.3.3   Fluorescence Quantum Yield of HPIMP

To calculate Q_f, one must measure the thermal lens signal intensity for all the concentration at which fluorescence spectrum was recorded. The dependence of the thermal lens signal on concentration and on excitation wavelength is as shown in Figure 5.6(a). The graph shows a large signal for the highest frequency of excitation, which is complemented by a smaller fluorescence signal at this frequency as seen from Figure 5.6(b). This can take place when the excited molecule undergoes a radiationless transition to the various lower vibrational levels of S_1 or if there is energy transfer to a nearby chromophore (energy transfer ET) or intersystem crossing (ISC) to a triplet state. The thermal lens

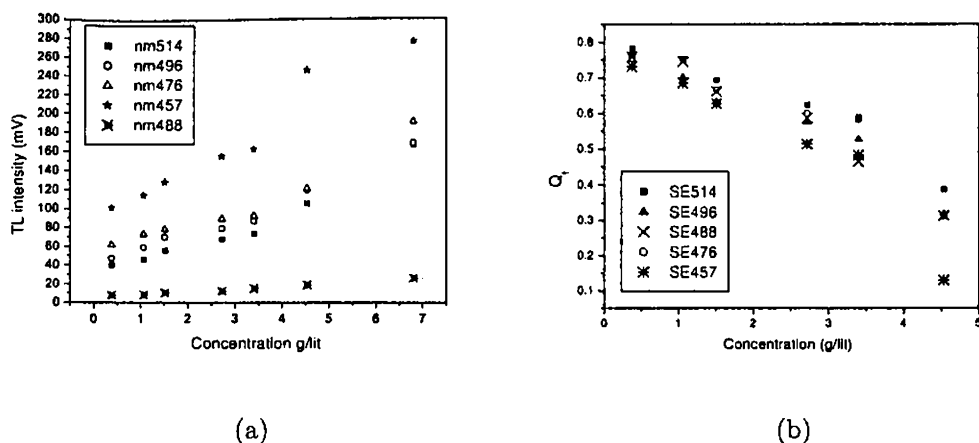(a)   (b)

Figure 5.6: (a) Thermal lens signal intensity and (b) Fluorescence quantum yield of HPIMP for all excitation wavelengths of Ar laser given as a function of concentration. The error in the calculated values are in the range from 12% to 27%.

was produced by the excitation of the sample with a continuous-wave (CW) argon-ion laser that generates the pump field at wavelengths 457 nm, 476 nm, 488 nm, 496 nm, and 514 nm. The power was attenuated to 5mW for all these wavelengths so as to avoid aberration in the signal due to full-wave shifts. In addition, at these power levels we expect no multiphoton processes or nonlinear effects in the medium. The pump beam is intensity modulated using a chopper operating at a low frequency of 8Hz (model SR 540). This frequency was selected because we found that the maximum thermal lens signal will be obtained at this chopping frequency. The formation of the thermal lens was probed with an intensity-stabilized He-Ne CW laser (JDS Uniphase model 1507) as explained earlier, with the power attenuated to 1mW. The absorption of the molecule at the probe wavelength is negligible compared to that at the pump wavelengths. Both the pump and the probe were focused using the same lens of focal length 35 cm, forming a mode matched configuration, and are made collinear by a dichroic mirror. The sample was placed in a quartz cuvette of path length 1 cm and positioned at one confocal distance past the beam waist of the probe beam. This position which gives maximum value for TL signal, was determined by recording the signal intensity at various sample positions along the pump beam path. The formation of the thermal lens causes the probe beam to expand and is detectable at the far field. This is detected as a change in the output voltage of a photomultiplier tube (PMT). The signal was processed using lock-in

amplifier and thus the values of η and η_α are obtained. The characteristics of fluorescence spectrum is independent of the excitation wavelengths, but the obtained intensity is more for higher wavelengths of excitation. It can be assumed that, the higher energy levels that are populated by the laser excitation, favor non-radiative decay, that results in reduced fluorescence. It has further been observed that the thermal lens signal increases with the energy of excitation.

The calculated quantum yield is highest for a concentration of 0.3775 g/lit, and varies slightly with excitation wavelength. It is seen that at higher concentrations the yield is significantly lower for 457-nm excitation. One reason is the increased probability of nonradiative de-excitation, which results in a higher thermal lens signal as seen from Figure 5.6(a). The complementary nature of TL and fluorescence signals is also clear from Figures 5.6(a) and 5.6(b), in which there are clear enhancements in the TL signal with rise in concentration, which also results in strong fluorescence quenching. To determine the cross section for other nonradiative decay processes like resonance energy transfer to other fluorophores, triplet to triplet excitation, etc.,more detailed structural and chemical analysis is necessary. It is assumed that the aggregation of the compound in solution is negligible.

5.3.4   Energy Transfer Processes in HPIMP

The observations of fluorescence spectrum show the usual concentration dependent red shift in the fluorescence emission. This effect can be explained on the basis of solvent relaxation and Stokes shift. It has been observed that the peak fluorescence wavelength increases with concentration of the dye. This implies a loss of energy of the emitted photons or an increase in Stokes shift with concentration. This is due to several dynamic processes which include energy losses due to dissipation of vibrational energy, redistribution of electrons in the surrounding solvent molecules induced by the altered dipole moment of the excited fluorophore, reorientation of the solvent around the excited state dipole, and interactions between the fluorophore and the solvent or the solute. The relative intensity of the LE and SE are concentration dependent. As the concentration increases the intensity of the LE increases and that of SE decreases. This can be seen from the Figure 5.4. It can also be seen that the concentration quenching of SE is faster. The collissional de-excitation increases with concentration. The absorption spectrum of the material shows a clear peak structure representing transition between vibronic levels of S_0 and S_1. As in the usual case, fluorescence spectrum is the mirror image of the absorption spectrum. As con-

centration increases, the intensity of LE peak increases with respect to that of the SE peak. This is due to collissional non radiative relaxation of the vibronic levels of S_1.

5.4 Effect of Silver Nanosol on FQY of Rh6G

The application of dual beam thermal lens technique for the determination of the effect of silver sol on the absolute fluorescence quantum yield of the laser dye rhodamine 6G is discussed in this section. A 532-nm radiation from a DPSS laser was used as the excitation source. It has been observed that the presence of silver sol decreases the fluorescence quantum efficiency. This is will have a very important consequence in enhancing Raman scattering which is an important spectrochemical tool that provides information on molecular structures. We have also observed that the presence of silver sol can enhance the thermal lens signal which makes the detection of the signal easier at any concentration.

5.4.1 Important Applications of Silver Nano Particles

Nano particles have a variety of unique spectroscopic, electronic and chemical properties due to their small size and high surface to volume ratios. Nano structured noble metals have very important applications in diverse fields as photovoltaic, catalysis, electronic and magnetic devices etc. The coherent oscillation of the free electrons in the conduction band exhibits surface plasmon oscillation and the resulting absorption is called surface plasmon absorption. In the case of noble metal nano particles the surface plasmon absorption band appears in the visible region. Because of this, the optical properties of noble metal nano particles have received considerable attention. They have a very important role in enhancing the Raman scattering and thus to provide important contribution towards sensing and bio-medical applications. It also helps in determining the molecular structure of specific analyte molecules. However it is inherently a weak effect, often masked by fluorescence. Raman scattering can be enhanced either by resonance or by surface enhancement. In resonance enhancement the laser frequency is tuned to an energy transition of the analyte. In surface enhancement the analyte is adsorbed onto a suitable metal surface. It should also be possible to enhance it, if fluorescence could be reduced by some method. The objective of our experiment is to find out the role played by silver sol in the fluorescence efficiency of rhodamine 6G which is a Xanthene dye, having very high quantum yield.

5.4.2   Preparation and Characterization of Silver sol

Reagents - Double distilled water was used throughout the experiment. Analytical grade silver nitrate (99.5% Merck), extra pure Sodium Borohydride (95%, SRL), rhodamine 6G (LOBA) are used as received. Silver hydrosol is prepared by reducing $AgNO_3$ with sodium borohydride. For this both solutions are prepared in double distilled water and chilled by ice-cold water prior to mixing. $AgNO_3$ is added to $NaBH_4$ solution by drops from a burette while continuously stirring by a magnetic stirrer [10].

The formation of silver sol is indicated by the change in color of the solution. At the end point the solution becomes light yellow. The steady state absorption spectrum (taken using a spectrophotometer, Jasco-V-570) of the prepared Ag colloidal solution has a single peak at 410 nm as shown in Figure 5.7(a), which is in agreement with the reported value and consists of roughly spherical Ag particles of diameter in the range 1-50 nm. The colloid thus prepared is yellow in color and is stable at room temperature for several weeks. The sample solution is prepared by an accurately weighed amount of rhodamine 6G and dissolving it in double distilled water to obtain stock solution of concentration 10^{-2} molar. From this stock solution, samples of various concentrations in the range from 10^{-3} M to 10^{-6} M are prepared. For comparative studies, dye solutions of equal concentrations are prepared both in the presence of silver sol and in the absence of it.
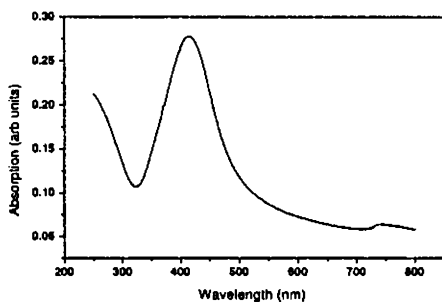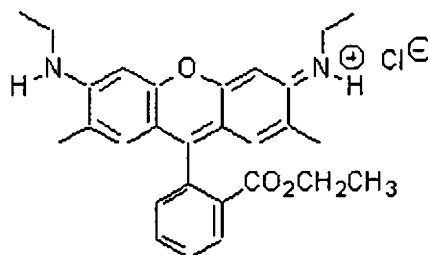
(a)   (b)

Figure 5.7: (a) Absorption spectrum of silver sol showing the plasmon resonance peak at 410 nm (b) Chemical structure of rhodamine 6G

5.4.3   Structure and Spectroscopic Properties of Rh6G

Rhodamine is a family of related chemical compounds, xanthene dyes. Examples are rhodamine 6G and rhodamine B. It is often used as a tracer within water to determine the rate and direction of flow and transport. Rhodamine dyes are generally toxic, and are soluble in water, methanol, and ethanol. Rhodamine 6G is also known as rhodamine 590, R6G, Basic rhodamine Yellow, or C.I. 45160. Its chemical structure is (Molecular Formula: $C_{28}H_{31}N_2O_3Cl$) shown in Figure 5.7(b). It is a highly fluorescing dye, often used as fluorescence standard. Rhodamine 6G is a laser dye, widely used in systems pumped by the second harmonic from an Nd:YAG laser. This is because it has a remarkably high photostability, high quantum yield, low cost, and its absorption maximum is close to the second harmonic of Nd:YAG (approximately 530 nm). The lasing range is 555 to 585 nm with a maximum at 566 nm.

5.4.4   Fluorescence Studies on Rh6G in Silver sol Environment

Fluorescence and thermal lensing studies were carried out for the laser dye Rhodamine 6G dissolved in double distilled water in the presence and also in the absence of silver sol, for a wide range of concentrations and also for various values of pump power. The excitation wavelength used was 532 nm. The absorption spectrum of silver sol shows a peak at 410 nm and its absorption at the excitation wavelength is too small to be taken into account.

The absorption spectrum of the sample is shown in Figure 5.8(i). The fluorescence spectra taken with dye alone and dye sol mixture are shown in Figure 5.8(ii). Fluorescence spectroscopy provides a powerful methodology for investigating the dynamic properties of solutions. Because of Frank -Condon principle absorption spectroscopy can only yield information on the average ground state of the molecules which absorb light. Only solvent molecules that are immediately adjacent to the absorbing species will affect its absorption spectrum. In contrast fluorescence spectroscopic parameters are sensitive to functions of all processes which can occur during the excited state life time, and these processes can involve other molecules which are over 10 nm away from the fluorophore at the moment of excitation. Although the duration of 10 ns, which is the life time of the excited state, may appear to be very brief time span, it is actually long relative to the motions of small molecules in fluid solution. This means that the fluorescence is affected very significantly by the nature of the solvent or, more precisely, by the type of the environment of the fluorophore. Here also we

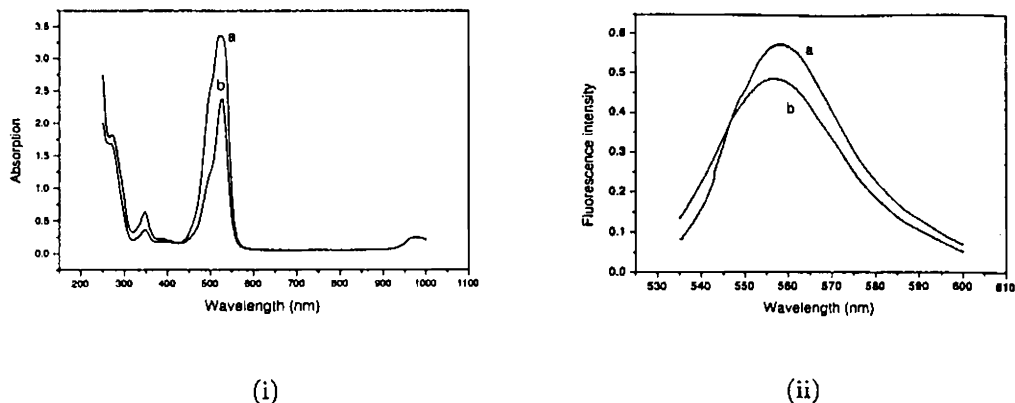(i)   (ii)

Figure 5.8: (i) Absorption spectrum of the samples in the presence (b) and absence of silver
sol (a) (ii) Fluorescence spectrum of the samples in the presence (b) and absence of silver sol
(a)

observed concentration dependant red shift of the fluorescence emission both in
the case of dye with and without the presence of silver sol. Such red shift with
concentration is more steep in the presence of silver sol. (Figure 5.9)

The physical properties of the solvent affect the fluorescence spectra in a
number of ways. The solvent can be regarded as a continuum in which the flu-
orophore is contained. The interaction between the solvent and the fluorophore
molecules affect the energy difference between the ground and the excited states.
This energy difference in (cm^{-1}) is a property of the refractive index (n) and the
dielectric constant (ϵ) of the solvent and is described by Lippert equation[19]

$$\overline{\nu_a} - \overline{\nu_f} = \frac{2}{hc}\left(\frac{\epsilon-1}{2\epsilon+1} - \frac{n^2-1}{2n^2+1}\right)\frac{(\mu^*-\mu)^2}{a^3} + constant \qquad (5.4)$$

where h is Planck's constant, 'c' is the speed of light and 'a' is the radius of
the cavity in which the fluorophore resides. ϵ is the dielectric constant of the
medium and $(\mu^* - \mu)$ is the change in dipole moment. The increase in peak
fluorescence wavelength with concentration of the dye indicates that the ground
and the excited states take larger time to get stabilized after the excitation
which results in decrease in energy difference between them and greater Stokes
shift. One of the reasons can be a decrease in refractive index which restricts
the movements of electrons within the solvent molecules. Since hydroxyl groups
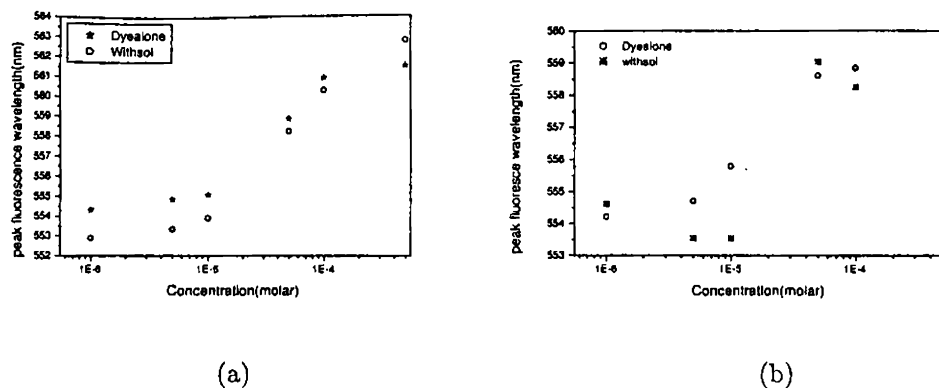are present in the solvent, there will be second order effects due to induced

(a)   (b)

Figure 5.9: Peak fluorescence wavelength from the Rh6G-silver sol mixture at (a) 14 mW and (b) 28 mW incident power

dipoles. A decrease in ϵ can also make the stabilization time large and thereby increase Stokes shift. But this occurs only after the reorientation of the solvent dipoles. This requires the movement of the entire solvent molecules and not just its electrons. Therefore, in our case where the stabilization of the excited state depends on ϵ, it can be assumed that as the concentration increases the reorientation of the solvent dipoles becomes slower thereby shifting the excited states to lower energy on the timescales compared to solvent reorientation time.

The Q_f values are calculated using Equation 5.3 for various values of dye concentrations. The experiment was done under identical conditions for a wide range of concentrations with and without the presence of silver sol. The Q_f variations with concentration are as given in Figure 5.10 at two different pump powers of 14 mW and 28 mW. As is seen from the figure, at higher pump power there is only about 10% reduction in the quantum yield at low concentration in comparison with about 50% reduction at low pump power of 14 mW. At higher concentrations the percentage reductions are almost identical in both cases. The fluorescence will be affected by the electromagnetic interaction among the optical fields, the fluorophore molecules and the electronic plasma resonance. This plasma resonance can also affect normal Raman scattering and resonance Raman scattering in different ways. The silver particles provide an additional decay mechanism, which arises from the possibility of very rapid transfer of the excitation from the dye molecule to the silver particles via the excitation of the plasma resonance. This additional excitation can be either radiative

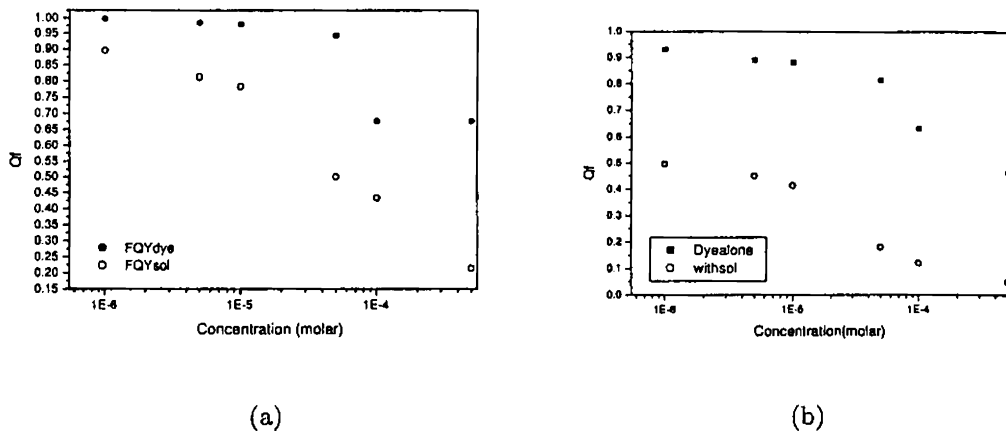(a)   (b)

Figure 5.10: Fluorescence quantum yield of the Rh6G-silver sol mixture at (a)28 mW and (b)14 mW incident power

or non radiative. But since the excitation wavelength that we have used in our experiment (532 nm) is far removed from the plasma resonance wavelength (410 nm) it can be assumed that fluorescence is not much affected by this additional decay mechanism induced by resonance.

5.4.5 Twisted Intramolecular Charge Transfer Processes in Dye-sol Mixture

Another possible mechanism for the non radiative decay is the twisted intramolecular charge transfer (TICT) which accounts for many processes taking place in the fluorophore-solvent environment after the excitation of the dye molecules. Solvent dependence of fluorescence lifetimes of Rh6G has been studied earlier for a number of solvents like H_2O, D_2O, MeOH, EtOH, i-PrOH etc.[20]. The dye is proved to be relatively insensitive to the solvent effect, with lifetime restricted in the range from 4.36 ns to 3.83 ns. This is because the ionization potential of its monoethyl amino group (Figure 5.7(b)) is too high to favor TICT state formation. TICT state formation is an important nonradiative decay channel from the planar excited state and therefore if this channel is absent in Rh6G, in electromagnetically inert environment, its fluorescence quantum yield should be nearly equal to unity. This has been proved to be so in our experiment with $Q_f \approx 1$ with water as the solvent at low concentrations. The fluorescence measurements from the molecules on the silver island film shows
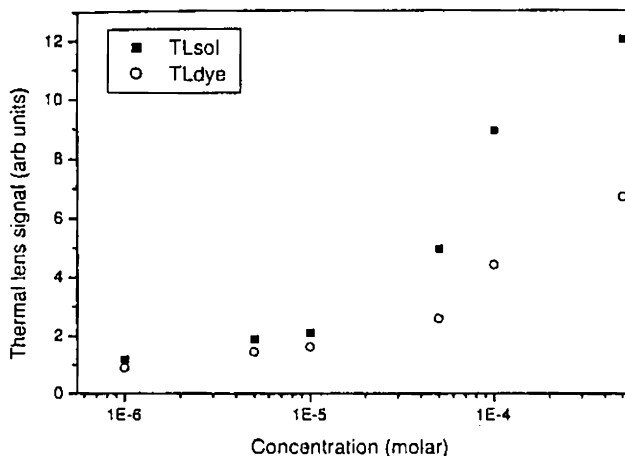
Figure 5.11: Thermal lens signal intensity as a function of concentration from Rh6G-silver sol mixture

a reduction in fluorescence lifetime [21] up to three orders of magnitude which invariably means the appearance of an additional non radiative decay channel due to the electric field in the vicinity of Ag particles which was otherwise absent. Therefore it can be assumed that the presence of silver particles produces a greater optical field for the excited fluorophore and induces the formation of charge transfer complexes. Moreover, reduction in absorbed light quanta due to scattering by the silver particles also results in reduced fluorescence. Many researchers have already proved that the presence of nano particles like Ag and Au enhance the Raman scattering and resonance Raman scattering [20, 21]. There was no significant reduction in Q_f as the intensity of the pump laser is increased, at low dye concentration (Rh6G). This means that the additional deexcitation process in the presence of silver sol is not intensity dependant.

5.5 Enhancement in Thermal Lens Signal Intensity from Rh6G in the Presence of Silver sol

As a consequence of the reduction in fluorescence from the Rh6G molecules in the presence of silver sol, it was further observed that there is an accompanying increase in thermal lens signal as seen from Figure 5.11.

As explained in the previous section, the silver particles provide an additional decay mechanism through the formation of TICT states, which accounts for many processes taking place in the fluorophore-solvent environment after the excitation of the dye molecules. Therefore, it can be assumed that the presence of silver particles produces a greater optical field for the excited fluorophore and induces the formation of charge transfer complexes. Formation of these resonance hybrids provides a nonradiative decay channel for the excited fluorophore and thereby reduces its fluorescence quantum yield. It is this additional decay channel that accounts for the enhancement in thermal lens signal. Formation of these resonance hybrids provides a nonradiative decay channel for the excited fluorophore and thereby reduces its fluorescence quantum yield.

5.6   Conclusions

In conclusion, the fluorescence quantum yield of the synthesized schiff base was calculated using a dual-beam thermal lens method. The moderately high value of the fluorescence and the extremely high stability of the material will make it useful as a fluorescent marker for biological applications. Gain studies and photobleaching studies will assess the suitability of the material as a laser dye. It is also shown that the presence of Ag sol reduces the quantum yield of Rh6G. Its favorable outcome is the enhancement of Raman scattering signal which is inherently weak. A discussion is presented on the possible reasons for this decrease in Q_f in terms of the formation of charge transfer complexes. Also, we have observed that the presence of silver sol can enhance the thermal lens signal which makes the detection of signal easier at any concentration.

References

[1] J.N.Demas, G.A.Crosby, *J.Phys.Chem.*, 75 (1971) p.8.

[2] D.Cahen, H.Garty, R.S.Becker,*J.Phys.Chem.*, 84 (1980) p.3384

[3] A.A.Krashenikov, A.V.Shablya,*Opt.Spec.*(USSR), 52 (1982) p.159

[4] C.Hu, J.Whinnery, *Appl.Opt.*, 12 (1973) p.72

[5] J.H.Brannon, D.Magde, *J.Phys.Chem.*, 82 (1978) p.705

[6] H.L.Fang, R.L.Swofford, in *Ultrasensitive Laser Spectroscopy,*ed. by D.S.Kliger(Academic, London 1983) p.176

[7] C.V.Bindhu, S.S.Harilal, V.P.N.Nampoori, C.P.G.Vallabhan, *Mod. Phys.Lett.B*, 13 (1999) p.563

[8] C.V.Bindu, S.S.Harilal, V.P.N.Nampoori, C.P.G.Vallabhan,*J. Phys. D: Appl.Phys.*, 29 (1996) p.1074

[9] M.Fischer, J.Georges, *Spec. Acta Part A* 54 (1998) p.101

[10] A.Santhi, M.Umadevi,V.Ramakrishnan, P.Radhakrishnan,V.P.N.Nampoori,*Spec. Acta Part A* 60 (2004) p.1077

[11] M.L.Baesso,*Phys. Rev. B*, 57,10 (1998) p.545

[12] R.T.Bailey, F.R.Cruickshank,*Chem. Phys.*, 77 (1983) p.243

[13] M.Fischer, J.Georges,*Chem. Phys. Lett.*, 260 (1996) p.115

[14] A.A.Andrade,*J. Non-Cryst. Solids*, 284 (2001) p.255

[15] Achamma Kurian, *Characterization of Photonic Materials using Thermal Lens Technique,*PhD thesis,2002, International School of Photonics, CUSAT

[16] D.L.Klayman, J.P.Scovill,*J. Med. Chem.*, 26 (1983) p.35

[17] Santhi et al,*App. Phy.B.*, 79 (2004) p.629

[18] C.V.Bindu, S.S.Harilal, V.P.N.Nampoori, C.P.G.Vallabhan,*J. Phys. D: Appl. Phys.*, 29 (1996) p.1074

[19] Joseph.R.Lakowicz,*Principles of Fluorescence Spectroscopy*, 1/e.,Plenum press, New York and London,(1983)

[20] D.Roy, Z.H.Barber, T.W.Clyne,*J. Appl. Phys.*, 91 No:9 (2002) p.6085

[21] D.A.Weitz, S.Garoff, G.I.Gersten, A.Nitzan,*J. Chem. Phys.*, 78 No:9 (1983) p.5324

Chapter 6

Thermal Lens Effects in Z-scan Experiments

"The greatest challenge to any thinker is stating the problem in a way that will allow a solution."- Bertrand Russell

ABSTRACT

The theory of photo thermal lens formation and also that of pure optical nonlinearity, can be applied to account for the phase modulation in a beam as it traverses a nonlinear medium. It is used to simultaneously determine the nonlinear optical refraction and the thermo-optic coefficient. This technique is demonstrated using some metal phthalocyanines dissolved in dimethyl sulphoxide, irradiated by a frequency doubled, Q switched Nd:YAG laser with 10 Hz repetition rate and a pulse width of 8 ns.

6.1   Introduction

The z-scan is a simple and sensitive technique introduced in 1990 to measure the nonlinear refractive index of optical materials. Relevant details of this technique are given in the first part of this thesis. In this technique the sample is moved in the intensity pattern generated along the z-axis by focusing a laser beam. The on-axis transmitted signal is measured in the far field by a detector placed behind a small aperture, which is referred to as closed aperture z-scan. Changes in the refractive index due to optical nonlinearities in the sample are detected as characteristic intensity variations of the transmitted signal as a function of the sample position. However, a closed-aperture z-scan is also sensitive to refractive index changes due to density variations induced by linear or nonlinear

absorption of light in the sample, i.e., to thermal lens effects. For this reason the z-scan setup has been used to detect small linear absorption using low power continuous wave (CW) lasers, and also two-photon absorption (TPA) using a two-colour, pumb-probe, technique with a pulsed pump laser and a CW probe laser [1]. There are differences in the ways in which the thermal nonlinearity acts in a particular experimental scheme, mainly depending on the excitation pulse duration and repetition rate. Some of the commonly encountered situations are briefly discussed below.

6.1.1   Thermal Effects in Z-scan Experiments with High Repetition rate Sub pico second Lasers

In evaluating the potentialities of a nonlinear material for applications requiring operation at high repetition rates, one has to use experimental methods capable of separating the contribution of the purely optical Kerr nonlinearity from that of the thermo-optical effects. The nonlinear response of materials when irradiated by very intense femtosecond or sub pico second laser pulses at verify high repetition rates ($\sim$ 50-100 MHz) will largely be influenced by slow cumulative thermal effects [2].

6.1.2   Thermal Effects in Z-scan Experiments with CW Lasers

The rise time of thermal lens signal in a typical z-scan experiment is of the order of a few tens of nanoseconds and the thermal decay time is typically hundreds of milli seconds. These values are governed by beam parameters like beam radius, pulse width and material constants like thermal diffusivity, thermal conductivity etc. If the pulse width is larger than the decay time of the thermal lens, then diffusivity will come into play and will affect the phase of the propagating beam. For this reason, z-scan signals using CW lasers will have a slowly rising thermal component.

6.1.3   Thermal Effects in Z-scan Experiments Using nano second Lasers

Thermally induced refractive index changes caused by absorption of light in a material have been intensively investigated both experimentally and theoretically in various time scales of the input laser pulses [3, 4]. Most of these studies addressed the problem of thermal lensing produced inside the material using

microsecond and longer pulses (up to CW). Several authors have considered shorter (nanosecond) pulses to be a source for the refractive index change. In this case the effect of thermally induced index changes can be highly transient for focused beams [5].

6.1.4 Methods to Uncouple Thermal Effects from Z-scan Signals

1. Time Resolved Z-scan

   In the case of z-scan experiments with sub-nanosecond response Kerr-like media, in a spectral region where the sample is transparent, the nonlinear susceptibility is fairly small, and its measurement demands a high intensity light. However, there is an alternate technique, which is an extension of the usual single-beam method to study slow response absorbers. In this case, the nonlinear susceptibility is large because the laser frequency is close to a resonance and thus, even a low power CW laser would be suitable for its measurement. Moreover, if the optical nonlinearity arises due to the population of a long-lived electronic state or if it has a thermal origin, the medium will present a slow response. In this situation, it is possible to separate out the slow componet to nonlinearity, from the fast components, by means of a time resolved technique. Experimental arrangement for time resolved z-scan is given in chapter 1, (Figure 1.11). The main difference of this scheme from the usual experiment, is in the use of a chopper to modulate the excitation beam. It is this component that allows time resolved measurements.

   In this technique, transmission can be measured at various point of time, during the chopping cycles. As explained in chapter 1, the transmittance is purely linear at t=0. As the time evolves, the sample heats and/or excited states become populated and nonlinear effects start to manifest themselves. For times much longer than the characteristic relaxation time T_1 , the steady state is reached and the final transmittance will contain both linear and nonlinear contributions. The data-acquisition system measures the intensities at t=0 and $t = \tau$ ($> T_1$), and evaluates their ratio. By suitably setting the chopper opening time, one can thus eliminate the thermal effects from the nonlinear refraction measurements [6, 7].

2. Recording the time evolution of z-scan signal

   This is another method to uncouple the thermal effects from z-scan data

This is suitable for experiments with high repetition rate lasers, where, the real part of the refractive index could be altered by cumulative sample heating, giving rise to the time evolution of the CA curve. On the other hand, the OA curve usually does not evolve in time regardless of the laser repetition rate since optical absorption is generally weakly influenced by a change in the sample temperature. The equation for transmittance should be suitably modified, by taking into account the phase distortion induced by thermal diffusion in addition to that due to optical Kerr effect. [8]

6.2   Thermal Lens Formalism to Interpret Z-scan Data

It is possible to use the thermal-lens model to interpret z-scan experiments when the sample is weakly absorbing. In this situation, the energy absorbed from the laser beam is converted into heat due to non radiative relaxation. The non-linearity arises from the dependence of the refractive indices on temperature. Due to the diffusion of heat, the spatial temperature profile can differ significantly from the laser intensity profile. Z-scan experiments probe the intensity-dependent nonlinear susceptibility. In the case of laser heating, this depends on the thermo-optic coefficient $\partial n / \partial T$, where n is the refractive index and T is the temperature, and on the thermal diffusivity, D. One can therefore expect to evaluate these quantities by this method.

6.2.1   Theory

The effects of local heating due to the absorption of light on the propagation of a Gaussian beam were studied by Gordon et al in 1964. This study forms the foundation of the thermal-lens model (TLM). In this application, as the Gaussian beam propagates through a weakly absorbing sample, light is absorbed and consequently gives rise to local heating. Diffusion of heat is assumed to take place in the radial direction (perpendicular to the z direction), giving rise to a spatially varying temperature field that is not proportional to the local light intensity. The refractive index is assumed to depend linearly on temperature, and the nonlinearity is due to this nonlocal dependence of the refractive index on the light intensity. The effects of laser heating by a Gaussian beam on its far-field intensity can be analyzed using a parabolic approximation to the temperature field and on approximating the optical effects due to temperature as being the same as those of a simple lens. The time dependent expression for

the far-field on-axis transmittance is [9]

$$T_N(z,t) = \cfrac{1}{1 + \left(\frac{\Delta\phi}{1+t_c/2t}\right)\frac{2x}{1+x^2} + \left(\frac{\Delta\phi}{1+t_c/2t}\right)\frac{1}{1+x^2}} \qquad (6.1)$$

where $x = z/z_0$ and the thermal diffusion time t_c is given by $\frac{\omega^2}{4D}$

Thermal parameters like diffusivity, D and thermal relaxation time, t_c of the sample can be extracted by assuming that the phase modulation of the propagating beam is caused by thermal lens formation as given in this equation. A theoretical fit of the z-scan data to Equation 6.1 will therefore give the values of all these quantities.

6.2.2   Experimental Results Using Metal Phthalocyanines

To verify the above method, samples of cobalt and nickel phthalocyanines were prepared in DMSO at a concentration of 0.5 mM. There is no special absorption band for any of the metal Pc's around 532 nm, which is the excitation wavelength used. The experimental arrangement is as given Chapter 2. The laser source used was a frequency doubled, Q-switched Nd:YAG laser emitting at a wavelength of 532 nm at a repetition rate of 10 Hz and with pulse duration of 8 ns. To satisfy the thin lens approximation we used a cuvette of path length 1mm. The transmitted pulse energy in the presence of a far field aperture was probed by a detector (Rj 735, Laser Probe Inc.) as a function of sample position z, obtaining the closed aperture (CA) z-scans.

Evaluation of Thermal Diffusivity and Thermal Decay Time constant

The z-scan measurements were performed with on-axis peak intensities I_0 ranging from 0.29 to 0.631 GW/cm^2. The phthalocyanine samples shows some linear absorption in the wavelength 532 nm, which will lead to thermal effects. Figure 6.1 shows an example of the CA z-scan trace for CoPc in DMSO at I_0=0.631 GW/cm^2 with theoretical fit using Equation 6.1. The presence of prefocal maximum and the post focal minimum in the z-scan signal indicates that the nonlinear refractive index is negative, i.e., $n_2 < 0$. The analysis of this data is done using the equation for position dependent TL signal. In the fitting procedure, the value of z_0 is fixed by initially giving a trial value using the equation $z_0 = \omega_0^2/2k$, and then refine the fit by two or three trials. Two free fit parameters are used here; one for $\Delta\phi_0$ and the other is for t_c. The value of Rayleigh range, (z_0) will yield the value of beam waist and this and t_c will give the value of the thermal diffusivity from equation $t_c = \omega^2/4D$. For the data in
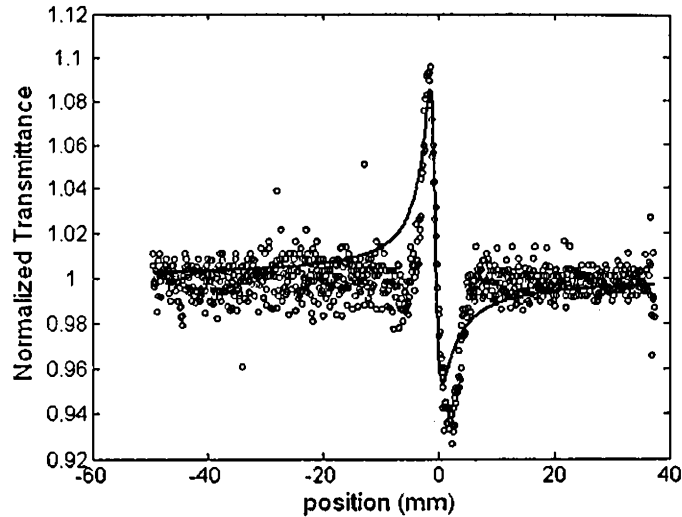
Figure 6.1: Closed aperture z-scan data and theoretical fit using thermal lens formalism

Figure 6.1, the thermal decay time was calculated to be 6 ms yielding thermal diffusivity of $0.525 \times 10^{-3} cm^2/s$. This in turn will furnish the value of thermal conductivity. This suggests that thermally induced nonlinearity is also present in the refractive studies using the Q switched envelope of ns laser pulses.

Source of Errors in Thermal Lens Formalism

Figure 6.1 shows that the thermal lens formalism does not give a good fit to the transmittance data. The main reason can be that, during 8 nanosecond time the thermal diffusion does not begin to act, to significantly affect the phase of the transmitted beam. Therefore this analysis may be more suitable for CW lasers.

6.3 Simultaneous Determination of Thermo Optic Coefficient and Nonlinear Optical Parameters in Transient Regime

The thermal lens formalism given above can be modified to correctly account for purely optical and thermo optical nonlinearities in the transient regime [10, 11].

This will act as a tool to simultaneously determine thermo optic coefficient and nonlinear optical parameters. It is done as follows.

6.3.1   Theory

If we have a few nanosecond duration pulse, focused to a spot diameter of $10 \sim 40 \mu$m, for typical values of the sound velocity in liquids $(1 \sim 2 \mu$m/ns) the acoustic wave generated by the front end of the pulse traverses the beam and creates an index change affecting the tail end of the pulse. If the pulse width, τ_p, is longer than the acoustic transit time, $\tau_p > \omega / C_s$, where ω is the beam waist size and C_s is the sound velocity, the thermal lensing effect is given by $\Delta n = (\frac{dn}{dT}) \Delta T$ where $\frac{dn}{dT}$ is the thermo optic coefficient [5].

The z-scan method to measure the nonlinear absorption β, nonlinear refraction γ etc are well documented [12, 13, 14]. The nonlinear refraction encountered by an intense laser beam as it propagates through a liquid medium, can have various physical origin like electronic, molecular or thermal. Under specific experimental conditions, there is the possibility of thermal lens (TL) formation which will be reflected in the z-scan signal. A transient TL signal will be formed in liquid samples, even in the nanosecond regime [5, 10], which we exploit here to simultaneously determine thermo-optic coefficient, $\frac{dn}{dT}$ and the nonlinear optical parameters. The experimental arrangement is as given in chapter 2 and also in reference [15]. However some differences in the optics were made in the experimental configuration, to satisfy the condition for formation of transient thermal lens signal. The laser source used was a frequency doubled, Q-switched Nd:YAG laser with a repetition rate of 10 Hz and pulse duration of 8 ns. A spatial filter was used to limit the beam size, and then it was focused by a short focal length convex lens, producing a Gaussian spot of 15.4μm in radius. Reducing the beam spot size to this value, ensures that the acoustic waves build up during the time in which the pulse lasts in the medium. The sample taken in a quartz cuvette was translated through the focus and the transmitted pulse was measured as before, which gives the closed aperture (CA) z-scan signal. The thermo optic coefficient, $\frac{dn}{dT}(K^{-1})$ and some of the nonlinear optical parameters are extracted as follows.

Here, we are considering the changes in refractive index due to purely optical nonlinearity and also that due to TL formation. The effect of this nonlinear refractive index is to produce a phase shift, which varies across the beam profile, resulting in transmittance change when viewed through an iris placed at the center of the beam spot in the far field. As mentioned in reference [1], the best

procedure to extract both these nonlinearities is by a fit of the z-scan signal, taking into account both these effects. This can be done by modifying the on-axis phase shift at focus $\Delta\phi_0$, used in the derivation for far-field transmittance in reference [15], by including the phase shift due to transient TL formation. We write this phase-shift as

$$\Delta\phi_0 = \Delta\phi_0(opt) + \Delta\phi_0(ther) \qquad (6.2)$$

where $\Delta\phi_0$ is related to the total change in nonlinear refraction as

$$\Delta\phi_0 = \frac{2\pi}{\lambda}\Delta n_0 L_{eff} \qquad (6.3)$$

In the time scales in which this experiment was carried out, and for the focussed beam spot size of $15.4\mu m$, the rise time for thermal nonlinearity, t_{ther} is of the same order of magnitude as that of the pulse duration (t_p). The former is governed by acoustic transit time $\frac{\omega_0}{v_s}$, where the sound velocity v_s is nearly 1-5 $\mu m/ns$ in most solvents. So the condition $t_{ther} < t_p < t_c$ is satisfied and results in efficient transient TL signal. Here t_c is characteristic time for TL signal given by $\frac{\omega_0^2}{4D}$ where ω_0 is the beam spot size and D is the diffusivity. Since we are interested in the on-axis index change, we do not consider the effect of diffusion. Under these approximations, the on-axis refractive index variation due to thermal effects can be expressed as $\Delta n_0(ther) = \frac{\alpha p_0}{2\rho_0 c_p}\frac{dn}{dT}$ [16]. The corresponding value index change due to pure optical nonlinearity is given by $\Delta n_0(opt) = \gamma I_0$, where the remaining unexplained terms are; p_0-incident fluence (Jcm^{-2}), ρ_0-density (gcm^{-3}), α-linear absorption coefficient (cm^{-1}), c_p-specific heat capacity $(Jg^{-1}K^{-1})$, γ-the nonlinear index (cm^2W^{-1}), $L_{eff} = \frac{(1-e^{-\alpha L})}{\alpha}$ is the effective sample path length and I_0 is the irradiance (Wcm^{-2}).

Since the TL built up is instantaneous, both $\Delta n_0(ther)$ and $\Delta n_0(opt)$ will contribute to $\Delta\phi_0$ through Equation 6.3. This situation is different from the case of cumulative TL effect present when high repetition rate pulses are used. If the heating effect is cumulative, we need to take into account thermal diffusion which contributes to a slower component to nonlinearity. In such cases one can uncouple the purely optical (fast) and thermal (slow) nonlinearities as done by Yang et al where they obtain thermal conductivity and two photon absorption cross sections from a single z scan signal [17]. For 8 ns pulse of 10 Hz repetition rate, conductivity or diffusivity will not significantly affect the propagating pulse. In other words the thermal nonlinearity due to the fast rise time of TL signal is more significant than that due to the decay of the TL [10]. Since in transient regime, the TL peaks up and distorts $\Delta\phi_0$ while the pulse

lasts in the medium, and also since the TL created by one pulse does not affect the subsequent pulses, the problem of uncoupling it from the purely optical nonlinearity becomes less complicated.

Following the method adopted by Weaire etal [18] and Sheik Bahae etal, we can approximate the normalized transmittance for a Gaussian TEM_{00} beam at the aperture plane as

$$T(z) = 1 - \frac{2\pi}{\lambda} L_{eff} \left(\frac{\alpha p_0}{2\rho_0 c_p} \frac{dn}{dT} + \gamma I_o \right) \frac{4x}{(1+x^2)(9+x^2)} \tag{6.4}$$

where x is the dimensionless sample position $\frac{z}{z0}$, z_0 being the depth of focus. This expression is used to fit the experimental z-scan signal by treating $\frac{dn}{dT}$ and γ as fit parameters. The detailed curve fitting is done using a trial value for c_p as $1.2 Jcm^{-3}K^{-1}$ and obtain initial guess values for thermo optic coefficient and γ. With these initial values we refine the fit by varying c_p values from 1.2 to 3.0 which is typical for organic solvents and obtain best fit parameters.

6.3.2   Experimental Results Using Metal Phthalocyanines
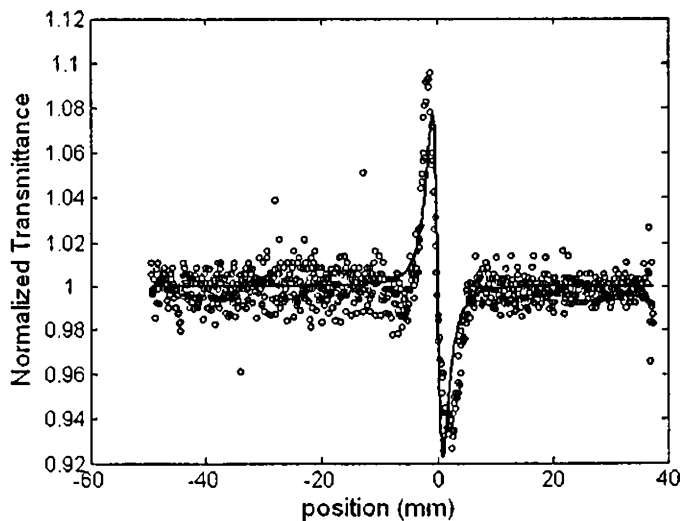
Figure 6.2: Closed Aperture z-scan data and theoretical fit in the case of CoPc in DMSO, using the modified expression taking into account both TL effect and phase distortion due to purely optical nonlinearity. The values used to obtain best fit are, $\gamma = 8.35 \times 10^{-5} cm^2/GW$, dn/dT = $5.02 \times 10^{-4}/K$, $c_p = 1.5J$ cm^3/K

Sample used	Method 1		Method 2			
	$D^{(e)}$	$D^{(r)}$	$\gamma^{(e)}$	$\gamma^{(r)}$	$dn/dT^{(e)}$	$dn/dT^{(r)}$
	$(\times 10^{-3} cm^2/s)$		$(\times 10^{-5} cm^2/GW)$		$(\times 10^{-4}/K)$	
CoPc,DMSO	0.525	$1 \pm .03$	8.35	—	5.02	$4.3 \pm .2$
NiPc,DMSO	0.43	$1 \pm .03$	7.78	—	4.86	$4.3 \pm .2$
CoPc,DMF	0.49	—	8.1	—	4.3	—
NiPc,DMF	0.51	—	8.4	—	5.1	—

Table 6.1: Summary of the experimental results. Method 1 is the TL formalism and Method 2 is the use of modified expression for T, which takes into account both thermal and purely optical nonlinearities. Superscripts (e) stands for experimental and (r)for the reported values. The experimental values of D have an error of 35%, γ 17% and dn/dT values have error of approximately 21%

Cobalt and nickel phthalocyanines (CoPc and NiPc), dissolved in dimethyl sulphoxide (DMSO) at a concentration of 0.5 mM, were used for this study. The z-scan measurements were performed with on-axis peak irradiance I_0 ranging from 0.1 to 0.6 GW/cm^2. Figure 6.2 shows an example of the CA z-scan trace for CoPc in DMSO at I_0=0.171 GW/cm^2 with theoretical fit using equation 6.4. The values of γ and the thermo-optic coefficient obtained in this case are also shown in the figure caption. The corresponding values for NiPc are $7.78 \times 10^{-5} cm^2/GW$ and $4.86 \times 10^{-4} K^{-1}$ respectively, with the same value of c_p. The thermal parameters extracted in both the cases are nearly equal and is close to the $\frac{dn}{dT}$ value of DMSO. Therefore it can be concluded that, the small difference in $\frac{dn}{dT}$ value from that of DMSO is due to the presence of impurity, which is Pc in the present case. The nature of the metallic nuclei in the Pc does not affect the thermal expansion of the solution.

The entire results are summarized in Table 6.1. Method 1 refers to the thermal lens formalism used to find out the thermal diffusivity, and the Method 2 is the use of modified expression to fit the transmittance data taking into account both thermal and Kerr nonlinearities.

6.4   Conclusions

Under specific experimental conditions both thermal and purely optical nonlinearities can be present in an z-scan data. One should be careful in uncoupling them while interpreting the results. By making use of these effects, it is also possible to simultaneously determine some of the nonlinear optical parameters and thermo-optic coefficient of a sample in liquid form. This has been demonstrated in metal Pc's dissolved in DMSO and DMF, using an Nd:YAG laser of 8 ns pulse

width and 10Hz repetition rate. The experimentally obtained values of thermal diffusivity and thero-optic coefficient are of the same order of magnitude as the actual values. This proves the presence of thermal nonlinearity through the formation of transient thermal lens, even in nano second regime. This method can be applied to materials that are weakly absorbing at the excitation wavelength.

References

[1] Mauro Falconieri, *J. Opt. A: Pure Appl. Opt.*, 1, (1999) p.662

[2] M. Falconieri, G. Salvetti, *Appl. Phys. B*, 69,(1999) p.133

[3] C. K. N. Patel and A. C. Tam, *Rev. Mod. Phys.*, 53, (1981) p.517

[4] J. N. Hayes, *Appl.Opt.*, 11, (1972) p.455

[5] Dmitriy I. Kovsh, David J. Hagan and Eric W. Van Stryland, *Optics Express*, 4(8), (1999) p.315

[6] R A Ganeev, M Baba, M Morita, A I Ryasnyansky, M Suzuki and H Kuroda, *J. Opt. A: Pure Appl. Opt.*, 6, (2004) p.1076

[7] L. C. Oliveira and S. C. Zilio, *Appl. Phys. Lett.*, 65 (17), (1994) p.24

[8] A.Gnoli, L.Razzari and M.Righini, *Opt.Express*, 13(20) (2005) p.7976

[9] C. A. Carter and J. M. Harris, *Appl. Opt.*, 23, (1984() p.476

[10] Pascale Brochard,Valrie Grolier-Mazza and Rgis Cabanel, *J. Opt. Soc. Am. B*, 14(2), (1997) p.405

[11] Andrea Gnoli, Luca Razzari and Marcofabio Righini, *Optics Express*, 13(20), (2005) p.7976

[12] M. Sheik-Bahae, A. A. Said, and E. W. Van Stryland, *Opt. Lett.*, 14, (1989) p.955

[13] Wei-Ping Zang, Jian-Guo Tian, Zhi-Bo Liu, Wen-Yuan Zhou, Feng Song, Chun-Ping Zhang, and Jing-Jun Xu,*J. Opt. Soc. Am. B*, 21(2), (2004) p.349

[14] Lina Yang, R Dorsinville, Q Z Wang,P X Ye, R R Alfano, *Opt,Lett.*, 17(5), (1992) p.323

[15] Sheik Bahae, Ali A Said, Tai-Huei Wei, David J Hagan, E W Van Stryland, *IEEE j. QE*, 26(4), (1990) p.760

[16] B. L. Justus, A. L. Huston, and A. J. Campillo, *App.Phy.Lett.*, 63,(1993) p.1483

[17] R. F. Haglund, L. Yang, R. H. Magruder, J. E. Wittig, K. Becker, and R. A. Zuhr, *Opt.Lett.*, 18(5), (1993) p.373

[18] D.Weaire,B. S. Wherrett,D. A. B.Miller, and S.D. Smith, *Opt.Lett.*, 4(10), (1979) p.331

Chapter 7

Conclusions and Future Prospects

7.1 General Conclusions

Nonlinear optical materials use nonlinear dependence of the refractive index on the applied electric field to produce other frequencies. This results in either harmonic generation or frequency shifting. The importance of nonlinear optical materials in lasers and electro-optics became clear in the early days of lasers, since it enabled expansion of their limited spectral regime. Presently, there are a large number of nonlinear optical materials for specific wavelengths, with various damage thresholds, and with various optical characteristics. The unique characteristics of each nonlinear optical material and its various applications are mutually connected.

The nonlinear optical properties of single metal substituted phthalocyanines are investigated using the closed aperture and open aperture z-scan experiments that provide information regarding the refractive and absorptive nonlinearities of the materials. Phthalocyanines find several applications in dyes, photo-conducting materials, cancer therapy etc. The synthesis and applications of Pc materials is a dynamic and multidisciplinary field of research. The materials used for studies in the present thesis are CoPc, NiPc, CuPc and ZnPc. The nonlinear absorption and nonlinear refraction coefficients of all these materials were calculated. The calculated values of nonlinear absorption coefficient for these materials when DMF was used as the solvent, was in the range 5.66 to 6.46 cm/GW at 532 nm, and 3.25 to 7.68 cm/GW at 1064 nm excitation. There was not much change in these values when the solvent was changed to DMSO.

Nonlinear absorption spectrum of ZnPc was extensively studied which resulted in an interesting observation of the nonlinear mechanism changing from RSA to SA when the excitation wavelength changes to the rising edge of Q-band [1]. A 5-level model has been developed using the density matrix formalism to account for the spectral dependence of nonlinear absorption mechanisms. All of these materials are good RSA based optical limiters. The optical limiting studies carried out in ZnPc using the fundamental and second harmonic of the Nd:YAG laser reveal that, the material has a limiting threshold of approximately 2.5 J/cm^2 at 532 nm and 2.2 J/cm^2 at 1064 nm excitation, for a concentration of 0.5 mM in DMSO. Moreover, the spectral dependence of nonlinear susceptibility shows that ZnPc can act as an RSA based limiter at wavelengths ranging from 527 to 616 nm and also at 1064 nm. The cross-sections for nonlinear absorption and nonlinear refraction of all these materials were also calculated [2].

Solving the rate equations for a five level system, we can find out the expression for the spectral dependence of nonlinear susceptibility and also the excited state dynamics of the material system [3]. The procedure reveals that triplet to triplet excited state absorption is the reason for RSA behavior of ZnPc.

Fluorescence is a central technology in medicinal testing, drug discovery, biotechnology and imaging. In almost all uses of fluorescence, the fluorophores are in free space condition, in which they radiate energy with minimal interaction with their surroundings. Fluorophore interactions with the local environment affect non radiative decay processes such as quenching, but do not alter the intrinsic rate of radiative decay. Remarkably, proximity of fluorophores to metallic particles can dramatically alter their fluorescent spectral properties in ways that alter the quantum yield and photostability and improve detectability. This aspect was investigated in a commonly used fluorescing material rhodamine 6G in silver nano particle environment. The fluorescence quantum yield was calculated using the thermal lens method. In this study it was observed that rhodamine 6G in liquid form, with silver nanoparticles in its surroundings, has a decreased fluorescence efficiency compared to the case when the nano metals were absent [6]. However since the dye is highly fluorescing on its own, with a quantum yield of more that 95%, this result may not be very surprising. Metal particles usually finds biological applications in enhancing the intrinsic emission of DNA, which exhibits an extremely low quantum yield ($\sim 10^{-4}$ to 10^{-5}) in solution. The reduction in quantum yield of rhodamine 6G was complimented by the increased thermal lens signals. This study was carried out using the 532 nm CW excitation from a DPSS laser. It was also observed that the presence of silver particles results in an increased thermal lens signal from rhodamine 6G

[8].

The fluorescence quantum yield of a newly synthesized material Hydroxyphenyl imino methyl phenol was also calculated using the same technique [4]. For this study five wavelengths from CW Ar-ion laser was used. This material has remarkable stability such that its fluorescence spectrum did not vary appreciably even after keeping it in dissolved form in chloroform for several days. Its reasonably good fluorescing ability with a quantum yield of nearly 78% is promising and by carrying out photostability and laser emission studies one can verify its suitability as a laser dye.

Thermal nonlinearities are commonly much larger than the electronic nonlinearities of the same material, often by several orders of magnitude. The apertured z-scan data contains both nonlinear absorption and refraction. With the aperture in the far field, the measured values of normalized energy transmission can have two contributions to the nonlinear refraction: one derived from a change in density with heating of the sample, and the other derived from the excited-state contribution to the index. The change in phase $\Delta\phi$ of the electric field through the sample should therefore be suitably modified to take into account of these two influences. Depending on the experimental conditions and the characteristics of the laser pulse, the nature and influence of the thermal effects on the propagating beam will be different. Thermally induced refractive index changes caused by absorption of light in a material have been intensively investigated by various scientists, both experimentally and theoretically for various time scales of the input laser pulses. At these different time scales of the input pulse, the thermal lensing has different manifestations. If the pulse width is longer than a few microseconds, density changes occurring via acoustic propagation may be considered instantaneous for beams having radii of one hundred microns or less (sound velocity ($1\sim 2$ μm/ns). Hence, it is the shape of the beam, coupled with thermal diffusion, which dictates the temperature gradient and hence the phase change of the propagating beam in this regime. However, for the single pulses of shorter duration (nanosecond time scale), the refractive index of the medium changes with its the acoustic expansion, generated by local heating (absorptive mode) or by its compression due to the electromagnetic field of the laser beam (electrostrictive mode). Hence, although the refractive index varies linearly with the density, it does not follow the spatial variation of the temperature. If the pulsewidth is in the picosecond regime, the acoustic waves do not have time to propagate, and therefore the density and index cannot change significantly resulting in no lensing effect during the short pulse. However, with high repetition rate pulses there will be the effects of cumulative

thermal lensing. The presence of these two nonlinearities can be made use of in calculating the thermo-optic-coefficient and the nonlinear optical parameters from a single z-scan signal [3,5]. This has been demonstrated using metal phthalocyanines. In the transient regime, one can take into account the refractive index changes due to both purely optical and thermo optic nonlinearity and the phase of the propagating pulse gets affected accordingly. Therefore this method will enable one to find out the nonlinear refractive index and the thermo-optic coefficient simultaneously. Two materials were used for demonstration of this method, CoPc and NiPc dissolved in DMSO. The extracted values of γ and dn/dT are in agreement with the values obtained for single metal phthalocyanines and for DMSO respectively.

7.2   Future Prospects

There are a lot more aspects of these materials that can further be explored using various techniques. Wavelength dependence of refractive nonlinearities in the same materials can be studied and the theoretical model developed for nonlinear absorption spectrum can be generalized to incorporate both nonlinear refraction and absorption terms as the real and imaginary parts of susceptibility. It is also possible to use a CW laser for the studies of nonlinear properties so that one can adjust the chopping frequency and vary the 'pulse' duration and thus study the nature and dynamics of the thermal nonlinearity. It is also possible to carry out a time resolved z-scan measurement. Extensive investigations can be carried out on the fluorescing ability of the newly synthesized material. It will be interesting to study its amplified spontaneous emission probably by incorporating it into a solid matrix like PMMA.

List of Publications

(References)

1. Spectral dependence of third order nonlinear optical susceptibility of Zinc Phthalocyanine, Santhi.A, Vinu V N, P Radhakrishnan and V P N Nampoori, **Journal of Applied Physics**, Am.Instt.Phys, USA, Sept 2006 (in press)

2. Excited state absorption of metal Phthalocyanine studied using z-scan technique, Santhi.A, Vinu V N, P Radhakrishnan and V P N Nampoori, **Physical Review A**, Am.Phys.Soc, USA, (under review)

3. Simultaneous determination of nonlinear optical parameters and thermal diffusivity of liquid samples, **Santhi.A**, Vinu V N, P Radhakrishnan and V P N Nampoori, **Applied Physics Letters**, Am.Instt.Phys, USA (under review)

4. Thermal lens technique to evaluate the fluorescence quantum yield of a schiff base, **Santhi.A**, U.L. Kala, R.J.Nedumpara, A. Kurian, M.R.P. Kurup, P. Radhakrishnan, V.P.N. Nampoori, **Applied Physics.B**, Springer, UK, 79, (2004) p.629-633

5. Dual beam thermal lens and z scan studies of the thermo optical properties of some nonlinear materials, **Santhi.A**, Vinu V N, M R P Kurup, J Kesavayya, P Radhakrishnan and V P N Nampoori **Proceedings of SPIE**, Photonics West 2005, San Jose, USA, Vol. 5710, p.91-98

6. Effect of silver nano particles on the fluorescence quantum yield of Rhodamine 6G determined using dual beam thermal lens method, **Santhi.A**, M Umadevi, V Ramakrishnan, P Radhakrishnan, V P N Nampoori **Spectrochimica Acta Part A**, Elsevier, USA, 60 (2004) p.1077-1083

7. Photoacoustic investigations on the photostability of Coumarin 540 doped PMMA, Ritty J.Nedumpara, **Santhi.A**, Binoy Paul, P. Radhakrishnan, V.P.N.Nampoori, and C.P.G.Vallabhan **Spectrochimica Acta Part A**, Elsevier, USA 60 (2004) p.435-439

8. Enhancement in Thermal lens signal from molecules of Rhodamine 6G Dispersed in Silver sol and its Effect on Quantum yield Measurements **Santhi.A**, Ritty J Nedumpara, V S Abraham, V Ramakrishnan, P Radhakrishnan, C P G Vallabhan and V P N Nampoori **Proceedings of SPIE**, APOC 2003, Nov 4-6, Wuhan, China, p.661

9. Fibre optic based chemical sensor to detect endpoint in volumetric analysis, **Santhi.A** , S. Thomas Lee, Ginu Rajan, Veena Gopal , P. Radhakrishnan and V.P.N Nampoori, **National Laser Symposium** 2002, SCTIMST, Thiruvananthapuram, Nov 14-16

10. Laser excited fluorescence characteristics of chemical ligand hydroxyphenol salicylaldehyde oxime, **Santhi.A**, P. Radhakrishnan and V.P.N. Nampoori **National Laser Symposium** 2002, SCTIMST, Thiruvananthapuram, Nov 14-16

APPENDIX : A

SIGNIFICANCE OF TIMESCALES IN NONLINEAR OPTICAL INTERACTIONS.

The origin of optical nonlinearity depends on the relevant time scales of the light interaction with the material. For ultra-fast process in the femtosecond time domain, distortion of the atom's or molecule's electron cloud leads to an induced electronic nonlinearity which is weak but very fast. Longer time interactions, for example in the picosecond domain, can lead to coupling with the intrinsic vibrational nuclear motions in a molecule, or can reorient small molecules, leading to a stronger but slower, nonlinear coupling.The vibrational resonant processes, although highly detuned from the very large optical frequency of $\approx$ $10^{15} second^{-1}$ (their resonances lie around $10^{13} second^{-1}$), can be driven through a three wave interaction involving the original incident optical wave, the above material oscillation and a spontaneously generated scattered optical wave (Stimulated Raman scattering (SRS)). Interaction times of the order of nanoseconds can stimulate hypersonic acoustic waves via a similar three wave interaction called Stimulated Brillouin Scattering (SBS). Even longer interactions can induce thermal coupling which poses a major problem in CW optical devices such as semiconductor lasers, amplifiers and repetitively pumped pulsed systems.

APPENDIX : B

CONSEQUENCES OF INTENSITY DEPENDENT REFRACTIVE INDEX .

There are mainly two consequences of intensity dependent refractive index. One is Optical bistability and the other is Self-focussing/Trapping. A commonly used realization of optical bistability uses a Fabri-Perot resonator,of length d, which contains a medium with intensity dependent refractive index of the form $n_{tot} = n + n'_2 I$. The intensity I of the transmitted beam from the Fabri-Perot resonator is given by the Airy-formula,

$$I_2 = \frac{T_0 I_1}{1 + F . sin^2(\delta/2)} = T . I_1 \tag{1}$$

I_1 is the incoming intensity, T is the total transmission with $T_0 = T(\delta = 0)$, F is a constant connected with finesse, whereas the phase shift for a whole round-trip is

$$\delta = k_0 n_{tot} 2d = k_0(n + n'_2 I_i)2d \tag{2}$$

and I_i is the intensity in the resonator. The output intensity I_2 can be expressed also with I_i:

$$I_2 = B . I_i \tag{3}$$

where B depends on the mirror transmission; thus,

$$T = \frac{I_2}{I_i} = \frac{BI_i}{I_1} \tag{4}$$

The graphical solution for the two sets of equations, for $T = T(I_i)$, Eq. 1 plus Eq. 2 and Eq. 4 yields for small values of I_1 only one point of intersection in the curve $T(I_i)$, for larger I_1 values three or still more points of intersection. See figure ??. From this result we get $T(I_1)$ and $I_2(I_1)$. Bistability is very important for optical data processing in purely optical logic and computer systems. The switching effect is similar to phase transition. The nonlinear system has positive feedback and can lead to bifurcation and chaos in the output.

self focussing is another effect that originates from the nonlinearity of the index of refraction: $n_{tot} = n + \delta n(I)$ Laser light which is propagating in the z direction and which has a Gaussian transverse intensity distribution, experiences the highest refractive index on the axis, where optical path lengths are maximum. Therefore the medium acts as a convex lens. This focussing can compensate the diffraction effects. Depending on the ratio of the light power $\mathcal{P}_0$ to some critical power $\mathcal{P}_c r$, either diffraction or focussing predominates. The limiting case, (neither diffraction nor focussing is called *self-trapping)*

The effect of self-focussing is caused by a single field

$$\hat{E}(\mathbf{x}, f) = \mathrm{e}(f) \cdot \bar{E}(\mathbf{x}, f) \cdot exp[-jk(f)z], \quad k = k_0 n = (\frac{\omega}{c})\sqrt{\epsilon_r} \tag{5}$$

with frequency f, but now with a dependence also from the transversal coordinates x,y; the polarization unit vector e is directed along the x-axis.

APPENDIX : C

PHOTO PYRO TECHNIQUE FOR CALCULATION OF EXCITED STATE ABSORPTION SPECTRUM.

Pyroelectric technique can be used to detect the temperature change caused as a result of the heat released by various optical processes. Pyroelectricity is the manifestation of a spontaneous temperature dependent electrical polarization. This property results in a temperature dependent potential difference occurring between the two, properly chosen, opposite surfaces of a pyroelectric material [1]. In photo pyroelectric (PPE) technique modulated or pulsed temperature rise in a material is detected by a pyroelectric film sensor attached either at the back of the sample (standard or rear detection scheme with sample being illuminated Figure 1(a) or to its surface (inverse pyroelectric technique with pyroelectric sensor being illuminated Figure 1(b). The heating gives rise to a temperature distribution in the system which depends on the modulation frequency, the geometry and thermal parameters of the assembly. Commonly used PPE sensors are Lithium Tantalite $LiTaO_3$, Lead Zirconium Titanate (PZT)
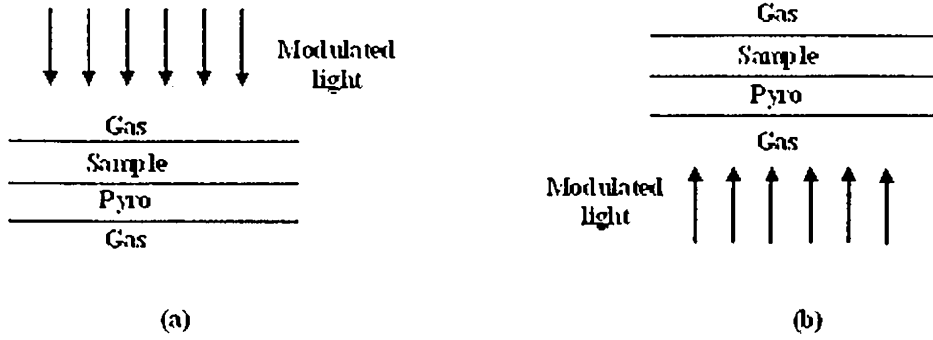
Figure 1: Conventional pyro electric detection schemes (a)rear detection scheme (b) inverse pyroelectric technique

and Polyvinylidene Flouride (PVDF). The principal advantages of the PPE technique over other photothermal techniques are flat frequency response over a very wide bandwidth, a relatively simple sample cell and the considerable reduction of noise [2].

When a pulsed light source is used, the temperature at a depth 'x' and at a time 't' following the surface absorption of an optical pulse is given by

$$\theta(x, t) = \frac{Q_0}{2\sqrt{\pi\rho\, ckt}}\ exp\left(-x^2/4\alpha t\right) \tag{6}$$

where Q_0 is the heat source, ρ , c and k are the density , specific heat and the thermal conductivity of the sample.

The pyroelectric voltage in time domain is given by

$$V(t) = e^{t/\tau} \int_0^t dt' e^{t'/\tau} \frac{pA}{C_a + C_p} \frac{d}{dt'} \overline{\theta_p(t')} \tag{7}$$

where $\overline{\theta_p(t')}$ is the spatial average of the temperature in the pyroelectric element. For very short pulses, if the thickness of the sample is considerable, then no heat would reach the pyroelectric sensor. However in these cases, as most of the pyroelectric sensors are piezoelectric, pressure changes caused by the heat release in the sample will result in piezoelectric signals [3]. Hence the signals in these cases should be analyzed as the piezo signals rather than the pyro signals. We tried to measure the excited state absorption cross section, excited state lifetime and triplet state absorption with a pyroelectric setup. As a test sample we used Rhodamine 6G dissolved in water. The excitation source used is a pulsed Nd: YAG laser (9 ns pulses). The pyroelectric sensor used is an electrode coated PVDF film. The pyro signals obtained with 532 nm excitation is shown in figure 2 The PA absorption spectrum recorded using this technique in the same sample at a very high concentration ($\sim 10^{-2}$molar) is shown in figure 3

(a)   (b)
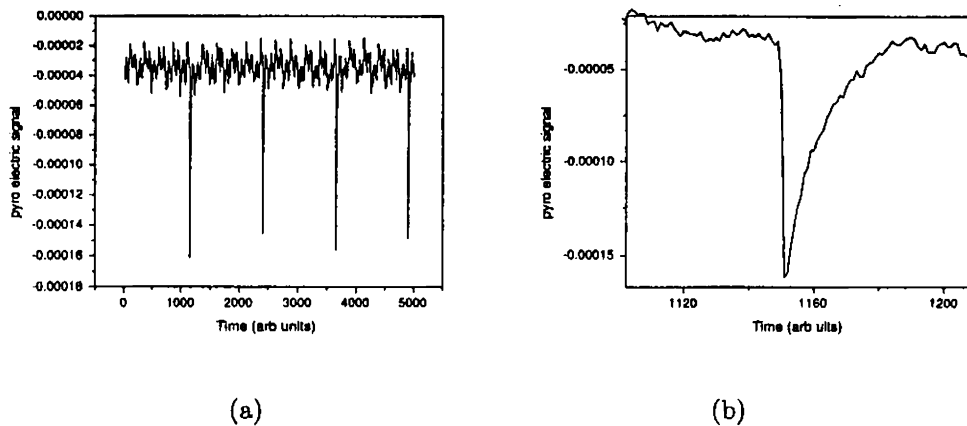
Figure 2: (a) Typical pyro electric signal obtained with Rhodamine 6 G using 532 nm pulsed excitation (b) Enlarged section of one of the peaks in 'a'
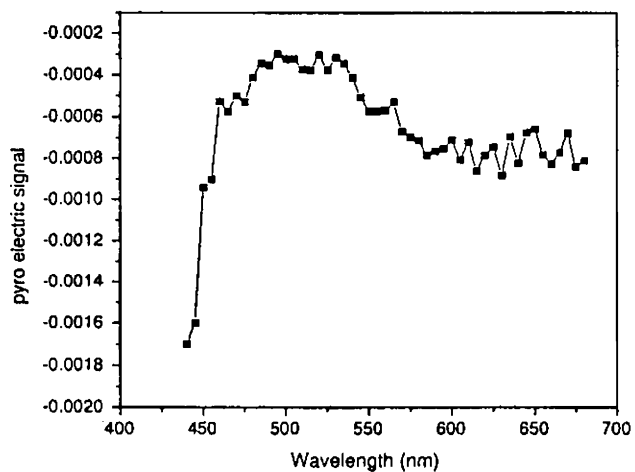
Figure 3: photo pyro absorption spectrum of Rh6G at 10^{-2} molar concentration in water

References

[1] Q. Zhong, Z. Wang, Y. Sun, Q. Zhu and F. Kong, *Chem. Phys. Lett.*, 248, (1996) p.277

[2] L. J. Rothberg, J. D. Simon, M. Bernstein and K. S. Peters, *J. Am. Chem. Soc.*, 105, (1983) p.3464.

[3] K. C. Thomas, V. B. Biju, M. V. George, D. M. Guldi and P. D. Kamat, *J. Phys. Chem. A*, 102, (1998) p.5341

Index

Index